FOSSIL ENERGY

DOE/BC/14990-14
(DE97000793)

APPLICATION OF RESERVOIR CHARACTERIZATION AND ADVANCED TECHNOLOGY TO IMPROVE RECOVERY AND ECONOMICS IN A LOWER QUALITY SHALLOW SHELF CARBONATE RESERVOIR

Final Report
August 3, 1994 to December 31, 1996

By
Archie R. Taylor
Greg Hinterlong
George Watts
Jim Justice
Keith Brown
T. Scott Hickman

October 1997

Performed Under Contract No. DE-FC22-94BC14990

Oxy USA, Inc
Midland, Texas

National Petroleum Technology Office
U. S. DEPARTMENT OF ENERGY
Tulsa, Oklahoma

DISCLAIMER

This report was prepared as an account of work sponsored by an agency of the United States Government. Neither the United States Government nor any agency thereof, nor any of their employees, makes any warranty, expressed or implied, or assumes any legal liability or responsibility for the accuracy, completeness, or usefulness of any information, apparatus, product, or process disclosed, or represents that its use would not infringe privately owned rights. Reference herein to any specific commercial product, process, or service by trade name, trademark, manufacturer, or otherwise does not necessarily constitute or imply its endorsement, recommendation, or favoring by the United States Government or any agency thereof. The views and opinions of authors expressed herein do not necessarily state or reflect those of the United States Government.

This report has been reproduced directly from the best available copy.

Available to DOE and DOE contractors from the Office of Scientific and Technical Information, P.O. Box 62, Oak Ridge, TN 37831; prices available from (615) 576-8401.

Available to the public from the National Technical Information Service, U.S. Department of Commerce, 5285 Port Royal Rd., Springfield VA 22161

DOE/BC/14990-14
Distribution Category UC-122

Application Of Reservoir Characterization And Advanced Technology To Improve Recovery And Economics In A Lower Quality Shallow Shelf Carbonate Reservoir

Final Report
August 3, 1994 to December 31, 1996

By
Archie R. Taylor
Greg Hinterlong
George Watts
Jim Justice
Keith Brown
T. Scott Hickman

October 1997

Work Performed Under Contract No. DE-FC22-94BC14990

Prepared for
BDM-Oklahoma/
U.S. Department of Energy
Assistant Secretary for Fossil Energy

Chandra Nautiyal, Project Manager
National Petroleum Technology Office
P.O. Box 3628
Tulsa, OK 74101

Prepared by:
Oxy USA, Inc
PO Box 50250
Midland, TX 79710

ABSTRACT

The Oxy West Welch project is designed to demonstrate how the use of advanced technology can improve the economics of miscible CO_2 injection projects in a lower quality shallow shelf carbonate reservoir. The research and design phase primarily involves advanced reservoir characterization and accelerating the production response. The demonstration phase will implement the reservoir management plan based on an optimum miscible CO_2 flood as designed in the initial phase.

During Budget Period 1, work was completed on the CO_2 stimulation treatments and the hydraulic fracture design. Analysis of the CO_2 stimulation treatment provided a methodology for predicting results. The hydraulic fracture treatment proved up both the fracture design approach and the use of passive seismic for mapping the fracture wing orientation.

Although the 3-D seismic interpretation is still being integrated into the geologic model and interpretation of borehole seismic is still underway, the simulator has been enhanced to the point of giving good waterflood history matches. The simulator-forecasted results for an optimal designed miscible CO_2 flood in the demonstration area gave sufficient economics to justify continuation of the project into Budget Period 2.

TABLE OF CONTENTS

	Page
Executive Summary	1
Introduction	3
Technology Transfer	7
Acknowledgement	11
Chapter 1. Optimization of Fracture Treatments	
Introduction	12
Prefracture Analysis and Design	12
Fracture Treatment Results	14
Summary of Results	16
Conclusions	17
Table	19
Figures	20-25
Chapter 2. CO_2 Stimulation Treatments	
Introduction	26
Treatment Design	27
Field Results	29
Summary of Results	34
Conclusions	35
Figures	37-38
Chapter 3. Geologic and Petrophysical	
Introduction	39
Data Base	39
Geological History	40
Petrophysical Analysis	41
Petrophysics-Seismic Intergration	42
Permeability Determination	42
Geologic Model	47
Summary of Results	48
Conclusions	49
Tables	51
Figures	52-68
Chapter 4. 3-D Seismic Evaluation	
Introduction	69
Scope and Objectives of 3-D Seismic Evaluation	69
3-D Seismic Data Base	70
Field Data Acquisition	70
Data Reprocessing	70
Seismic to Well Log Calibration	71
Seismic Structural Interpretation	72
Seismic Stratigraphic Interpretation	72
Seismic Attribute Data	74
Statistical Correlations within the Data	76
Calibrating Attributes to a Property	76

Seismic - Guided Reservoir Property Maps 78
Geologic Model 78
Summary of Results 79
Conclusions 80
Tables 82-86
Figures 87-118
Chapter 5. Borehole Seismic Program
Introduction 119
Interwell Seismic Surveys 120
Data Acquisitions 123
Processing 127
Summary of Results 132
Conclusions 133
Figures 135-139
Chapter 6. Reservoir Simulation Study
Introduction 140
Fluid Characterization 140
Relative Permeability Data 141
Reservoir Description 141
History Matching Process 142
Forecast Simulations 143
Summary of Results 143
Conclusions 143
Figures 144-149

EXECUTIVE SUMMARY

All tasks scheduled for Budget Period 1 have been undertaken and accomplished with the exception of obtaining interpretable tomograms and VSP sections from the interwell seismic surveys and preparing a seismic-guided geologic model for the final simulation runs. However, since this is leading edge technology, the original management plan anticipated that interpretation of the wellbore seismic data might continue into Budget Period 2.

The availability of a high quality 3-D seismic survey across the demonstration area was an added bonus for the project. Not only has it been possible to identify, across the total seismic volume, the two depositional parasequences that make up the main pay section, but a methodology has been developed to generate porosity and pore volume values from seismic attributes. Because the vertical resolution of the 3-D seismic in the San Andres formation is approximately 35 ft, the seismic interpretation to date has been used only to qualitatively refine the geological interpretation and quantitatively verify the total pore volume in the upper and lower main pay sections. If usable reservoir characterization is obtained from the interwell seismic surveys, the results will be integrated with the 3-D seismic in an attempt to distribute the interpretation across the demonstration area.

Meanwhile, work is progressing on an approach to improve the vertical resolution of the 3-D seismic so it can be used directly to enhance the geologic model. This approach uses well control to proportion pay thickness and pore volume between the reservoir model layers contained within the mappable seismic intervals - M1 to M3 and M3 to M5. This information is gridded and used to subdivide the seismic-derived maps of pay thickness and pore volume into intervals to match the layering.

Although the enhanced geologic model was not available in Budget Period 1, the basic geologic model was adequate enough to enable the simulator to obtain reasonable performance history matches. This created confidence in the performance predictions for various secondary and tertiary operating scenarios, which allowed design of a CO_2 flood for installation in Budget Period 2 to proceed. This progress was due in part to the base geologic model being further enhanced by the advanced petrophysical analysis, particularly the log-derived permeability profiles. The methodology developed to obtain continuous permeability from conventional log response was an important advancement. Permeability determination in shallow shelf carbonates is usually limited to cored intervals or a very data-intensive approach that derives a permeability/porosity transform for each rock type.

Analysis of the simulation runs indicates that the installation of a miscible CO_2 flood in the demonstration area will result in the economic recovery of an additional 2 million barrels of oil over the next 14 years compared to continuation of current

waterflood operations. This is significant since Oxy had originally determined that tertiary operations would not be economical in the lower quality reservoir under the West Welch Unit.

Continuation of the project is justified not only economically, but to complete the demonstration of some of the important technologies from Budget Period 1. The ability to accurately characterize the interwell space in shallow shelf carbonates would add tens of millions of barrels to the U.S. oil reserve base. The innovative use and interpretation of seismic signals is the only existing technique with the potential to achieve this goal. Progress is also being made in reducing the 3-D seismic vertical resolution below the current ± 35 ft limit. A considerable amount of time and money has been invested in conducting interwell seismic surveys, processing the data and attempting to interpret the results. Efforts to refine the processing and interpretation should be greatly enhanced once CO_2 injection begins since there is a high probability that wellbore seismic can distinguish the CO_2 saturated rock.

Not all new technology proves effective. Benchmarking the improvements in the simulation history matches for each enhancement to the geologic model allows practical judgements to be made as to the worth of a particular approach. This process will become even more meaningful during Budget Period 2 once response from the CO_2 injection occurs and comparisons can be made on the basis of simulation predictive accuracy.

Other work to be pursued during Budget Period 2 includes fracturing a row of injection wells. The simulation results indicate that this will increase the sweep efficiency in lieu of infill drilling. The fracture treatment on WWU 4807 demonstrated that a 3-D model can be used to design a treatment that gives satisfactory fracture wing length without extending downward into the water zone. The CO_2 stimulation treatment results were also promising. A careful analysis of the data indicated that the payout of a CO_2 flood can be accelerated with this approach when pipeline CO_2 is available. A method for predicting the incremental oil recovery was developed and 17 treatments are planned during Budget Period 2 for an estimated incremental oil increase of 40 MB.

Three separate written requests were made to extend the completion date for Budget Period 1 that resulted in an extension from August 31, 1995 to December 31, 1996. The major factor in extending the completion date was the delay in starting the main project task and the time involved in processing the wellbore seismic information. Also, more time was spent on technology transfer then originally anticipated due to the aggressive schedule that was followed during Budget Period 1. Twenty-three oral presentations were made, six poster sessions conducted, and ten articles were published.

INTRODUCTION

In response to the DOE's 1992 solicitation for Class 2 Shallow Shelf Carbonates (SSC) Reservoir demonstration projects, OXY USA Inc.'s Western Region in Midland, Texas submitted a proposal titled "Application of Reservoir Characterization and Advanced Technology Improves Economics in a Lower Quality Shallow Shelf San Andres Reservoir." The proposal was aimed at proving lower quality San Andres reservoirs can be economically flooded by applying advanced reservoir characterization and a combination of EOR methods that are not widely utilized. Because of the various technological expertise required by this project, OXY formed a team consisting of service companies and consultants as shown on Table 1. The reservoir characterization efforts would demonstrate new technologies which include borehole seismic and 3-D seismic. The proposal focused on using commercial resources available to most operators. The EOR methods involved both miscible CO_2 flooding and cyclic CO_2 stimulation in reservoirs more heterogeneous and of lower quality than current CO_2 projects. The proposed site was representative of DOE Class 2 reservoirs and was uniquely suited for the successful application of advanced technology.

The DOE selected the OXY proposal as one of the successful candidates for a mid-term Class 2 project. A contract was finalized during 1994 which provided for 50-50 cost sharing arrangement of the $22.2 MM estimated budget. The project, which officially started August 3, 1994, was divided into two phases. Budget Period 1 was the design phase in which advanced reservoir characterization was used to build a geologic model for insertion in a reservoir simulator. The enhanced simulator is being used to optimize the miscible CO_2 flood design and maximize the economics. Depending upon the results obtained during Budget Period 1, a decision will be made on whether to proceed with Budget Period 2 which would be the actual installation and operation of the miscible CO_2 project in the demonstration area.

The initial reservoir characterization used conventional geological and petrophysical methods to construct the basic geologic model. The model was to be enhanced by the innovative application of 3-D seismic and borehole seismic to characterize the interwell reservoir volume. The resulting geologic model is used in a compositional simulation model to provide production forecasts for optimizing the design of the conventional miscible CO_2 flood and maximizing the project economics.

The cyclic CO_2 stimulation process can provide an almost immediate production increase, and thus has the potential to reduce payout time which is long, due to the large capital outlay required up front in a CO_2 flood. The ability to accurately forecast production during this early phase is essential to performing a realistic economic evaluation of the project. CO_2 stimulation treatments were conducted during Budget Period 1 to determine if performance could be predicted accurately with the enhanced compositional simulation or some alternate approach.

Another factor influencing CO_2 floods is unfavorable mobility ratios which cause poor sweep efficiency, limiting the CO_2 processing of the hydrocarbon pore volume to only a small portion of the reservoir. Injecting CO_2 along a linear flood front would improve the areal sweep thereby increasing recovery. A linear flood could be emulated by a row of injectors whose fracture wings are aligned. This would increase injectivities and sweep efficiencies at a significantly lower cost than infill drilling. The ability of the compositional simulator to reasonably forecast the effect of the fracture wing alignment will be tested as the project progresses.

The proposal addresses methods to improve the vertical sweep by the use of borehole seismic in tracking the CO_2 front for WAG cycle optimization and mobility control. Recent work shows the effectiveness of mobility control agents for vertical sweep control, especially where thief zones are present. This project would attempt to address the sweep problems before CO_2 breakthrough and associated gas-handling problems occur by the use of tomography surveys and simulation to determine if this technology is cost-effective for reservoir management.

Overall, the project addresses five of the six primary producibility problems for shallow shelf carbonates described in the PON. The demonstration site is located in the Welch Field which is designated as a Class 2 reservoir in the TORIS database. The reservoir is in the Permian-age San Andres formation within the Northern Midland Basin of West Texas. The reservoir is comprised of layered porous dolomite, anhydritic dolomite and anyhdrite with average porosity of 12% and geometric average permeability of less than 1 md. The net pay interval averages 65 ft at an average depth of 4800 ft.

The reservoir characterization study area consists of the OXY-operated West Welch and South Welch Units, comprising over 10,000 ac and 800 wells. The actual field demonstration site consists of a 520-ac area with 62 wells in the West Welch Unit. The field demonstration site is in lower-quality reservoir rocks, where the commercial application of CO_2 flooding has yet to be demonstrated. This type of lower-quality reservoir is typical of many Permian Basin fields that are in danger of abandonment. Therefore, the focus of this project is on the lower-quality shallow shelf carbonate reservoirs whose remaining reserve potential is at greatest risk.

This area was uniquely appropriate for an advanced technology demonstration since OXY had completed the majority of the foundational work required and the field demonstration site was selected to maximize the technical benefit of the project to other operators.

The unique aspects of the field demonstration site are summarized as follows:

1. Reservoir heterogeneities and producibility problems characteristic of SSC reservoirs exist, but they are not extreme. The technical challenge is therefore solvable, and thus, success is likely.
2. OXY had an existing reservoir characterization model over both units based on detailed analysis of core from 147 wells, logs from 770 wells, and 78 mi of 2-D seismic data. The time-consuming work of building a digital database had already been completed.
3. Reservoir simulation of a successful CO_2 pilot in the South Welch Unit has obtained an excellent history match. Many of the difficult fluid and rock property problems that are so time-consuming in modeling have been resolved. The ability to do reservoir characterization in the better-quality reservoir at South Welch has been successfully demonstrated.
4. A high resolution 3-D seismic survey completely covering both units was available.
5. OXY has installed a limited CO_2 flood in the South Welch Unit and a CO_2 pipeline runs through the West Welch Unit. Therefore, the costs to bring CO_2 to the demonstration site will be minimized.
6. The Welch Field has been under water injection since the 1960's and has gone through the process of orienting the injection wells to take advantage of the preferential fracture direction of this formation. This facilitates the initiation of a linear flood front. The field demonstration site includes both fully developed 20-ac line drive patterns and patterns where infill injectors have not been drilled. Having both types of patterns in the pilot area allows for an accurate comparison of fracture wing alignment vs. infill drilling.
7. The project area is large enough that there are significant variations in reservoir properties. This gives comprehensive results that should be applicable not only to the rest of the West Welch Unit, but to other similar shallow shelf carbonate reservoirs.

The project utilizes six advanced technologies to solve producibility problems in lower quality SSC reservoirs. The advanced technologies being applied are as follows:

1. Borehole seismic to determine if the geologic model in interwell areas can be refined, and to determine if CO_2 flood advance can be monitored to maximize sweep efficiency.
2. 3-D seismic to determine if the results of the reservoir characterization refined by the borehole seismic can be applied field-wide.
3. Enhanced compositional reservoir simulation to improve prediction of CO_2 recovery processes in a lower-quality reservoir.
4. Fracture stimulation of injection wells to determine if the number of required injection wells in a CO_2 project, and thus the required capital,

can be reduced, and to determine if areal sweep efficiency can be increased.

5. Directional fracture propagation detection to determine if the induced fracture phase can be mapped.
6. The use of mobility control agents with CO_2 injection to determine if vertical sweep efficiency can be increased.

In summary, the project uses 3-D seismic and cross wellbore tomography to improve reservoir characterization in an attempt to reduce the risk involved in the large investment required to obtain and inject CO_2. This project demonstrates a variety of new and advanced techniques for applying EOR technology in marginal shallow shelf carbonates.

TECHNOLOGY TRANSFER

In their project application, the OXY team made a significant commitment of time and money for technology transfer activities. This commitment was discharged during Budget Period 1 by a very aggressive transfer program that included 23 presentations and six poster sessions before a wide variation of industry groups (Table 1). Although the exact attendance at all of these events is not available, a conservative estimate would be over 2,000 industry professionals have been exposed to information about the West Welch Unit DOE Project. In addition, articles have been published in the proceedings of meetings where presentations were made. Also, articles have appeared in two widely circulated industry publications. Table 2 lists publications to date.

This high level of technology transfer activity came about in spite of no usable tomograms being obtained yet from the borehole seismic program. This prevented finalizing the geological model and hence delayed the compositional simulation runs for optimizing the miscible CO_2 flood design and maximizing the economics. These functions will produce important information that would make worthwhile presentations. The technology transfer on these activities will take place during Budget Period 2. Fortunately, the unforeseen gap that developed as a result of the borehole seismic was taken up by reporting the success in developing techniques for obtaining permeability from conventional logs and porosity from seismic attributes. Industry has demonstrated a keen interest in these subjects to the extent that the amount of technology transfer activities by some team members threatened to interfere with progress on other aspects of the project.

A majority of DOE Class 2 reserve potential exists in SSC reservoirs located within the Permian Basin. An increasing number of these reservoirs is controlled by independent operators. This audience was specifically targeted in the original technology transfer plans. Nine of the presentations to date have been made within the Permian Basin and several others were at large meetings of technical societies where Permian Basin professionals would be in attendance. The most significant activity involving independent producers was two all-day seminars conducted at the CEED/Petroleum Industry Alliance facility located between Midland and Odessa, Texas. Five different team members made presentations concerning the engineering, petrophysics, geological, 3-D seismic, and borehole seismic aspects of the project. Included was an actual demonstration of the seismic attributes to log property conversion methods using inexpensive, commercially available software on a PC. Nearly 200 individuals attended the two seminars.

The majority of the presentations to date have been before a mixture of technical societies for the engineering, geological, and geophysical disciplines. This reflects not only the multi-disciplinary nature of the project, but also the fact that most of the activity in Budget Period 1 involved detailed technical analysis relating to the

reservoir characterization. In the future, the project will produce results that will be of more interest to operators. The original OXY proposal not only targeted operators and technical professionals, but also working interest partners, investors, and financial institutions that the independent must have on board to initiate a tertiary project. Not much of the technology developed during Budget Period 1 is directly applicable to this audience, but the focus will change during Budget Period 2.

The DOE-required quarterly and annual reports have been provided and these, along with future DOE reporting, will create a vast repository of information available to future investigators and other interested parties. As the project moves toward finalizing some of the reservoir characterization and optimization activities, an increase in articles written by the team members for various technical journals is anticipated along with industry-wide coverage through trade journals such as the Oil and Gas Journal.

A project of this magnitude also generates a lot of informal technological exchanges. This is particularly true in the Midland-Odessa area where there is a large concentration of operators and industry professionals that interact daily in professional and social settings. Some of the team members are from service organizations that have an economic incentive to commercialize technology from the project as soon as possible. The principal in ART, for example, teaches industry short courses which incorporate some of the data from the West Welch Unit Project.

The aggressive technology transfer pace established during Budget Period 1 will be continued into Budget Period 2.

TABLE 1

Technology Transfer Activity
Budget Period 1
West Welch Unit - DOE Class II Project
Dawson County, Texas

Date	Forum	Sponsoring Organization	Location	Topic	Attendance	Presenter
3/94	Permian Basin Oil & Gas Recovery Conference	SPE	Midland	Poster Session: Objectives of Project		A. Taylor
12/94	Panel on Review of the Oil Recovery Demonstration Programs of the DOE	NRC	Houston	Objectives & Goals of the Project		A. Taylor S. Hickman J. Justice
2/95	3-D Seismic Symposium	RMAG DGS	Denver	3-D Seismic Prediction of Reservoir Properties	350	G. Watts
4/95	Geophysical Short Course	SEG	Lafayette	Selected Examples from West Welch DOE Project		J. Justice
5/95	Regional Convention of Earth Science Societies	AAPG, etal	San Francisco	Overview of Reservoir Characterization at West Welch DOE Project	496	G. Watts
5/95	Annual Exploration Meeting	PBGS	Midland	3-D Seismic Predictions of Reservoir Properties	88	G. Watts
6/95	Contractors Review Meeting	DOE	Oklahoma	Review of Progress on Project		A. Taylor S. Hickman
9/95	Monthly Meeting	WTGS	Midland	Converting Seismic Attributes to Log Properties		G. Watts
9/95	Industry Seminar	Oxy/CEED	Midland	Reservoir Characterization for Low Permeability Carbonates	105	Team
10/95	Fall Industrial Associates Meeting	BEG	Carlsbad, NM	Poster Sessions: 1) Converting Seismic Attributes to Log Properties 2) Examples of Tomograms		P. Lufholm
11/95	Industry Seminar	Oxy/CEED	Midland	Reservoir Characterization for Low Permeability Carbonates		Team
11/95	In-House Seminar	Oxy	Bakersfield	Reservoir Characterization for Low Permeability Carbonates		G. Watts
11/95	Monthly Meeting	SEG	Bakersfield	Converting Seismic Attributes to Log Properties		G. Watts
3/96	Annual Meeting	SIPES	Dallas	Converting Seismic Attributes to Log Properties		G. Watts G. Hinterlong A. Taylor
3/96	Workshop on Platform Carbonates in Southern Midcontinent	OGS	Oklahoma City	1) Converting Seismic Attributes to Log Properties 2) Reservoir Characterization using Intergrated Log and Core Analysis		G. Watts G. Hinterlong
3/96	Permian Basin Oil & Gas Recovery Conference	SPE	Midland	1) Fracture Monitoring Using "Low Cost" Passive Seismic 2) Characterization of Rock Types with Mixed Wettability Poster Session: Cyclic CO2 Results and Evaluation		G. Hinterlong A. Taylor
4/96	Southwest Petroleum Short Course	Texas Tech	Lubbock	Fracture Monitoring using "Low Cost" Passive Seismic		A. Taylor
5/96	Annual Meeting	PBGS	Midland	Converting Seismic Attributes to Log Properties		G. Watts
5/96	Annual Meeting	AAPG	San Diego	Poster Session: Converting Seismic Attributes to Log Properties		G. Watts
5/96	Permian Basin Reservoir Engineering Study Group	SPE	Midland	Panel: Status of DOE Class II mid-term projects in the Permian Basin	110	A. Taylor
/96	In-House Seminar	Oxy		Fracture Monitoring Using "Low Cost" Passive Seismic		A. Taylor
9/96	Section Meeting	SPE	Oklahoma City	Application of Advanced Technologies in Characterizing Complex Carbonate Reservoirs	105	S. Hickman
9/96	Section Meeting	SPE	Duncan, OK	Application of Advanced Technologies in Characterizing Complex Carbonate Reservoirs	30	S. Hickman
11/96	Fall Symposium	WTGS	Midland	Use of Multiple Log Curves to Predict Permeability in a Dolomite Reservoir Poster Session: Converting Seismic Attributes to Log Properties		G. Hinterlong G. Watts

Organization Abbreviations
AAPG - American Association of Petroleum Geologists
PBGS - Permian Basin Geophysical Society
SEG - Society of Exploration Geophysics
SPE - Society of Petroleum Engineers
DOE - Department of Energy
NRC - National Research Council
RMAG - Rocky Mountain Association of Geophysics
DGS - Denver Geophysical Society
WTGS - West Texas Geological Society
CEED - Center for Energy and Economic Diversification
BEG - Bureau of Economic Geology
SIPES - Society of Independent Professional Earth Scientists
OGS - Oklahoma Geological Society

TABLE 2

Publications
Budget Period 1
West Welch Unit - DOE Class II Project
Dawson County, Texas

Authors	Title	Publications	Note
Watts, G. and Lions, T.D. and Taylor, A.R.	3-D Seismic Predictions of Reservoir Properties - West Moose Field, Ector County, Texas	"High Definition Seismic" Guide Book - RMAG	November 1995
Taylor, A.R., Brown, K etal	Fracture Monitoring Using "Low Cost" Passive Seismic SPE 35230	Proceedings: Permian Basin Oil and Gas Recovery Conference	March 1996
Hinterlong, G.D. and Taylor, A.R.	Characterization of Rock Types with Mixed Wettability Using Log and Core Data - SPE 35160	Proceedings - Permian Basin Oil and Gas Recovery Conference	March 1996
Lyle, D.	Huff'n Puff CO2 Enhancement Works, But the Economics Need Some Tuning	Hart's Oil and Gas World	March 1996
Hinterlong, G.D. and Taylor, A.R.	Improved Reservoir Characterization Through Integrated Log and Core Data; Example from the Permian San Andres Formation Welch Field, Dawson County, TX	Proceedings: Platform Carbonates of the Southern Midcontinent	March 1996
Watts, G.P., Hinterlong, G.D. etal	Seismic Estimation of Porosity in the Permian San Andres Carbonate Reservoir, Welch Field, Dawson County, Texas	Proceedings: Platform Carbonates of the Southern Midcontinent	March 1996
Watts, G.P., Hinterlong, G.D.	Seismic Estimation of Porosity in the Permian San Andres CarbonateReservoir, Welch Field, Dawson County, Texas	OGS Circular: Platform Carbonates of the Southern Midcontinent	March 1996
Hinterlong, G.D. and Taylor, A.R.	Improved Reservoir Characterization Through Integrated Log and Core Data: Example from the Permian San Andres Formation, Welch Field, Dawson County, Texas	OGS Circular: Platform Carbonates of the Southern Midcontinent	March 1996
Taylor, A.R. etal	Passive Seismic Data used to Design and Analyze Fracture Treatments	American Oil and Gas Reporter	July 1996
Hinterlong, G.D. and Taylor, A.R.	Use of Multiple Log Curves to Predict Permeability in a Dolomite Reservoir, San Andres of Welch Field, Dawson County, TX	Proceedings: WTGS Fall Symposium	November 1996

ACKNOWLEDGMENT

This document reports the findings and results of the investigations and analysis performed during Budget Period 1 by the OXY West Welch Unit DOE project team, which included personnel from OXY, USA; Advance Reservoir Technologies (ART); Geomatic (formerly Reservoir Simulation Resource Corporation); Halliburton and T. Scott Hickman and Associates (TSH&A). The information for the technical sections of this report was prepared by the principal investigators - Archie R. Taylor, OXY; Gregg D. Hinterlong, OXY; George P. Watts, OXY; and James Justice, ART. The report was compiled and edited by T. S. Hickman, TSH&A. Hickman also prepared the introduction, executive summary and technology transfer sections.

Appreciation is expressed to OXY USA, the West Welch Unit DOE project sponsor, for their full cooperation in the preparation of this report.

Chapter 1 - OPTIMIZATION OF FRACTURE STIMULATION TREATMENTS

Introduction

The Welch field is located in the northwestern portion of Dawson Co., Tex, and produces from the San Andres formation at average depths of 4800 ft-4900 ft. The field was discovered in 1936, with waterflooding initiated in 1958 and reaching full field implementation by 1972. The Unit has been further developed by infill drilling and pattern modification, and is currently producing from 20-acre line drive patterns, with some areas where the infill injectors have not been drilled. The southern part of the DOE project area (Fig. 1-1) shows an example of this.

Wellhead injection pressures have varied over time, from 400-1800 psig. The current injection pressure is about 1600 psi, which is at, or slightly above, formation parting pressure. Due to the high injection pressures, fractures at injection wells were initiated. In addition, propped hydraulic fracture treatments have been performed on a large portion of the injection wells to increase injectivity. Water breakthrough and pressure testing over time showed fractures were generally oriented east-west. The current east-west line drive injection pattern was installed to take advantage of the orientation. It was reasoned that by optimally fracturing a row of east-west injectors, a linear CO_2 flood front could be established that would improve the sweep efficiencies of the tertiary process. An additional benefit would be the elimination of infill injectors. During Budget Period 1, a fracture simulator was used to design an optimum fracture treatment that would obtain maximum fracture wing length while keeping the fracture height within zone. To verify the model design, passive seismic measurements were used to map fracture growth when the demonstration well, WWU 4807, was fracture treated in 1995.

An initial data review revealed that all the wells in the project area on the wider spacing have already been hydraulically fractured. WWU 4807 was chosen for the analysis. Data gathering and analysis included evaluation of well log, core, and pressure transient data that were then incorporated into the 3-D fracture model. The 3-D fracture model was built, then refined, through history-matching the previous treatments and production and injection volumes for the WWU 4807 and offset wells. To arrive at a final model for designing the optimum fracture treatment the designed treatment was pumped with tagged injectants, while seismic events were recorded in an offset well. Post fracture analysis included, (1)using the 3-D model, (2)logging to evaluate the tagged injectants and fluid injection intervals, and (3)falloff testing to determine the effective fracture area after closure.

Prefracture Analysis and Design

Well log and core data from area wells were used to set up the initial 3-D fracture model, with most of the data indicating the fracture would grow out of the

pay interval. Analysis of the Full Wave Sonic (FWS) log showed that the layer stresses would cause the fracture to grow down into the water zone below the main pay (Fig. 2-1). This was supported by core testing samples taken from different intervals (Table 1-1) and the match of fracture pressures, obtained from the FWS, with step rate test results. The fracture pressure, obtained from the FWS analysis, was 3200 psig, while the step rate results gave a fracture pressure of 3150 psig.

The injection survey just prior to the treatment showed 50% of the water injection going into the very top of the perforated interval, 25% going into the middle of the interval,and 25% going into the bottom (Fig. 3-1). In contrast, earlier surveys on the well indicated injection was better distributed over the main pay, corresponding to the balanced injection and total produced fluid volumes that were occurring in the area. If significant volumes of water were going out-of-zone, injection-production ratios would be considerably higher than the approximately 1:1 being experienced. Permeability values are less than 0.01 md above the N marker, a dense, primarily anhydrite zone. Therefore, the likelihood of injection occurring above the pay interval would be negligible. The lower water zone, however, does have good permeability and significant injection volumes could be lost below the pay interval.

The 3-D fracture stimulator was used to model the 1966 fracture treatment. The model shows a fracture area of 29,000 sq ft remaining after fracture closure, compared to the falloff test results of 15,000 sq ft in 1995. The difference is attributed to setting a liner, and a cement squeeze in the mid 70's. A fracture length of 139 ft and a fracture height of 208 ft at the wellbore were calculated by using the stimulator. Injection profile data indicating that injection is in the main pay interval only do not support the model results, which show the fracture being propped out of the main pay interval. If the height calculated by the model is shortened, the effective fracture length would increase. The longer fracture length is supported by the results of the optimum refracture treatment.

Since the previous treatment was shown to grow out-of-zone by the 3-D model, the new fracture treatment was designed to place proppant in the main pay interval, and keep it out of the lower water zone. The resulting treatment used a high density pad, followed by low density nitrogen foamed stages of 20/40 mesh sand, pumped at 8 bbl/min (Table 2-1). The purpose of the foam was to utilize density override to place the sand higher in the fractured interval away from the water zone and still obtain as much propped length as possible after fracture closure. The water zone was estimated to be 45 ft below the bottom perforation, separated by a dense, impermeable zone. The bottom barrier is the interval from N8-N9 in Figs. 2-1 and 3-1. Fracture growth upward out-of-zone was not a concern, since there are no upper zones with permeability that would allow out-of-zone fluid loss to occur.

Fracture Treatment Results

Passive Seismic. An observation well was used to monitor the seismic events created by the fracturing process. Both the treated well and the observation well had directional surveys run for more accurate bottomhole location. The observation well, located 560 ft south of the treated well, had four geophone stations spaced 50 ft apart vertically across the treated interval. Each station consisted of three geophones to measure the X, Y, Z components of events, allowing individual seismic events to be located in three dimensions[1]. Another approach uses multiple stations, which allows triangulation of the source location[2] using velocities check shot . The velocity check shot was acquired prior to the fracture treatment by detonating a dynamite charge in the well to be fractured and listening at the observation well.

Detection. Passive seismic events were recorded before, during, and after the fracture was pumped, with over 200 events identified, using a band pass filter to distinguish event signals from noise. After visual inspection of the signals revealed only weak signals, a signal detection program was used for finding potential signals. Since a small time lag would be expected between the different stations receiving a signal, a time window was used to find events that created at least four signals. Combining the time window and testing different band pass filters resulted in finding 229 events in the 0-50 Hz range, which other studies[3] have found to be fracturing-event related. Of the 229 events, 30 had at least six detections exceeding a signal-to-noise ratio of 3.0. Background noise, which masks the events, was higher during pumping, and resulted in almost zero detection rate. The highest detection rates occurred immediately following a cessation of pumping, even if the shut down was only for a short time.

Twenty-seven event locations remained after refining the initial 30 picked. Figure 4-1 is a 3-D representation of the 27 events. Once the events were found in the records, event locations were calculated from the relative amplitude of the signals and the difference in the shear wave and the P (compression) wave arrival times[4]. The P wave and shear wave should be 90 degrees apart; if the angle varied significantly from 90 degrees, the events were excluded. When different geophones gave greatly differing locations, the most common problem was getting the depths to agree. It is believed the interval at 4800 ft, where the velocities differ significantly, caused a large part of this problem.

Interpretation. A plan view of event locations shows significant variation from a linear symmetrical fracture even though the anticipated east-west trend is evident (Fig. 5-1). The east wing of the fracture created events up to 700 ft away, slightly over ½ the distance to the offset injection well. The hydraulic fracture treatment increases pressure in the pores causing the rock to rupture. The higher pressure of the adjacent injection well stopped the fracture from growing in length and forced it to widen and/or grow in height.

The areal scattering of the events generated by fracturing are controlled by the compressive forces created as the main fracture is widened. The eastern portion of the fracture was created by the earlier treatment, while the southwest fracture wing was induced by this demonstration fracture treatment. More events are located in the SW portion of the fracture and are more closely spaced than the events in the east. The location of the events on the east wing are wider spaced as expected because events associated with widening a pre-existing fracture are due to compression of the formation away form the fracture. Whether these events are due to simple collapse of vugs, etc., or from creating additional fractures is not known at this time. Further review to determine the origin may be done. Other studies[5,6] have shown that compression can create tensional and shear fractures along the main fracture at differing angles as determined by rock ductility. The effect of these fractures on the overall treatment is not known. However, this would impact the modeling and interpretation of fracture growth because the fracture height growth on a net pressure plot would be too optimistic if significant fluid loss volumes are not accounted for.

3-D Seismic. Interpretation of the 3-D seismic data for the field helped explain the asymmetrical orientation of the two fracture wings. Depth structure maps of the base of the Woodford and Atoka horizons were generated from the 3-D seismic volume. This was used to better define the deep seated (Pennsylvanian and deeper) faulting that lies beneath the producing San Andres formation. A coherency slice map of the base of Woodford horizon was produced to help delineate the small faults in the deep section.

These maps showed a fault running directly beneath WWU 4807. Figure 6-1 shows the fault line orientation (S-SW to N-NE) and its relation to the other wells in the area. Fault displacement occurs from the Woodford up through the Atoka formations. No evidence is seen that the fault extends up to the producing interval; however, the fault has created enough stress in the San Andres formation to change the fracture orientation as the fracture grows outward. Figure 7-1 shows the deeper fault identified on the seismic that is controlling the fracture orientation. The east wing of the fracture maintained the general E-W orientation, previously documented in the field, showing that the change in stresses is very localized. Thus the plans for using fracturing to improve the economics of the CO_2 flood have not changed.

Radioactive tagging during different stages of the treatment and post fracture injection surveys were performed to aid in the determination of fracture height. While the majority of the seismic events outside the main pay occurred above 4800 ft, post fracture logging showed that most of the tagged injectant stayed in the perforated interval, at least near the wellbore. Figure 8-1 shows the relative concentration of tagged injectant. The pad was tagged with antimony, the initial stages of proppant with scandium, and the final stage of proppant with iridium. The concentration of the tagged injectants is at background levels, above and below the perforated interval, showing the effective fracture near the wellbore is near the limits of the main pay.

A cross section of the passive seismic events (Fig. 9-1) shows height growth initially further from the wellbore, and later events occurring closer to the wellbore. The deepest event mapped is at 4989 ft, just reaching the water zone below the main pay. As the only seismic event in the water zone interval, it is isolated vertically and aerially, leading to the conclusion that the fracture did not grow down.

There is no indication from profile surveys or volume balances volumes that any fluid is leaving the pay interval. The injection surveys have shown an increase in injection volume into the middle of the pay interval following the fracture treatment, but little indication of out-of-zone injection. Above the N marker the intervals are mainly dense, tight, dolomites and anhydrites and there was not enough upward fluid movement to deposit significant amounts of proppant out-of-zone. It appears that the foamed gel produced enough of a gravity override effect to keep proppant out of the water zone.

Summary of Results

Passive seismic measurements were taken before, during, and after a fracture stimulation treatment to monitor the fracture growth and optimize future fracture treatments. The seismic events created by the fracture treatment showed an asymmetrical east-west trend during the treatment, with wide variations in the locations of events. The passive seismic measurements support the previous belief that the fracture orientation for the field is east-west. However, the recorded events showed more complexity to the fracturing process than had been anticipated. The events showed a southwest trend toward a producing well along with the widely scattered events to the east. The 3-D fracture simulation results, pressure transient analysis, and production injection data do not support the very large fracture geometry suggested by the more widely scattered events.

Fracture lengths and heights from the passive seismic events varied along with the directions. The length of the wing to the southwest showed seismic events over 1200 ft from the well, while the east wing events only reached about 700 ft. The shorter fracture length to the east is believed to be due to the well being offset to the east by another injection well. The higher pore pressure from the water injection stopped the fracture extension. The two wings also showed a large variation in the height at which events occur. Although the treatment interval was 4820-4910 ft, seismic events occurred from 4550-4900 ft for the southwest wing and 4600-5008 ft for the east wing.

The 3-D modeling of the initial 1966 fracture treatment showed a propped fracture wing length of 139 ft, with a propped area of 29,000 sq ft. The 1995 treatment model showed a wing length of 150 ft and an area of 26,000 sq ft. This matched very closely the pressure transient analysis results of 24,000 sq ft, indicating that the current model can predict fracture results adequately for most evaluation

purposes. However, for nonuniform pressure gradients a more detailed areal model will be needed.

Conclusions

Since actual propped fracture lengths and heights depend on fluid movement, each layer's properties, including permeability, are essential for accurate 3-D modeling in a fracture simulator. Passive seismic measurements can be used successfully in validating fracture design, especially in determining local fracture orientation.

Detection of fracturing events can be enhanced by short prime shutdowns during the treatments. This becomes more important as the distance from the treated well to the observation well(s) increases.

Variations in formation pressures can cause the fracture orientation to change on subsequent refracture treatments, consistent with Mukherjee et al.[7] Shutting in offset injectors and even flowing wells back may be useful for controlling fracture geometry.

The passive seismic measurements have recorded events that may be the result of additional fractures nearly perpendicular to the main fracture.

Multiple observation wells would place receivers closer to the sources enhancing event detection, as the fracture propagates on different sides of the wellbore.

Post fracture analysis has shown that foamed proppant was effective in keeping proppant in the desired interval.

References

1. Fix, J.E., Adair, R.G., Fisher, T.W., Maher, K.D., Mulcahay, C.C., Myers, B.C. Swanson, J.G., Woerpel, J.C., *Development of Microseismic Methods to Determine Hydraulic Fracture Dimensions*, Final Report, December, 1987-November, 1988, *Gas Research Institute Report.,* 89/0116: *Teledyne Geotech Technical Report* N. 88-11.

2. Vinegar, H.J., Wills, P.B., Demartini, D.C., Shlyapobersky, J., Deeg, W.F.J., Adair, R.G., Woerpel, J.C., Fix, J.E., Sorrells , G.G., *Active and Passive Seismic Imaging of a Propped Hydraulic Fracture in Diatomite*, paper SPE 22756 presented at the 1991 SPE Annual Technical Conference and Exhibition, Dallas, Texas

3. Woerpel, J.C., and Kalik, A.J., *Hydraulic Fracture Diagnostics Survey for Reuben L. Graham, Inc. E.D. Well F.M.C No. 78, Pike County, Kentucky*, report, *Teledyne Geotech Technical Report* No. 93-2

4. Woerpel, J.C., Justice, J.H., *Microseismic Mapping of a Hydraulic Fracture for OXY USA Inc.*, report, 1995

5. Griggs, D, and Handin, J., *Observations on Fracture and a Hypothesis of earthquakes*, Geological Society of America Memoir 79, p. 347-364.

6. Brace, W.., Paulding, B.W., and Scholz, C., *Dilatancy in the Fracture of Crystalline Rocks*: *Journal of Geophysical Research*, 1966, vol. 71, p.3939-3953.

7. Mukherjee, H., Poe, B., Heidt, H., Watson, T., Barree, R.D., *Effect of Pressure Depletion on Fracture Geometry Evolution and Production Performance*, paper SPE 30481 presented at the 1995 SPE Annual Technical Conference and Exhibition, Oct. 23-25.

Table 1-1. Core data from lab tests on the #4852 core.

Depth (feet)	Young's Modulus (psi x 10^{-6})	Poisson's (Ratio)	Compressive Strength (psi)
4836	12.6	.28	24455
4844	6.8	.26	15690
4852	5.1	.35	15324
4866	4.6	.24	10557
4900	9.5	.29	13222
4924	11.9	.28	24014

Table 2-1. 1995 Fracture Treatment Schedule

Stage	Planned Volume (gal)	Foam %	Actual Volume (gal)	Planned Proppant Concentration (lb/gal)	Actual Proppant Concentration (lb/gal)
1	1000	0	453	0.00	0.00
2	1000	0	1011	0.00	0.00
3	840	0	861	0.00	0.00
4	15000	0	14654	0.00	0.00
5	1500	0	1233	0.00	0.00
6	1500	70	1386	2.00	1.77
7	1500	70	1404	3.00	3.07
8	1500	70	1540	4.00	4.48
9	10000	70	3516	5.00	6.03
10	763	0	759	0.00	0.00
Total	33974		26818		

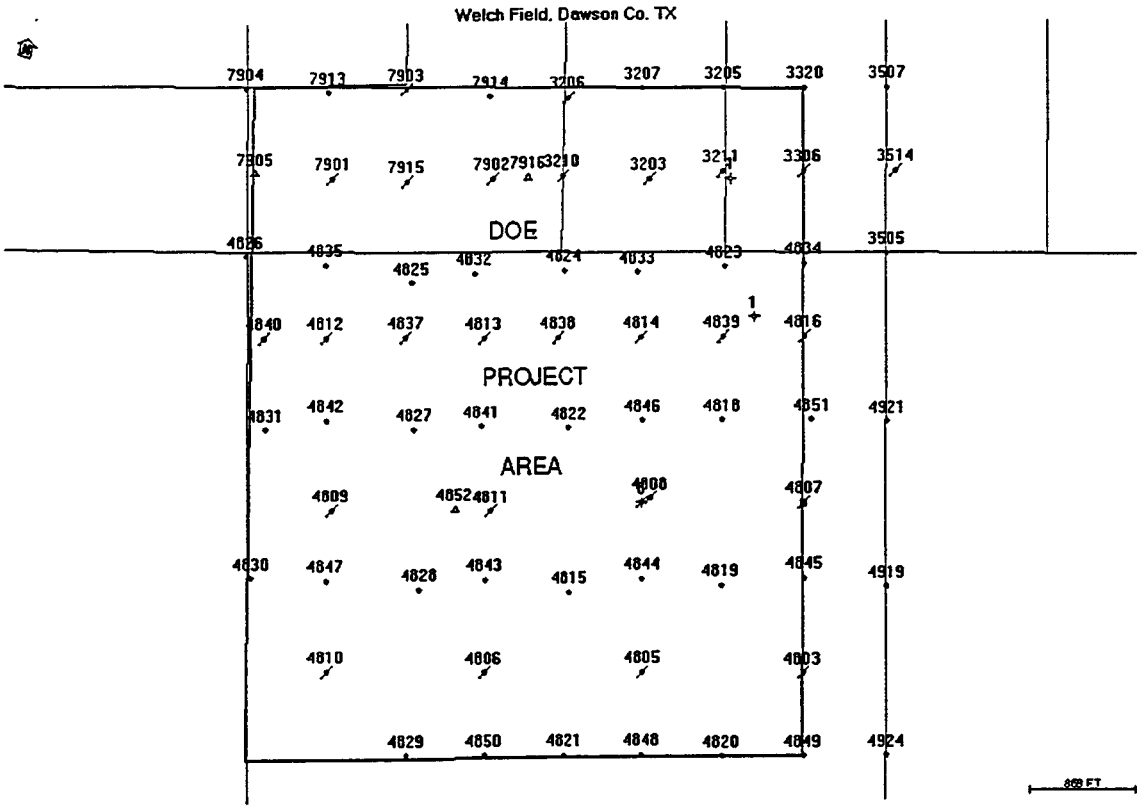

Figure 1-1 DOE Project Area showing the wider injection well spacing.

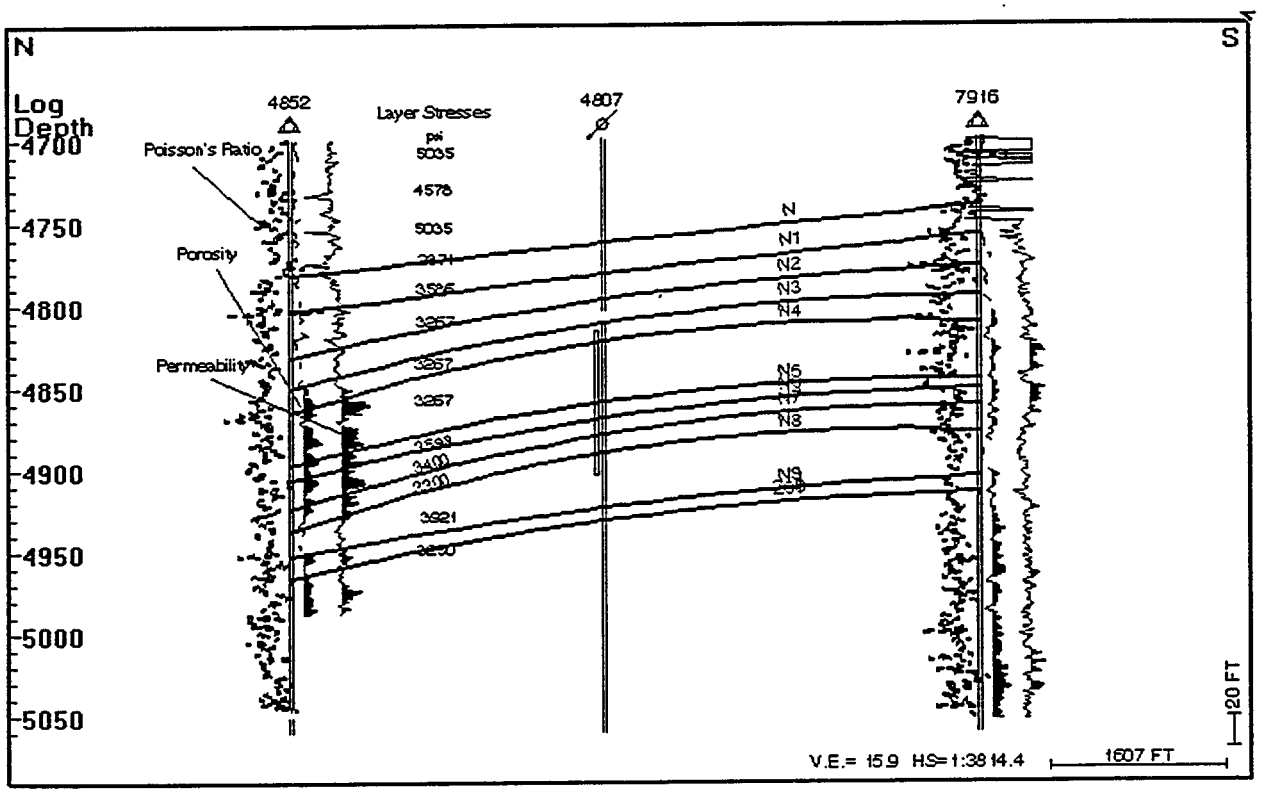

Figure 2-1 Layer stresses used in the fracture model.

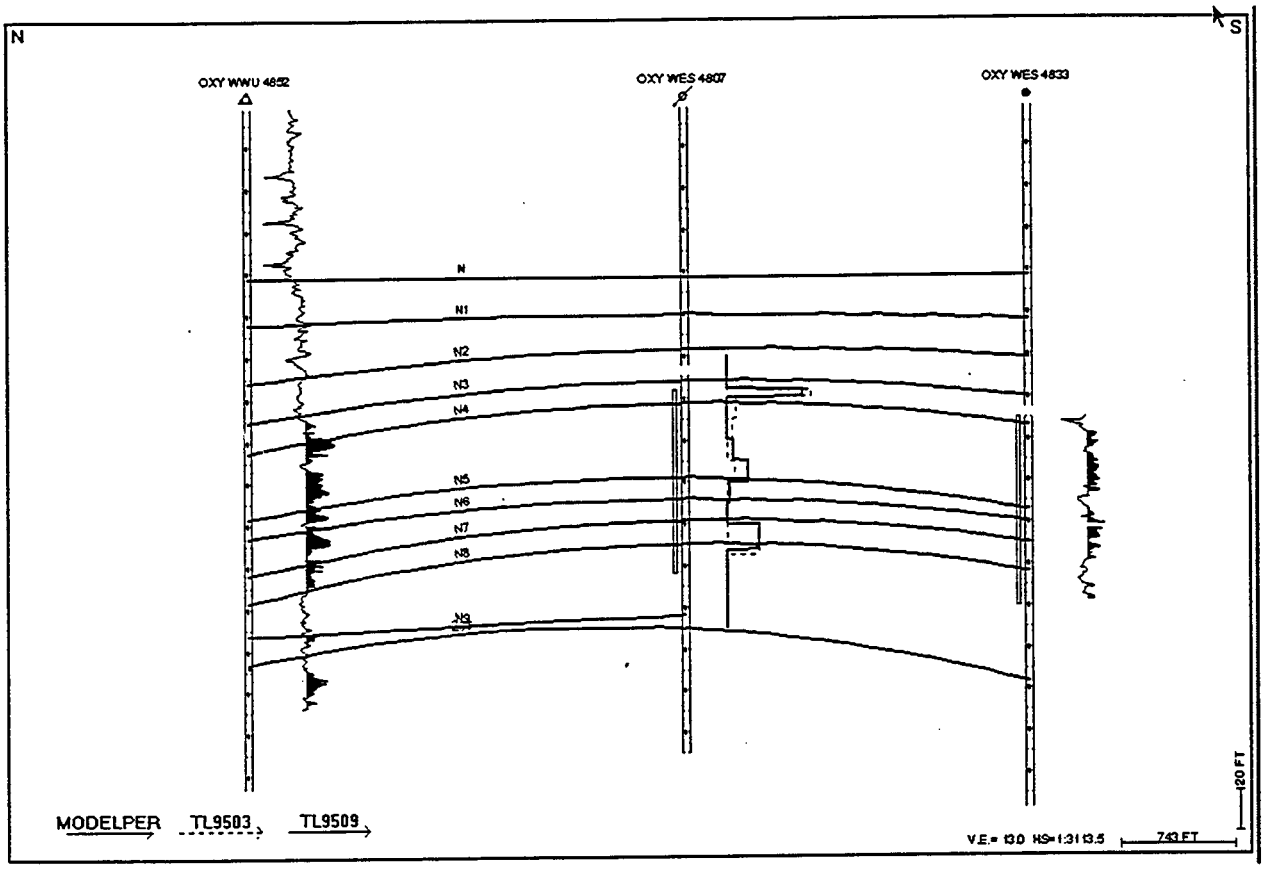

Figure 3-1 Cross section with the #4807 in center.

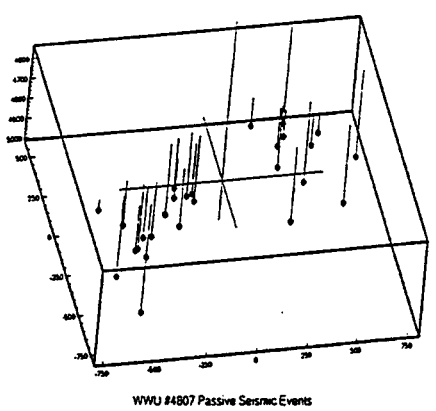

Figure 4-1 3D representation of seismic events.

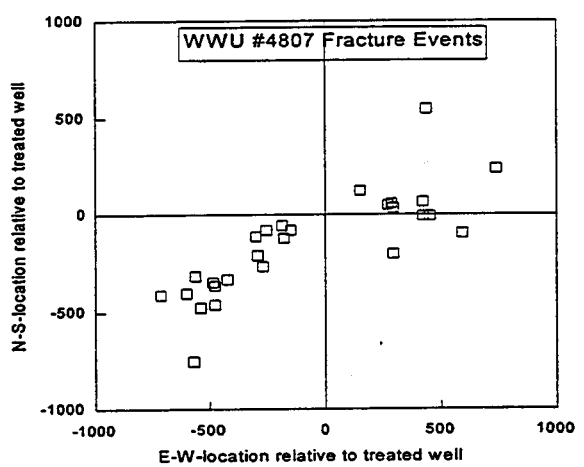

Figure 5-1 Areal view of seismic events centered around treated well.

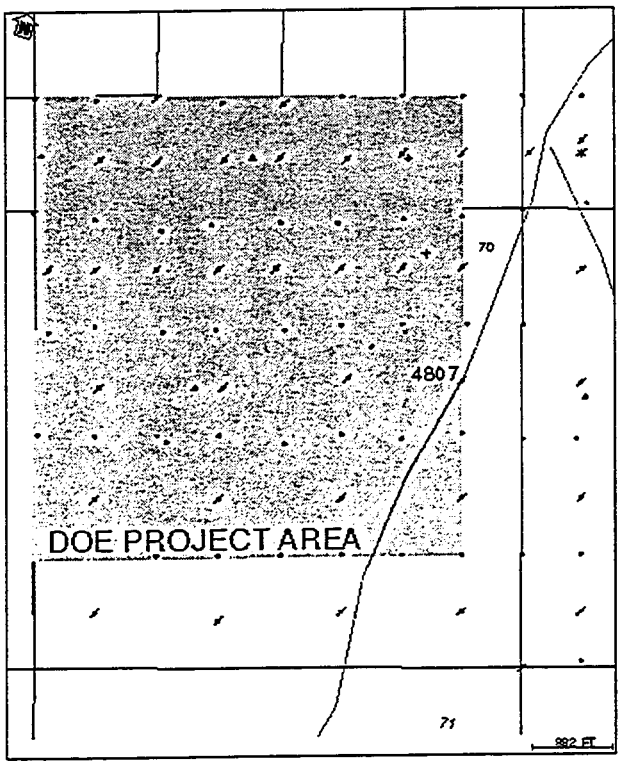

Figure 6-1 Sub San Andres fault running below the 4807w.

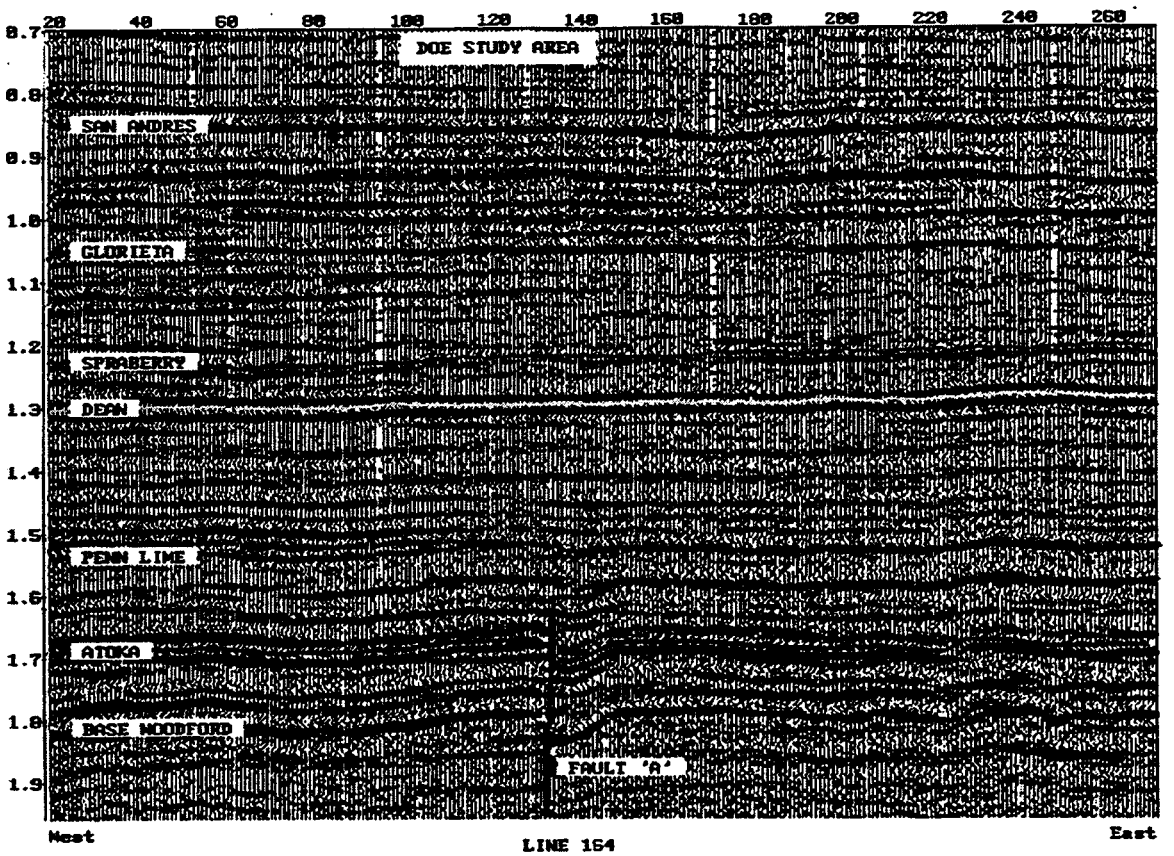

Figure 7-1 Seismic line showing the fault below the 4807w.

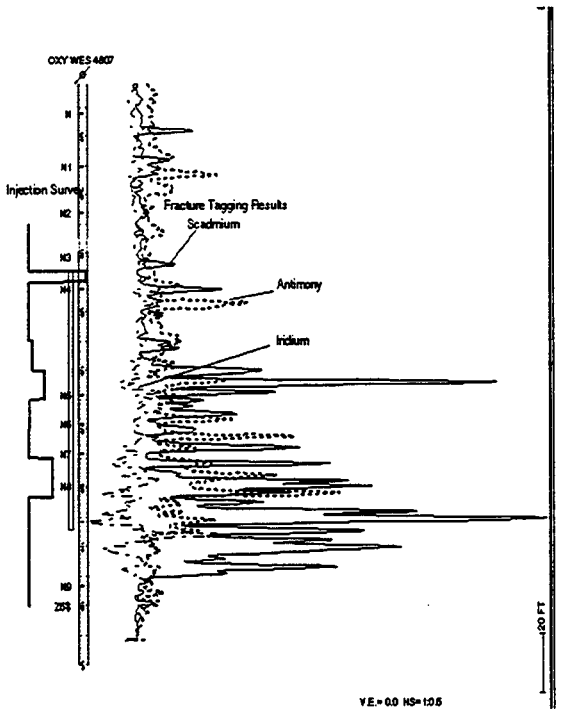

Figure 8-1 Concentration of tagged injectant after 1995 frac.

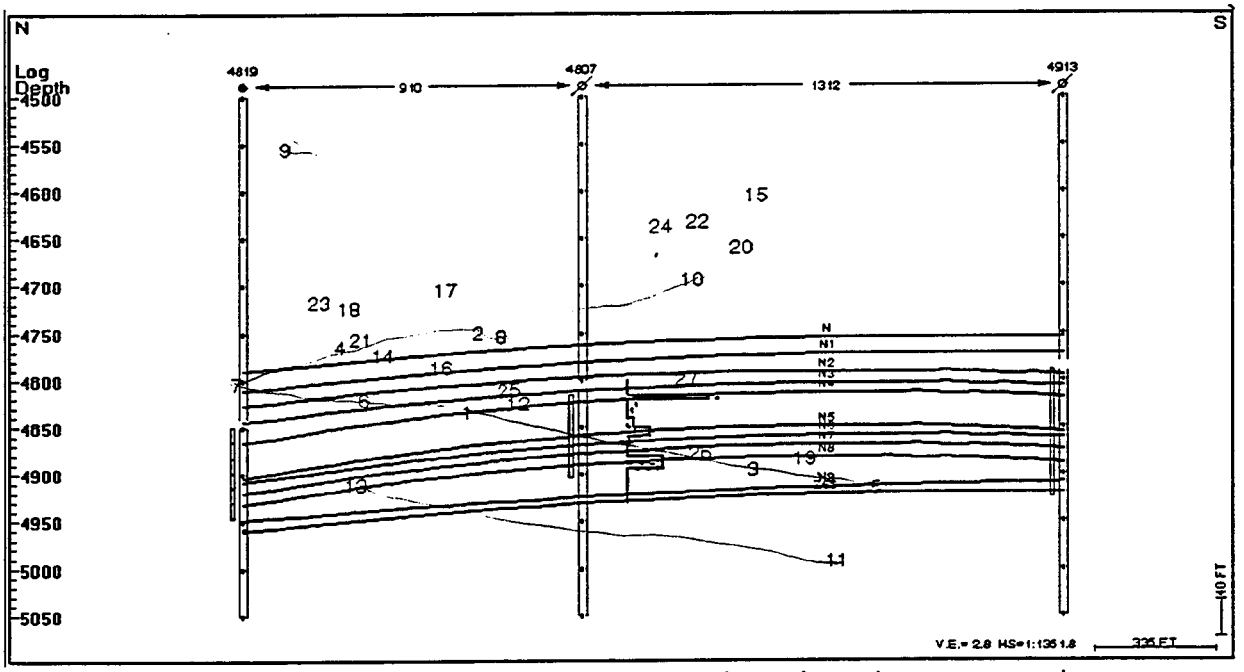

Figure 9-1 Cross section of seismic events numbered as they occurred.

Chapter 2 - CO_2 STIMULATION TREATMENTS

Introduction

The West Welch Unit is located in the NW corner of Dawson Co., Tex. and produces a 33°API oil under waterflood since the early 60's. The field is highly stratified and is producing at an average water-oil ratio (WOR) of 8:1. The average permeability is 2 md with average gross pay intervals of 74 ft; however, the net pay drops to 33 ft when a 1 md cutoff is used. Reservoir characterization has shown that two pore scale oil-water relative permeability characteristics are present. As a result, the residual oil saturation to waterflood varies from 20-45%, but reduces to a residual oil saturation of 8-10% with the presence of CO_2.

Reserves from CO_2 flooding were estimated at 10% of the original oil-in-place for the areas of the field that can be flooded. The original oil-in-place for the entire unit is estimated at 350 million barrels of oil. The economics of CO_2 flooding are often marginal due to the length of time between the beginning of CO_2 injection and the peak oil response. The time lag results from the reservoir's low permeability and heterogeneity. To make the recovery of the additional oil economic, applying various technologies to improve the economics is needed.

CO_2 stimulation treatment of producers was one method chosen for improving the economics. While treatment CO_2 has been shown to improve recovery in light oil reservoirs[1,2], wide application of CO_2 treatments has been limited due to the delivered cost of CO_2. In this instance, the CO_2 supply will be in place and thus provide a cheap source of CO_2 for treating producers at the start of the flood. The early increase in production from the CO_2 treatments will accelerate the payout, which should improve the economics for the overall project.

The goal of the initial demonstration was to quantify recovery from the CO_2 treatments and provide information for optimizing future treatments. Five wells were chosen for the demonstration with wide variations in producing and formation characteristics. The production rates varied from 3-30 BOPD with WORs ranging from 2 to 30. Another factor in well selection was excess pumping capacity since the wells would be producing extra volumes of oil and water.

CO_2 was trucked and stored at each wellsite during the pumping period at pressures and temperatures that would keep the CO_2 in liquid form. Having the CO_2 in liquid form was necessary for storage and improved the efficiency of the pumping system by reducing the volume of vapor being pumped. Initially, injection pressure was kept below miscibility pressure, but the resulting injection rates were too low. To obtain acceptable rates, the injection pressure was allowed to increase to just below the estimated fracture pressure. A minimal volume of CO_2, ranging from 5-15 MMCF was used in each well due to the high cost of trucked CO_2 (about six times the cost

for pipeline CO_2). Incremental production increases show that treating producers with CO_2 can accelerate the production response and improve the economics of CO_2 flooding in some cases.

Treatment Design

Laboratory data. Laboratory data used in the design and analysis of the stimulation treatment included oil swelling tests as a function of the CO_2 concentration, CO_2 oil diffusion rate tests, immiscible gas oil relative permeabilities, and slim tube miscibility data. Oil viscosity as a function of CO_2 concentration and pressure were also available from the CO_2 flooding evaluation. The only data gathered specific to the CO_2 producer treatment design were the diffusion rate data. Diffusion is the physical mechanism by which CO_2 moves through and mobilizes oil by swelling and viscosity reduction. The rate of diffusion, along with the formation heterogeneity, controls how long the shut-ins or "soak" periods need to last. Using the laboratory-derived diffusion rate, calculations of the shut-in time required for the CO_2 to diffuse through and swell the oil were made using both a viscous fingering model and a porosity-permeability layering model for the specific wellbore. The comparison of the two calculations showed that, in this reservoir, the permeability profile in the wellbore being treated controls the length of shut-in time needed. The high degree of heterogeneity actually reduces the soak time needed since the CO_2 has less distance to move to accumulate the concentration required to swell the oil. As a result, the shut-in time required after CO_2 injection was about 2 weeks.

Oil swelling appears to be the primary mechanism in incremental oil recovery for cyclic CO_2 treatment of producing oil wells. Since the oil phase will dissolve a larger volume of CO_2 than the water phase, the swelling is more pronounced in the oil phase and increases the oil saturation. Published data by Hara and Christman[3] show that 0.46 moles of CO_2 will dissolve in one barrel of water at Welch compared to the 2.86 moles that will dissolve in a barrel of Welch oil. The diffusion tests showed that CO_2 diffuses into the water phase faster than the oil phase.

A 50% CO_2 concentration will swell a volume of oil nearly 25% (Fig. 1-2), thereby increasing the oil saturation and relative permeability to oil. Special core analysis shows that the residual oil saturation to waterflood is about 35%. Therefore, if the residual oil swells by 25%, the resulting residual oil saturation increases to 44%. Addition of CO_2 to the oil also reduces the surface tension allowing oil trapped in large pores with small pore throats to flow. The percentage of pores included in this group is not known but could account for the increased recovery above that predicted by the design calculations.

The increase in saturations from the swelling also increases the oil relative permeability and reduces the produced WOR. The mobility of the oil is increased by the increased oil saturation and reduced oil viscosity. In contrast, CO_2 dissolved in the

water phase increases the viscosity of the water. The overall effect increases oil production rate and reduces the produced WOR. Depending on the initial oil cut, the total fluid production can increase significantly which can overload the production equipment. The resulting problems will be discussed in more detail in the field results.

Steady state oil-water relative permeability curves were used to estimate the change in relative permeability for use in forecasting producing rates. The produced watercut was used with fractional flow analysis to estimate the average saturations at the producing well. The change in oil saturation from swelling and the relative permeability curves were used to estimate the new relative permeabilities. A new producing rate was estimated based on a ratio of the old and new mobilities. The rates estimated from this method did not take into account the free CO_2 saturations near the wellbore and the effect of the gas saturation.

Gas-oil fractional flow curve data were used in design calculations to determine the volume of oil that could be treated for a given volume of CO_2. The fractional flow curve (Fig. 2-2)was generated from unsteady state gas-oil relative permeability curve data. The critical gas saturation was estimated at 5% and the critical gas saturation behind the front was estimated to be 11% during the injection period. Data from water alternating gas injection in corefloods showed that the trapped gas saturation with CO_2 was only about 5%.

Diffusion Tests. The only test performed that was not a standard laboratory measurement was the diffusion measurements. The test aim was to determine the rate at which CO_2 would diffuse through the reservoir oil. Knowing the diffusion rate would aid in determining the optimum shut-in time and, thereby, let the wells be put on production as quickly as possible.

Reservoir oil samples were obtained by recombining separator oil and gas samples from the reservoirs. The oil and gas were recombined to give the bubble point and solution GOR found from earlier PVT data. The diffusion test apparatus consisted of a vertical stainless steel tube containing water, oil, and CO_2 (Fig. 3-2). The tube was initially filled with water, then the water was displaced with oil to achieve a desired height of oil column. The oil was then displaced with CO_2 to achieve the desire oil column heights. Tests were run with the heights of the oil columns at 12, 24, and 36 in. A constant pressure was maintained on the CO_2 at the various test levels. Tests were run at pressures of 1000 and 2000 psi. An ohmmeter was used to measure and record the resistivity of the water over time. The water would undergo a decrease in resistivity as the CO_2 diffused through the oil and began to ionize the water.

The resistivity measurements were plotted versus time to identify when the change in resistivity would occur. Samples of oil from the bottom of the oil column were taken at the end of the test and the CO_2 concentration was measured by gas chromatograph. Fick's diffusion equation was solved for the diffusion coefficient from

the test. The results showed a diffusion rate of approximately 0.0015 cm^2/sec at 2000 psi and 0.00033 cm^2/sec at 1000 psi. Consequently, the soak period at higher pressures can be considerably shorter than generally used in low-pressure reservoirs.

Design Calculations. Pressure buildup surveys obtained by acoustic well sounders were run on the five demonstration producers to give an estimate of permeability and reservoir pressure in the treated area. Initial efforts to inject below miscibility pressure design were intended to keep the treatments from moving oil away from the wellbore, but only limited volumes of CO_2 could be injected without exceeding the targeted bottomhole pressure. It was necessary to forgo that miscibility pressure restriction and just keep the pressure below fracture pressure.

Multi-phase effective permeability obtained from the pressure buildup survey data was used to calculate total permeability for each well. The injection period pressures and rates were used to estimate the effective permeability to CO_2. The resulting relative permeability to CO_2 of 0.2 corresponds to a 20% gas saturation on the 2-phase gas oil relative permeability curves. This value is higher than the 15% expected from the fractional flow curve. The difference could be due either to the wells having been hydraulically fractured, since the calculations for injection rate versus time assumed radial flow and an improved skin, or from injection above the critical pressure and temperature where the CO_2 is a super critical fluid.

The methodology used in forecasting the oil recovery from CO_2 is shown in Appendix A. The average saturation (Sg) behind the front from the fractional flow curve was used to calculate the effective radius that could be treated by the CO_2 volume injected. This radius was used in volumetric calculations to determine the volume of oil and water available for absorbing CO_2 volumes. The volume of CO_2 dissolved in water was calculated, giving the volume available for swelling oil. Once the new oil saturations were determined, the difference between swelled oil saturations and the residual oil saturation to waterflood was used to calculate the volume of recoverable oil. Figure 4-2 shows the calculated versus actual recoveries for each of the five wells treated with CO_2.

Field Results

Injection. The CO_2 treatments were pumped into five wells with different producing characteristics to give representative results for the area. Treatment sizes were varied to study the effect of CO_2 volume pumped on the oil recovery. The wells had pressure buildup tests run to determine reservoir properties and producing tests conducted for baseline production data. Bottomhole pressure gauges were run to obtain a history of the injection pressures for establishing an average gradient needed to estimate bottomhole pressure from wellhead pressure and temperature. The data showed that standard pressure enthalpy charts for CO_2 could be used to obtain a reasonable

estimate of bottomhole pressure when wellhead injection pressure was above the critical pressure.

CO_2 injection on the first well was attempted while keeping bottomhole pressure below the minimum miscibility pressure of 1200 psi. The target rate of 500 MCFD of CO_2 was obtained only for about 12 hours before the rate fell below 250 MCFD. When the rate fell, the attempt to inject below miscibility pressure was abandoned and the pressure was raised to meet the goal of injecting at 500 MCFD with a total of 5000 MCF of CO_2. Treatment sizes for other wells varied from 5000 to 15,000 MCF. Injection equipment consisted of a 200-ton trailer-mounted supply tank, a trailer-mounted skid with a diesel powered positive displacement pump, a gas liquid separator and turbine meter supplied by the CO_2 supplier. A by-pass from the pump discharge to the CO_2 supply tank allowed injection rates to be kept lower than the pump minimum rates. Two-inch steel injection lines connected the pump to the wellhead. An orifice meter in the injection line was installed to measure the volumes injected, but the vibrations and pulsation of the positive displacement pump made the data unusable.

Injection pressures and temperatures varied between the wells treated. Wellhead injection pressures varied from 600 psi, when trying to stay below miscibility pressure, to 3200 psi on the wells receiving higher CO_2 volumes. Wellhead temperatures ranged from 10-25°F during injection with bottomhole temperatures staying close to the normal reservoir temperature of 95°F. The length of the injection periods varied from 125 hours on the well in the higher permeability area receiving only 5000 MCF to 265 hours on the well receiving 10,000 MCF in a low permeability area.

Soak period. The time required for CO_2 to diffuse through the oil and change the oil's properties is referred to as the soak period. This time can be estimated based on diffusion rates before the CO_2 is pumped, or determined from field measurements during the shut-in period. Pretreatment estimates were made by using a viscous fingering method[4] and by estimating the distance between high concentrations of CO_2 due to geologic heterogeneity. Field determinations of shut-in time have been made from monitoring changes in wellhead pressure. With the cross flow of fluids present in wellbores in the area, this method was expected to be reliable. The viscous fingering method is more applicable in homogenous formations. Therefore, soak periods were estimated based on diffusion rate of CO_2 obtained from laboratory data and reservoir layering.

$$t_s = \frac{\lambda^2}{.86400D}$$

Where: t_s = shut-in time in days
D = Diffusion Coefficient (cm^2/sec)
λ^2 = Half the distance between high CO_2 concentrations (ft)

The effective diffusion coefficient was calculated by using the relationship between diffusion and electrical resistivity[5,6] as shown:

$$D_o = D \cdot F \cdot \phi$$

where F is the formation factor and ϕ is the porosity used in log analysis.

Using the effective diffusion coefficient of 0.04 and an average layer distance of 20 ft, the estimated shut-in time needed was calculated to be 12 days. This was rounded up to 14 days. The production results indicated layering controlled the amount of diffusion. Early flowback was mostly CO_2, then oil, water, and free and dissolved CO_2. Finally, oil, water, and CO_2 were produced at ratios that indicated all the CO_2 was in solution in the oil or water.

Production. The five wells treated with CO_2 were chosen to give an estimate of the response for the whole project area. The wells all had different producing rates prior to the stimulation. Water-oil ratios varied from 2 to 30 and the reservoir properties exhibit the variation seen across the project area. The treatment volumes of CO_2 ranged from 5 to 15 MMCF. Of the five wells treated, three showed measurable increases in oil production. The two that failed to show a measurable response were the wells that received only 5 MMCF of CO_2 which was only 30 to 50% of the pore volume injected in the better wells. The best results came from WWU 4843, which received the largest volume of CO_2 and had the best reservoir properties. Thirty-seven to 55% of the CO_2 was produced back either as free CO_2 or as solution gas. The remaining CO_2 was either never produced or was produced back at such low volumes it was not measurable.

Producing WORs following the treatment were reduced, but not to the extent predicted from the laboratory data. This is probably due to the presence of the water being produced from high permeability layers swept during waterflood that are at a higher water saturation. After being pressurized by CO_2 injection, these permeable layers would produce back water initially, while the lower permeability intervals with high oil saturation would be slower in producing back oil production. Based on the average gas saturation, the volume of CO_2 typically available to dissolve in oil resulted in a fluid composition containing 40 mole percent of CO_2. From laboratory swelling data, this gives an oil volume increase of about 20%.

Flowback was initially through a stack pack and into a frac tank. The stack pack was used for the early flowback when wellhead pressures were too high to produce into the production lines and separation equipment without taking large pressure drops. The stack pack heated the fluid flowing back so pressure drops associated with high gas volumes would not cause freezing and plugging of flowlines. Fuel for the stack pack was supplied from a propane tank hauled to location. Prior to flowback, the

flowlines were cleaned out to prevent paraffin buildups from pressure-drop related cooling. The frac tank was used to provide a direct measurement of the produced liquids for totaling the volumes produced. The stack pack had 3-phase separation and the metering provided rate measurements for the produced fluids. The frac tank volumes were used as a check on the metering from the stack pack.

After flowback, the wells were put on artificial lift using rod pumps except on the first well where plunger lift was attempted since gas locking problems were anticipated. The plunger lift was not any more successful than flowing the well in this regard. As a result, the rest of the wells were switched directly from flowing to rod pump operation. No mud or gas anchor was run on one of the wells and severe gas locking problems occurred with the CO_2 present. Other wells had mud anchors and used tubing back pressure to avoid the pumping problems to a certain degree. The wells started out producing with high fluid levels that would gradually decrease to pretreatment levels. When the incremental production was calculated, the base production was adjusted for the difference in producing bottomhole pressure by multiplying the base rate by the ratio of the difference between average reservoir pressure and the producing bottom hole pressures. For example, the producing pressure was 150 psi before the treatment and the well was producing 10 BOPD and after the treatment, the new producing bottomhole pressure was 700 psi. The new base rate with an average reservoir pressure of 2000 psi would be 7 BOPD as shown below.

$$10BOPDx\left(\frac{2000psi-700psi}{2000psi-150psi}\right)=7BOPD$$

This provided the incremental production response due to CO_2 injection. The actual production streams would be scheduled and the difference in economic results compared for a true picture of the economic benefits.

WWU 4851. WWU 4851 is located in the east central portion of the project area and was the first of the five wells treated with CO_2. The well's prior production was 20 BOPD and 50 BWPD. Ten MMCF was injected over 265 hours with a maximum bottomhole pressure of 3210 psig, which is slightly below the estimated parting pressure. After a 17-day soak period, the well was opened for flow and began producing gas for the first 3 days while maintaining a wellhead pressure of over 350 psig. After the first day, a plunger lift system was installed to aid in liquid recovery and used for 28 days. During this time, various controller settings were tried in an unsuccessful effort to get the plunger to surface. Finally, the well was killed with brine and a rod pump run. A 3-in mud anchor was run to 4867 ft, slightly below mid-perforation, and the well was produced with a wellhead pressure of about 50 psig. The well was pumped down in 10 days at rates of 35-40 BOPD and 60-70 BWPD.

Using the previously described method, incremental reserves were estimated at 1552 barrels of oil. An oil saturation of 58% was calculated from the water-oil relative permeability curves using a 70% watercut. A total of 4621 MCF was estimated to be produced back. This includes the initial free CO_2 and the CO_2 produced back with the oil and water. The actual reserves estimated from post treatment production are 1858 bbl based on a total oil volume of 18,000 bbl effected by CO_2. The resulting utilization ratio was 5.8 MCF/B of incremental oil. Under reservoir conditions, there was 0.17 reservoir barrels of CO_2 injected per barrel of reservoir oil recovered.

WWU 3205. This well is located in the northeastern part of the project area and was the second well treated with CO_2. Prior production was 4 BOPD with a 97% watercut. The target CO_2 volume for this well was 5000 MCF with an actual volume of 4135 MMCF injected at a maximum pressure of 2830 psig. Initially, injection pressure was kept to a minimum to stay below the miscibility pressure. However, injection at acceptable rates was not obtainable so the pressure was increased. Injection was followed by an 18-day soak period. The well was put on production and flowed for 24 days before the rod pumping equipment was installed. While flowing, the well produced only CO_2 and water. Once on pump, the well returned to the pretreatment oil rate and a decrease in watercut from 97 to 93%. Thirty-seven percent of the injected CO_2 was produced back, of which 30% was estimated as either free CO_2 or CO_2 dissolved in the water phase. This well was put on pump without a gas anchor and experienced gas locking problems. A mud anchor was run and oil production increased from about 2.5 to 4.5 BOPD. An estimated 885 bbl of incremental oil was predicted to be produced. From the field measurements taken, this well actually produced 47 bbl of oil less than the volume expected without a CO_2 treatment. It is possible that any production increase could have been missed in the measurement process in view of the small volume involved and in the delay in re-establishing oil production.

WWU 4835. The third well treated with CO_2 was in the northwestern portion of the project area. Prior production was 15 BOPD at a 94% watercut. A total of 5121 MCF of CO_2 was injected over 187 hours followed by a 16-day soak period. The well was returned to production and flowed for 9 days before being put back on a rod pump. During the flow period, oil was recorded only on the third day. Once the well was put on pump, the oil rate ranged from 10 - 20 BOPD at the same 94% watercut as before the treatment. Incremental oil production was 678 bbl versus the calculated 865 bbl. The well produced back 48% of the injected CO_2 during the production period of which an estimated 8% was free CO_2, 19% from the water phase and 73% from the oil phase.

WWU 4847. This well provided the same lack of results as the other wells treated with only 5000 MCF of CO_2. It is located in the southwest portion of the project area, which generally has better reservoir properties. Prior to injection, the well was

producing 9 BOPD and 75 BWPD for an 89% water cut. The well was open after a 21-day soak period and flowed for 11 days with 27 BOPD reported the first day and no oil for the next 10 days until the well was put on pump. No mud or gas anchor was run on the well, but it appeared to pump normally. The WOR and production rates for this well showed no significant change after the CO_2 injection treatment. When the well initially started pumping, fluid level was at 1110 ft and was lowered to about 4000 ft over a 3-week period. The calculated incremental recovery was 642 BO with an actual incremental recovery of 71 bbl.

WWU 4843. This well is located in the southwest portion of the project area also and has some of the best reservoir properties in the project area. Prior production was 12 BOPD and 399 BWPD. A total of 15,471 MCF of CO_2 was injected into this well over 140 hours with a maximum bottomhole pressure of 3234 psig. The average rate of 3229 MCFD was far greater than the injection rates in other wells, possibly creating viscous fingering that kept the oil from being displaced from around the wellbore. The well was left shut-in for a 24-day soak period. The well flowed for 8-days before starting to produce oil. After 17 days, the well was put on a rod pump and produced 17-20 BOPD and 250 BOPW. The calculated incremental oil was 2382 bbl. The actual incremental production from the treatment was 2892 bbl of oil with 51% of the injected CO_2 produced back. The resulting utilization ratio was 5.3 MCF per barrel of oil.

Summary of Results

Five wells were tested to determine if CO_2 stimulation of producers could accelerate the payout of CO_2 flooding in a low permeability reservoir. The wells produce 33°API oil from the West Welch Unit, a waterflooded San Andres formation at a depth of 4800-5000 ft in Dawson Co., Tex. The wells chosen had a wide variation in producing characteristics to allow a more accurate evaluation of the expected results during an actual CO_2 flood. Water-oil ratios varied from 2 to 30 with a range of average porosities from 6-15% and average permeabilities ranging from 0.5 to 3 md. Data gathered included pressure testing, production logging, and compositional analysis of the produced fluids.

Operating experiences show what will be required to successfully stimulate the producing wells during a full CO_2 flood. Attempts to keep injection pressures below miscibility pressure and achieve significant injection rates were unsuccessful. Incremental recovery largely depends on the volume of CO_2 injected per porosity foot and the residual oil saturation. The well with the highest injection rates and pressures gave the best recovery per porosity foot. It also had the best reservoir quality. Incremental recovery estimates, using gas fractional flow theory to determine the reservoir volume treated, give reasonable agreement to actual incremental recoveries.

Conclusions

CO_2 stimulation treatments can provide economic increases in oil rates if pipeline CO_2 is available at a reasonable price. The production increase can be forecast with reasonable accuracy. If a number of treatments were conducted successfully at the beginning of a miscible CO_2 flood, the project payout could be shortened.

The single most important factor governing the incremental recovery from a well is the volume of CO_2 pumped per net foot of pay. The larger volume treatments also flowback initially, eliminating pumping problems associated with gas production. There are no significant increases in operating cost associated with the CO_2 stimulation treatments.

References

1. Thomas, G.A. and Monger, T.G., *The Feasibility of Cyclic CO_2 Injection for Light Oil Recovery*, Paper SPE/DOE 20208, presented at the SPE/DOE Seventh Symposium on enhanced Oil Recovery, Tulsa, OK, April 22-25, 1990.

2. Haskin, J.K., and Alston, R.B., *An Evaluation of CO_2 Huff 'n' Puff Field Tests in Texas*, paper SPE 15502 presented at the SPE 61st Annual Technical Conference and Exhibition, New Orleans, LA., Oct 5-8, 1986.

3. Hara, S.K. and Christman, P.G., *Investigation of a Cyclic Countercurrent Light-oil/CO_2 Immiscible Process*, paper SPE/DOE 20207, presented at the SPE/DOE Seventh Symposium on Enhanced Oil Recovery, Tulsa, OK, April 22-25, 1990.

4. Gardner, J.W. and Ympa, J.G.J., *An Investigation of Phase Behavior - Macroscopic Bypassing Interaction in CO_2 Flooding*, paper SPE 10686 presented at the SPE Symposium on Enhanced Oil Recovery, Tulsa, OK April 4-7, 1982.

5. Brigham, W.E., Reed,P.W. and Dew,J.N., *Experiments on Mixing during Miscible Displacement in Porous Media,* SPE Journal March 1961, Pg 1-8, Transactions AIME, Pg. 222.

6. Van der Poel, C. *Effect of Lateral Diffusivity on Miscible Displacements in Horizontal Reservoirs*, SPE Journal, December 1962, Pg. 317-26, Transactions AIME, Pg. 222.

36

36

37

37

38

38

Chapter 3. - GEOLOGIC AND PETROPHYSICAL INVESTIGATIONS

Introduction

The objective of the geologic and petrophysical investigation is to integrate and interpret the available reservoir data into a detailed reservoir model capable of forecasting the performance of the reservoir under CO_2 miscible flood and infill drilling conditions. The detailed description and modeling would allow for optimizing the design of the CO_2 flood to achieve economic tertiary recovery in a low permeability shallow shelf carbonate reservoir. The characterization is two-fold in nature: the initial geologic model uses only the wellbore data to describe the reservoir and the second model incorporates the wellbore data plus the geophysical data. By comparing the two models' performance forecast, the value of the geophysical data can be evaluated based on the model improvement. The actual response of the flood will ultimately determine which (if either) of the two models most accurately predicted the performance of the reservoir. Continuous monitoring will be required for validation.

The West Welch Unit produces from Permian-age dolomites of the San Andres Formation. The reservoir interval is encountered at an average depth of 4800 ft, approximately 400 ft below the top of the formation (Fig. 1-3). The West Welch Unit covers 12,000 surface acres. The general structure of the field is a gently-dipping monocline to the S-SE (Fig. 2-3). The present structure is a result of post-depositional movement of deeper fault blocks. The average gross thickness of the producing interval is 75 ft with an average net pay reservoir thickness of 67 ft. The porosity in the reservoir interval ranges from 0 to 22 %, with the average value of 9.5% for the entire unit and 12% for the project area. Permeability ranges from near zero to 87 md, with the geometric average for the unit of 1 md and an average for the project area of 2 md. The reservoir is highly stratified as a result of depositional processes, with Dykstra-Parsons values in the 0.75 range.

The producing interval is divided into two hydraulically separated intervals, the Main Pay and the Lower Pay. The oil/water contact (depth of 100% water production) for the Main Pay is at a subsea depth of 1890 ft. The same contact for the Lower Pay is subsea 1860 ft. These values vary slightly across the field due to the capillarity of the reservoir rock. The productive limits of the field are controlled by a combination of structure and permeability variations, with downdip locations producing excess water, and the loss of permeability in the Main Pay (generally to the north) creating uneconomic wells. San Andres production to the north of the West Welch Unit is from the Lower Pay which has moved into a more favorable structural position.

Data Base

Utilizing an OXY USA Inc. proprietary program called Stacked Log Curves for the Personal Computer (SCPC), a digital data base was assembled for the project area.

This data base would eventually incorporate 3-D seismic interpretation data, open hole and cased hole log data, production logging, production history, completion history, core analysis, and core description. The data base was compiled from multiple sources both commercially available and OXY USA Inc. files. Based on this framework of data, the reservoir description began to take shape. The validation of the basic data required a detailed effort of cross checking. Minor errors in the data can lead to significant interpretation errors of the reservoir. A computer simulation model requires a fairly standard set of data. These include pore volume, permeability distribution, thicknesses (gross and net), structure, fluid saturations, fluid properties, compressibility and continuity. The predictive capability of any model depends on the accuracy of input data and the validity of assumptions about the reservoir. The focus was to produce a deterministic model of the reservoir, which could be utilized in identifying additional optimal locations in the interwell area. A geostatistical approach to a stochastic model may yield accurate history matches and performance prediction on an area basis, but the predictive capabilities as to actual location of bypassed or trapped oil is unreliable.

Geological History

The first step was the determination of the depositional environments and diagenetic history of the reservoir. These were established from detailed interpretations of core samples within and surrounding the project area. The cyclic pattern of alternating depositional environments has been documented throughout the Permian basin. The depositional cycles were put into a sequence stratigraphic framework in order to insure that the correlation of individual reservoir layers remained consistent from well to well. The Bureau of Economic Geology was consulted to bring the Welch San Andres sequences into an established hierarchy. These deposits were emplaced on a shallow shelf ramp near the paleoshoreline (Fig. 3-3). Structural relief was very low, probably less than 3 ft of slope per mile, hence minor fluctuations in the sea level moved the shoreline several miles at a time. These depositional environments produced broad bands of sediments with variable textural characteristics depending upon the sub-environments associated with each major environment (Fig. 4-3). Tidal flat deposits are produced along the strand line as well as on islands within the lagoon. Higher energy tidal channels are seen dissecting the low energy tidal flats producing coarse grained sediments encased in lime muds. Small mounds of grainier rocks can also appear within the lagoonal settings.

Following the identification of the depositional environment and connection to the sequence stratigraphy, the post-depositional history had to be unraveled. This history details the diagenetic events that changed the physical properties of the reservoir rock. From the time of deposition, the sediments have been altered extensively in places to the point where the original fabric of the sediment is no longer recognizable. In some formations, particularly sandstones, the diageneses can be directly related to the depositional facies, making the prediction of reservoir quality much more robust. In carbonate rocks, especially in the case of dolomites, the

prediction of the alteration is less precise because the diagenitic fluids can cross depositional boundaries. Carbonate rocks are produced from the remains of living organisms making the distribution of the sediment dependent on processes quite different form those of sandstones. The result is a less uniform consistency to the composition of the carbonate. These processes are often termed random, because the controlling factors are often not known.

Petrophysical Analysis

In keeping with industry practices, prior studies of the reservoir had attempted to equate the total porosity of the rock to the permeability by a semilog cross plot (Fig. 5-3) although there is no theoretical basis to the relationship. The scatter in this plot produced a standard error of estimate for the regression line of several orders of magnitude in a permeability value for a single porosity value. This was compounded by the method used to analyze the cores prior to the project. The permeability was calculated based on water injection rates into partially cleaned cores. Investigations into the procedure determined that low permeability rock yielded values too high because of imbibition while the high permeability rock yielded values too low because of coked oil in the pore throats. Even after making corrections for theses factors, the porosity-to-permeability semilog plot still had a data band of two orders of magnitude (Fig. 6-3). Because of the critical nature of the permeability in the reservoir modeling process, a more accurate method of detailed permeability prediction had to be devised before modeling could proceed. This prediction method needed to be well log based as a simple matter of economics and data available. All wells can not be cored in cost effective development.

Because consistency of data is a serious problem in most San Andres reservoirs of this vintage, two observation wells (WWU 4852 and WWU 7916) were drilled, cored, and extensively logged over the reservoir (Fig. 7-3). These wells are used as the control points for the testing and calibration of the calculation models. The locations were selected to provide data in areas of differing reservoir properties within the project site to document as much of the reservoir variability as possible. Careful attention to the drilling fluids was maintained to prevent alteration of the cores prior to analysis. The cores samples were analyzed by both routine and special core analysis methods. The cores were described visually by thin section and by scanning electron microscopy[1]. Descriptions by both OXY USA Inc. personnel and the consulting firm of David K. Davies, and Associates (DKD) were used in the construction of the reservoir model. The multiple investigators allowed for independent description processes to be applied to the formation. This methodology aids in the determination of which geologic factors are most significant to the descriptive process. The independently-derived properties were compared to log response to aid in the extrapolation of facies to other wells in the project area.

Although the mineralogy of the reservoir is simple (Table 1-3), the structure of the pores is highly complex. DKD developed four rock types for the section while OXY USA initially developed a scheme of eight basic rock types. Comparison of rock types to the normally determined features of depositional fabric and depositional environment found little in the way of correlation. As described earlier, this is a function of the diagenetic process not being confined to the depositional fabrics. As can be seen in the Fig. 8-3, each of the rock types can occur within any depositional environment or fabric. Basing reservoir parameters on inferred depositional environments can yield erroneous data. This problem was also compounded when it became apparent even the facies could not be reliably determined from the log data alone. The explanation for the discrepancy came as a result of the special core analysis.

Petrophysics-Seismic Integration

Integration of the 3-D seismic volume into the petrophysical data base required specialized handling of the data. Comparison of the log data in the time domain to the 3-D seismic data provided the means of identifying which features could be resolved by the seismic. It was found that the M1, M3, and M5 tops could be identified throughout the seismic volumes, but the final reservoir layers were on too fine a scale to be resolved seismically.

To enable the calculation of seismic attributes, petrophysical values had to be calculated from the log data. Values for average porosity, average permeability, average water saturation, structure, and thickness were derived from the log data in the wellbores and compared to the seismic. The first attempt at determining any meaningful correlation of the seismic to the log data was unsuccessful to the extent that even the structure was not in the range of significant correlation. A review of the log analysis procedures indicated the problem. The first set of average log values was generated using generally accepted net pay criteria. In contrast, both the 'pay' and 'non-pay' rocks are averaged into the seismic response and cannot be differentiated. The lack of correlation to the structure was a different problem relating to the use of reference datums down loaded from a commercial data service. These datums were found to be 6 to 12 ft in error on many wells. Correcting the datums greatly improved the correlation to the seismic. The only reservoir property that did not improve after correction was average water saturation, probably due to the wide range of completion dates for the wells in an ongoing water flood.

Permeability Determination

Analysis of the relative permeability experiments on seven samples from the observation wells indicated the reservoir is of mixed wettability (Fig. 9-3). This implies that the distribution of the oil in the pore system changes through the reservoir. This change in the distribution of fluids affected the resistivity log response causing

inaccurate prediction of reservoir facies. This factor could not be recognized from visual description of the rock itself. To create a reasonable reservoir description, an accurate permeability profile had to be developed for the uncored wells. This was accomplished by a nonstandard log interpretation approach[2].

The Carman Kozeny equation is a descriptive model to predict the permeability of a porous medium assuming certain factors can be approximated[3,4].

$$k = \frac{\phi^3}{K_o \tau (1-\phi)^2}$$

Where:

k	=	total permeability
ϕ	=	porosity
K_o	=	Kozeny factor
τ	=	tortuosity

These factors relate to the length of the actual flow path, the total porosity, and the internal surface area of the pore system. These values must be consistent with the sample volume for which the permeability is being computed. Through a series of trial and error comparisons, certain log curves were found to approximate each of the factors in the CK equation.

In an attempt to employ newly developing technology, a neural net program was employed in an attempt to estimate permeability from log response. This technology is receiving greater acceptance as a valid way of determining nonlinear relationships. The comparison of the depth-corrected core permeability to the open hole log suite (neutron porosity, deep resistivity, shallow resistivity, bulk density, photoelectric, acoustic, and total gamma ray) showed the highest correlation to the gamma ray curve. This was surprising because local experience has contended that the gamma ray is unreliable in San Andres carbonate descriptions. The neural network analysis could approximate the permeability in a logged well but for applications by other operators, a more general model was required to formulate the permeability. Monicard[4] used a form of the CK equation to determine the specific surface area of the pore system that incorporated the routine porosity and permeabilitymeasurements.

$$k = \frac{\phi^3}{5\ Sg^2\ (1-\phi)^2}$$

Where:

S_g = Surface area of grains

By using this relationship, a continuous curve of the internal surface area was generated in the cored wells. This curve compared favorably to the total gamma ray log response (Fig. 10-3). The discrepancies between the two curves arise from the use of a single tortuosity value as input into Monicard's equation for the estimation of surface area. Another factor is that the gamma ray is a statistical curve and will read the response of differing volumes of rock at any one sample point. The computed specific surface area was determined for single station measurements (core samples) so each computed value is independent of the preceding or following samples. It should be noted that all log curves represent running averages of the response. The gamma ray and the specific surface area values differed by a factor of 10. The correlation was improved by normalizing the gamma ray to the reservoir interval response of maximum and minimum values using the following equation.

$$GR_{NORM} = \frac{GR - GR_{MIN}}{GR_{MAX} - GR_{MIN}}$$

Where:

GR_{NORM}	=	Normalized gamma ray response
GR	=	Total gamma ray response
GR_{MIN}	=	Minimum gamma ray response
GR_{MAX}	=	Maximum gamma ray response

The gamma ray minimum and maximum values are determined in each wellbore. The actual values are rounded down for the minimum values and rounded up for the maximum values to prevent the computation of zero values since the term is used as a multiplier of the denominator in the CK equation. These values were taken from the reservoir interval only, so other geologic processes would not be incorporated in the final curve response. The gamma ray curve could now be used to substitute for the Kozeny factor (K_o) in the CK equation.

The tortuosity of the system is much more difficult to determine, either from log response or by laboratory measurements. In the process of water saturation calculation, a factor similar to the tortuosity called the Archie 'm' factor has been

$$m = \frac{2\ Log(\phi_{Acoustic})}{Log(\phi_{Total})}$$

The assumption is that the acoustic porosity will determine the interconnected porosity (interparticle or intercrystalline) while the neutron/density describes the total pore space in the rock sample. Hence, the ratio of these independently derived values provides an approximation of the flow path or tortuosity in the rock.

Resistivity logs are approximately three times more abundant than acoustic logs in the project area. A resistivity-computed porosity was substituted for the acoustic porosity in the Nugent equation using the equation developed for the Gulf Coast area. Because of varying water resistivity due to waterflooding, the pad resistivity device (Rxo) was used for the calculation.

$$\phi_R = \sqrt[m]{\frac{Rmf}{Rxo}}$$

Where:

m = Archie cementation factor
R_{mf} = Temperature corrected mud filtrate resistivity (OHM)
R_{xo} = Flushed zone resistivity device reading (OHMM)

The resulting tortuosity (Nugent R) curve is inversely related to the acoustic-generated curve (i.g. higher numbers mean better permeability). This is consistent with the physics of the process in the wellbore during drilling and the basis of the resistivity-derived porosity. The resistivity-derived porosity indicates the length of the path that generated the resistivity measurement. Low porosity would indicate a short path for the current flow. The relationship was identified when the calculated curve was plotted alongside the logarithm of permeability. The two curves displayed almost a peak-for-peak match (Fig. 11-3). By changing the scale of the Nugent R curve, a reliable match for most of the reservoir interval could be calculated. There were significant intervals where the computed and laboratory permeabilities did not agree, but for the most part the computed permeabilities represented the changes in the permeability profile. From this relationship, a reasonable determination of the tortuosity (τ) could be generated from the log data.

The utilization of the electrical measurements as an indicator of the tortuosity is not new. Salem's[7] paper contains a summary of the efforts of investigators in the 1950's to determine tortuosity from electrical measurements. They attempted to relate the formation resistivity factor to the tortuosity. The formation resistivity factor is the ratio of the resistivity of a rock with 100% water saturation to the resistivity of the saturating water. Bore hole electrical measurements during this time were considerably more crude than those of today. As a result, the application of their laboratory work could not be applied effectively to the field and has not been actively pursued until recently.

The third factor required for the CK equation was the accurate determination of the porosity. Even though the lithological composition of the reservoir is fairly simple, variations in mineral content can adversely affect the porosity determination unless accounted for by calculation of mineral percentages. In this reservoir, a lithology-corrected density porosity was calculated using a three-curve model of the neutron, density, and either a photoelectric or acoustic curve. The computation was performed using commercially available log analysis software (Petcom®) for a personal computer. X-ray diffraction analysis of core samples from the reservoir showed the bulk of the rock to be dolomite and anhydrite in varying proportions. To a lesser degree silica (in the form of chert and fine quartz silt) and clay minerals (mostly illite and koalinite) were present. The clays present were found to be contained within the matrix and not within the pore system so their effects on permeability are minimal. After lithology correction, the calculated porosity was comparable to the core measured porosity (Fig. 12-3). Again the vertical resolution of the logs compared to the core measurements accounts for the few misties.

It was now possible to substitute terms based on the response of commonly available open hole logs to obtain a modified Carman-Kozeny Equation:

$$k = \frac{100\ \phi^3}{(GR_{NORM})^2 (NugentR)(1-\phi)^2}$$

where terms are as previously defined. The results from this approach compared favorably to whole core permeability over much of the pay interval.

By using the log measurements from the tools with the highest vertical resolution, a better match of the permeability profile was generated. A limiting factor that should be remembered is that these pad devises are on two separate pads in the logging string. It is possible that the portion of the wellbore where these measurements are taken may not coincide at all depths. Because of the regional

stress-strain pattern, a phenomenon called wellbore breakout occurs when drilling through the San Andres that tends to create an elliptical hole. In elliptical holes, the pad devises will preferentially follow along the long axis of the ellipse and track each other through the section. In areas of less tectonic stress, this scenario may not develop; however, new tools have been developed with both of these sensors on the same pad. Use of this type of tool would insure measurement of the same portion of the wellbore.

To this point, three methods have been described to determine the permeability from log measurements. Each of the methods is unique in that it is able to characterize certain portions of the reservoir more accurately than the other two. An integration of the three methods would provide the optimum results, but some means had to be developed to distinguish which interval responded most accurately to which method. The first distinction was the separation of water-wet from intermediate oil-wet rocks. Cross plot routines indicated that when the reservoir had greater than 4% porosity and a resistivity greater than 55 ohms, the rocks were intermediately oil-wet (Fig. 13-3). The increase in resistivity is caused by oil being distributed along the walls rather than the center of the pores. The modified CK equation characterized the oil-wet reservoir rock the best. The Nugent R curve scaled to the logarithm of permeability could characterize most of the remaining section. The intervals which were not reasonably characterized by these two approaches had a normalized gamma ray value less than 0.25. This rock was typically very similar to clastic-derived rocks and a porosity vs. permeability transform could give a satisfactory response. By following a logic flow chart (Fig. 14-3) permeability curves were computed for all wells with sufficient log data. Comparison of the final computed permeability showed close agreement to the whole core permeability and is well within the difference between the whole core measurements and the plug measurements (Fig. 15-3).

Geologic Model

The generation of the permeability profiles was not the final step in the characterization process because the reservoir must be subdivided into significant members to model the fluid flow. Although this methodology can calculate a permeability profile of the reservoir independent of the geologic description, it does not replace the need for the detailed description to create a geologic model for the reservoir simulator. The first approach was to subdivide the reservoir into depositional environmental deposits; however, as described earlier, variations within a depositional unit made this an unsatisfactory subdivision. From the comparison of the permeability profiles and the gamma ray logs, certain gamma ray spikes coincided with thin low permeability intervals. These boundaries could be correlated from well to well through the entire project area (Fig. 16-3). These became the basic layering of the reservoir model.

These nine layers did not necessarily have uniform properties through the area, but did exhibit bounded flow character. Comparison of the layering-to-injection profiles showed a similarity of flow characteristics to the proposed layering (Fig. 17-3). The typical method for layering is to group intervals with similar flow characteristics into a flow unit. In this reservoir, the position of these no flow boundaries has a strong affect on the flow characteristics. The formation of the nine layers appear to better characterize the performance of the reservoir. The permeability profiles were used to compute average properties by layer.

Much of the reservoir heterogeneities can be quantified by the lateral and vertical changes in each layer. Each layer is a continuous rock unit across the model area. The discontinuities are accounted for by rapid changes in the reservoir properties of porosity and permeability. The key factor is the actual interwell location of the discontinuities. Required reservoir parameters were computed on a layer-by-layer basis for the well locations and contoured. The gridded values were incorporated into the geologic model for use in the simulator.

In the first phase of reservoir description, a linear approximation has been used to distribute the wellbore data. The second phase will incorporate the geophysics to better determine the interwell properties and distribution.

Summary of Results

A geologic model for the demonstration area has been constructed incorporating available log and core data. After examination of the cores and thin sections the reservoir interval was divided into nine separate layers for the modeling. Each layer is continuous across the model but the reservoir properties vary considerably. The separation of the layers is based on the cyclic nature of the depositional process, where thin low permeability layers are formed during flooding stages. These were identifiable on the gamma ray response. The formation of these boundaries is consistent with the sequence stratigraphy of the basin.

Reservoir properties were determined for each of the layers. The properties of porosity and permeability were computed from a combination of laboratory core analysis and petrophysical analysis of wellbore logs. When multiple sources of data were available, the data with the highest confidence level were used. Water saturations for the model were determined from capillary pressure functions because log saturation data were not available prior to the water flood.

The layering and computed properties were entered into the geologic workstation (SCPC) to compute the values for the interwell area. Each wellbore was used as an end point and straight linear interpolation used to compute the interwell values. Wells outside the project area were also included to reduce the edge effects often seen in computer mapping. The computed values were examined to verify the

reasonableness of the extrapolated values. Obvious errors were removed and the data regridded. The final grids were exported to the reservoir simulator.

The second geologic model is currently under construction which will incorporate both the wellbore data and the geophysical data. The geophysical data will be proportioned according to the wellbore data, but honoring the total geophysical input.

Conclusions

The deceptively simple mineralogy of the reservoir masks the complexity of the flow system. Diagenetic processes which acted on the reservoir produced highly variable reservoir properties in a continuous rock layer. This variability has an adverse effect on the sweep efficiency of any flood mechanism. Based on the wellbore data, a reasonable approximation of the reservoir has been constructed for simulation purposes. The petrophysical analysis and permeability transforms provided reliable data for the determination of reservoir properties within the wellbore area. The permeability transform also provided a significant increase in the available data at a substantially lower cost over the acquisition of core data. The interwell areas have not been fully addressed by the first model due to the lack of data. The comparison of the first model (without geophysics) to the second model (with geophysics) should provide information as to the value of the additional information. As the CO_2 flood progresses, comparisons to both model runs will validate the accuracy of the predictions.

References

1. Vessel, R. K., and Davies, D. K. (1995) *Reservoir Characterization San Andres Dolostones West Welch Unit Dawson County, Texas; Unpublished Report to OXY USA Inc.*, David K. Davies & Associates, Inc., Kingwood, Texas, 245p.

2. Hinterlong, G.D., and Taylor, A.R., 1996(in Press) *Characterization of Rock Types With Mixed Wettability Using Log and Core Data* - DOE Project Welch Field, Dawson County, Texas. SPE 35160, Permian Basin Oil & Gas Recovery Conference, Midland TX, 27-29 March 1996.

3. Carman, P.C., 1937, *Fluid Flow Through Granular Beds*, Trans. Inst. Chem. Eng., v. 15, p. 154-155.

4. Kozeny, J., 1927, *On Capillary Movement of Water in Soil*, Wein. Akad. Wiss. Sitz. Berichte (IIA), v. 136, p. 271 - 306.

5. Monicard, R.P., 1980, *Properties of Reservoir Rocks: Core Analysis.*, Gulf Publishing Co., Houston, TX, 168p

6. Nugent, W.H.,1984, *Letters to the Editor*: The Log Analyst, v.25, no. 2, p.2-3

7. Salem, Hilmi S., 1993, *Derivation of the Cementation Factor (Archie's Exponent) and the Kozeny-Carman Constant from well log data, and their Dependence on Lithology and other Physical Parameters*, SPE Paper 26309, Society of Petroleum Engineers, 23 p. 6 Fig.

Table 1-3

Mineral	Average Percent of Reservoir *
Dolomite	77%
Anhydrite	17%
Quartz	4%
Gypsum	<1%
Calcite	<1%
Clay Minerals	<1%

*Tabulated from 74 X-ray Diffraction analyses.

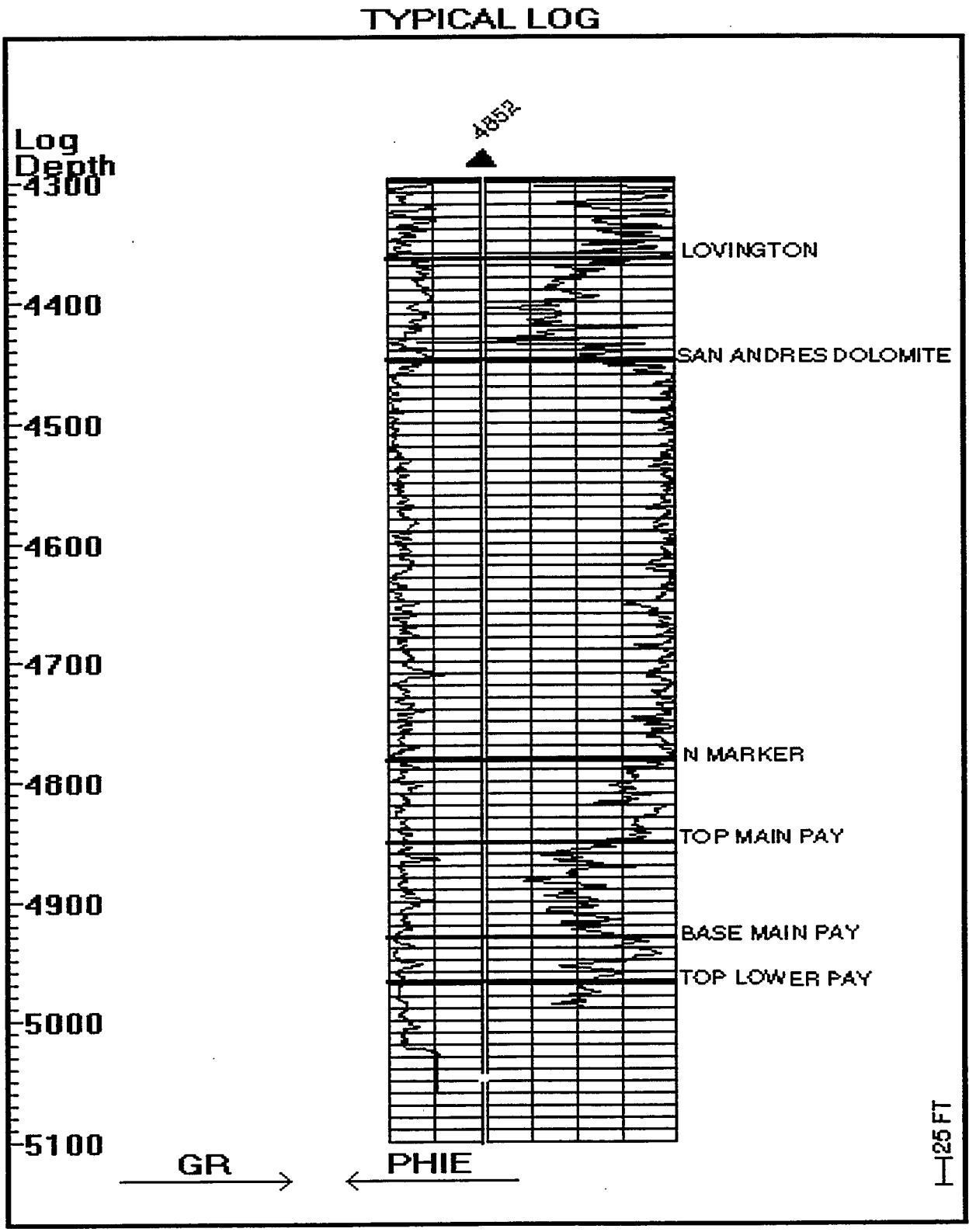
TYPICAL LOG
Log Depth
4300
4400
4500
4600
4700
4800
4900
5000
5100
4852
LOVINGTON
SAN ANDRES DOLOMITE
N MARKER
TOP MAIN PAY
BASE MAIN PAY
TOP LOWER PAY
GR
PHIE
25 FT

Figure 1-3

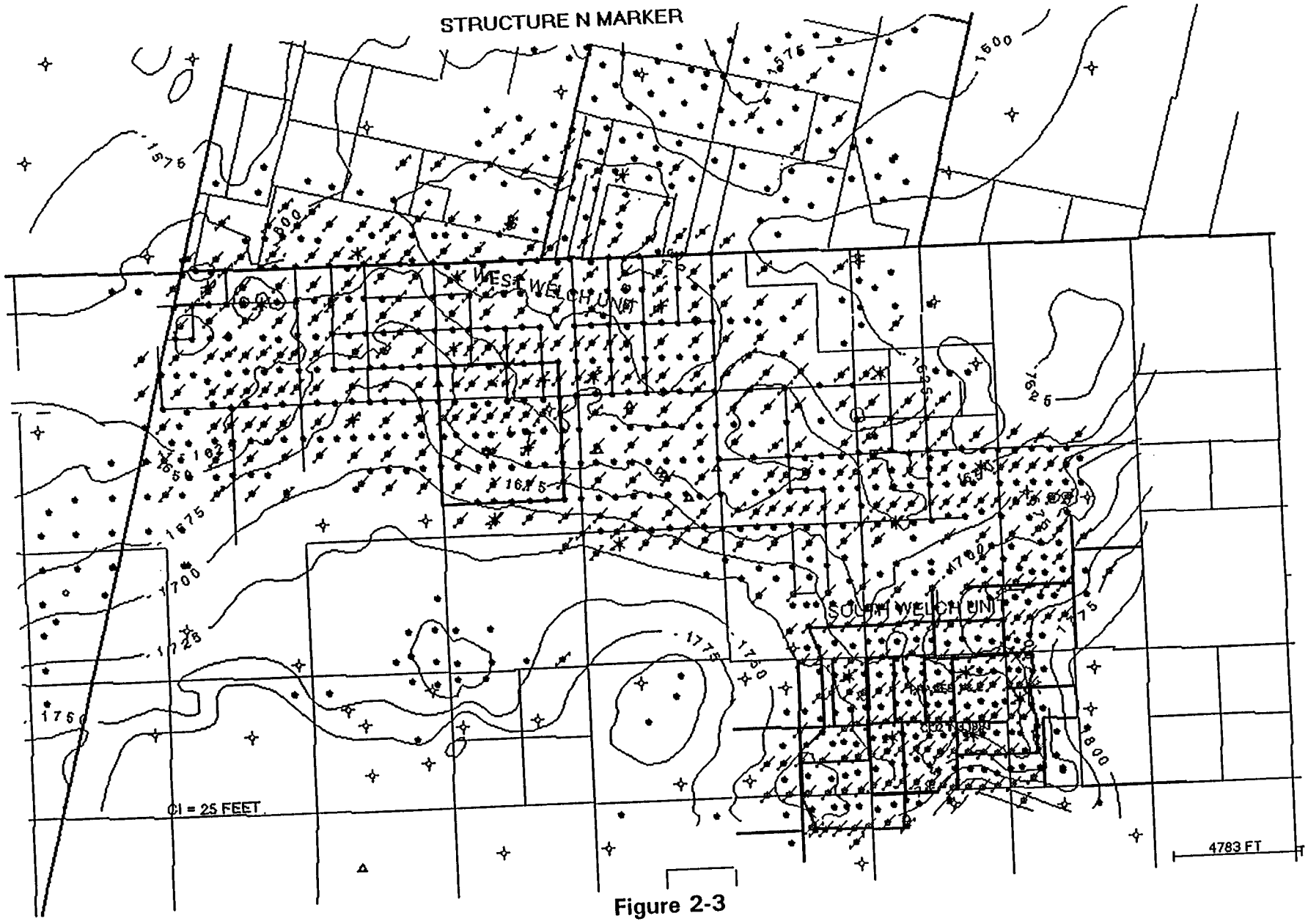
STRUCTURE N MARKER
WEST WELCH UNIT
SOUTH WELCH UNIT
CI = 25 FEET
4783 FT
1575
1600
1625
1650
1675
1700
1725
1750
1775
1800

Figure 2-3

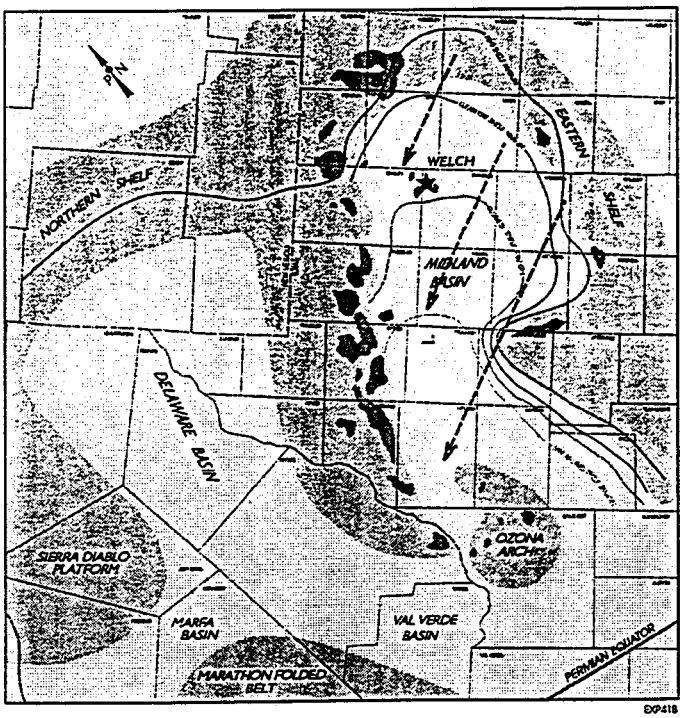

Grayburg-San Andres Oil Fields with Cumulative Production Greater than 10 MMB

Shelf/Platform/Arch

Basin

100 Miles

100 Km

Adapted from Longabre 1990

Permian Paleogeography of the Permian Basin

PERMIAN

PREVAILING WINDS

Figure 3-3

WELCH DEPOSITIONAL MODEL

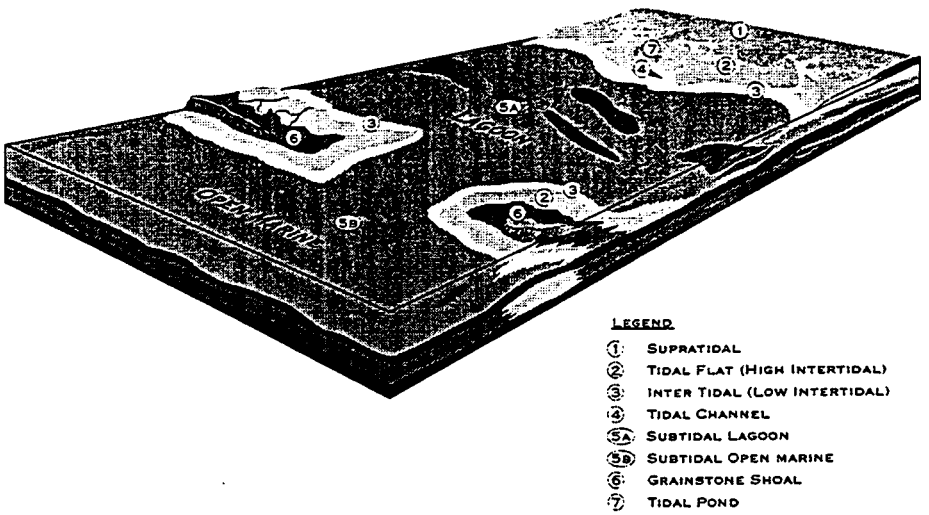

11/96 GN/JRR

Figure 4-3

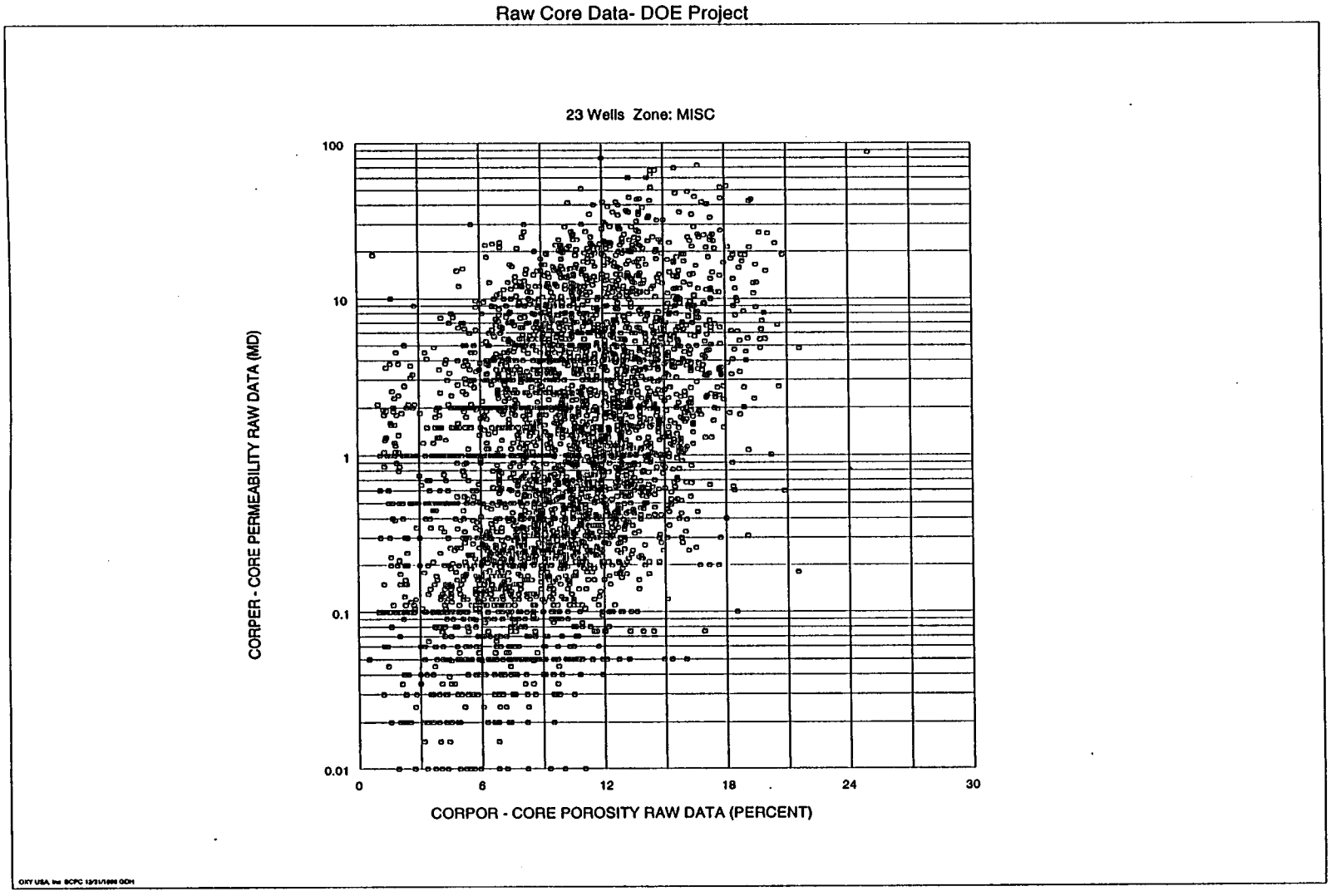
Raw Core Data- DOE Project
23 Wells Zone: MISC
100
10
1
0.1
0.01
0
6
12
18
24
30
CORPER - CORE PERMEABILITY RAW DATA (MD)
CORPOR - CORE POROSITY RAW DATA (PERCENT)

Figure 5-3

Corrected Core Data- DOE Project

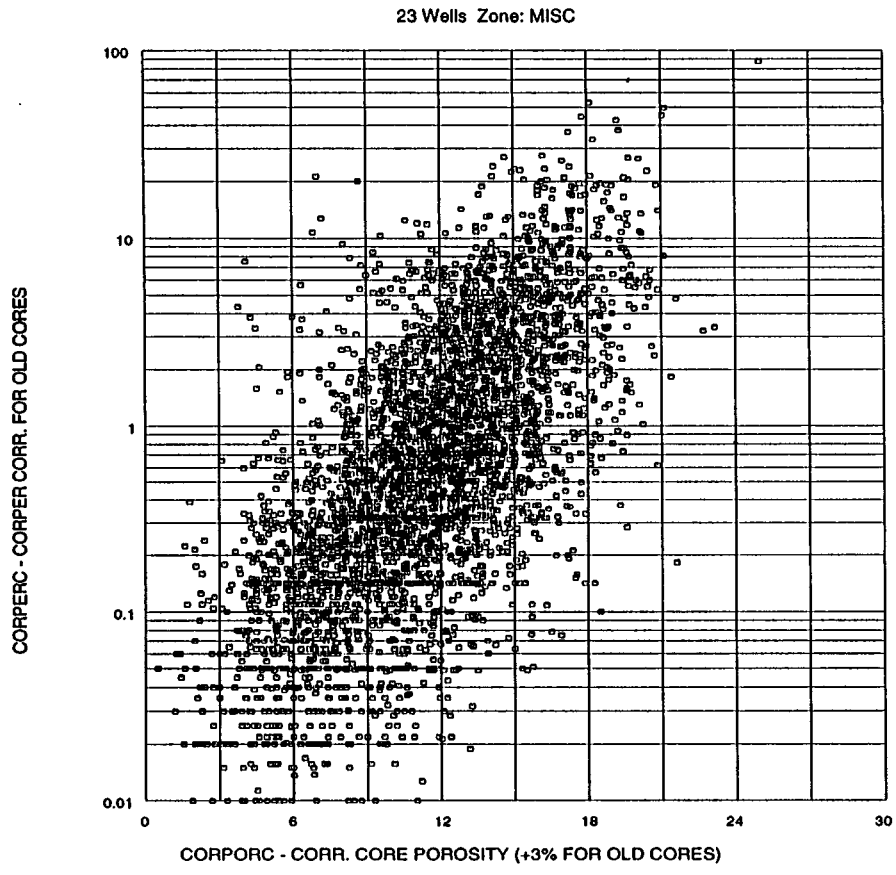

Figure 6-3

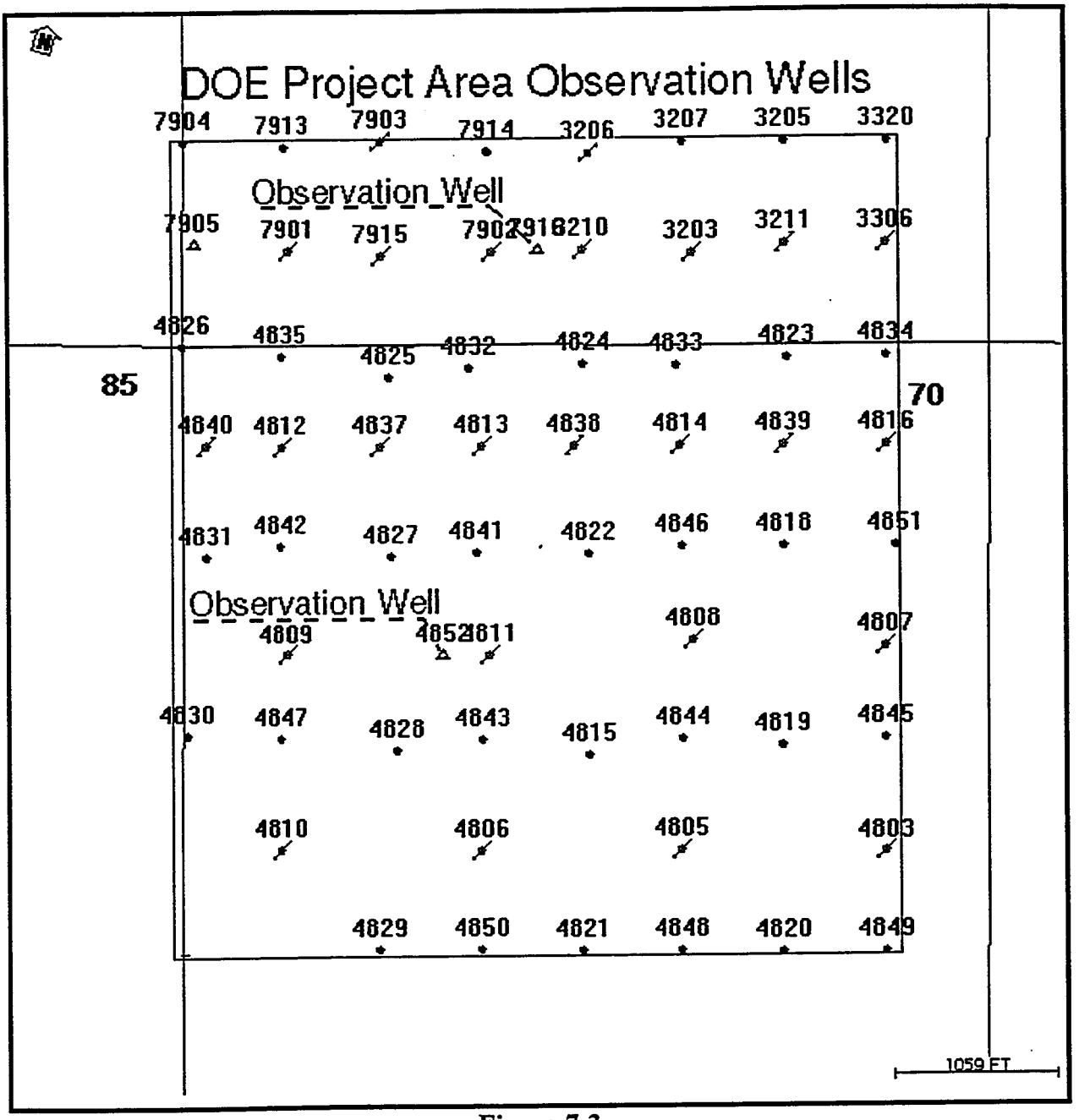
DOE Project Area Observation Wells
7904
7913
7903
7914
3206
3207
3205
3320
Observation Well
7905
7901
7915
7902
7916
3210
3203
3211
3306
4826
4835
4825
4832
4824
4833
4823
4834
85
70
4840
4812
4837
4813
4838
4814
4839
4816
4831
4842
4827
4841
4822
4846
4818
4851
Observation Well
4809
4852
4811
4808
4807
4830
4847
4828
4843
4815
4844
4819
4845
4810
4806
4805
4803
4829
4850
4821
4848
4820
4849
1059 FT

Figure 7-3

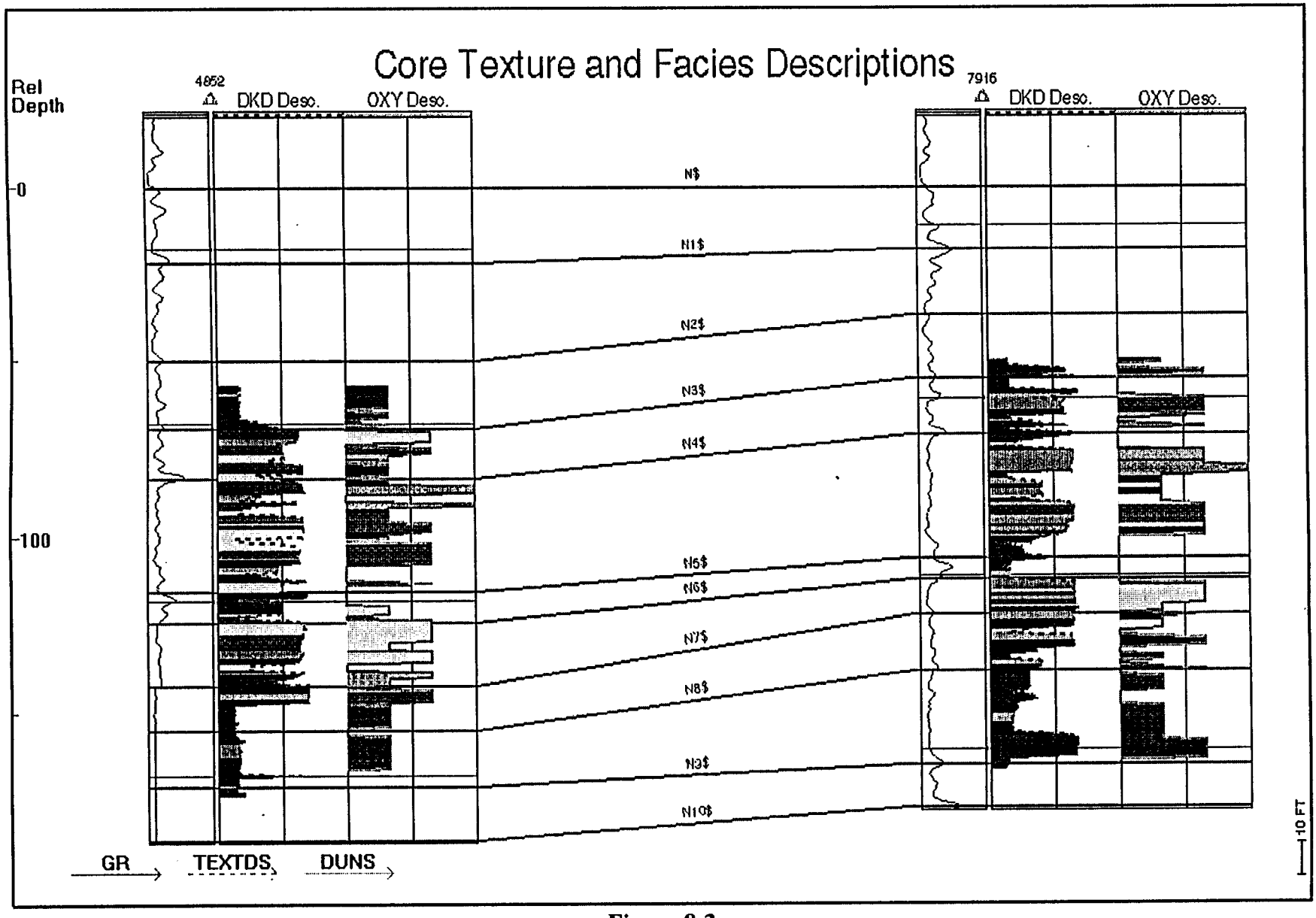
Core Texture and Facies Descriptions
Rel Depth
0
100
4852
DKD Desc.
OXY Desc.
7916
DKD Desc.
OXY Desc.
N$
N1$
N2$
N3$
N4$
N5$
N6$
N7$
N8$
N9$
N10$
GR
TEXTDS
DUNS
10 FT

Figure 8-3

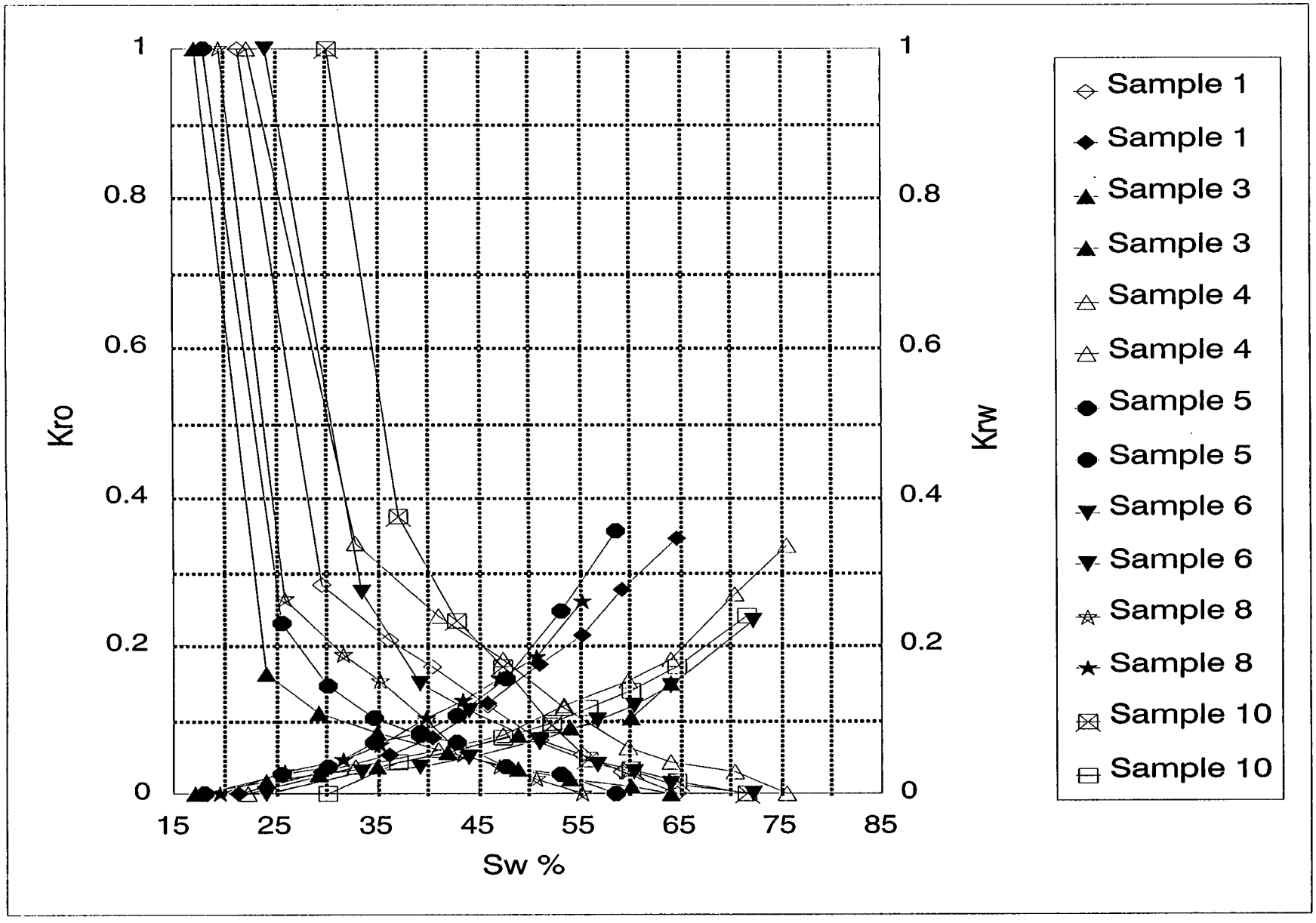
Kro
Krw
Sw %
1
0.8
0.6
0.4
0.2
0
15
25
35
45
55
65
75
85
Sample 1
Sample 1
Sample 3
Sample 3
Sample 4
Sample 4
Sample 5
Sample 5
Sample 6
Sample 6
Sample 8
Sample 8
Sample 10
Sample 10

Figure 9-3

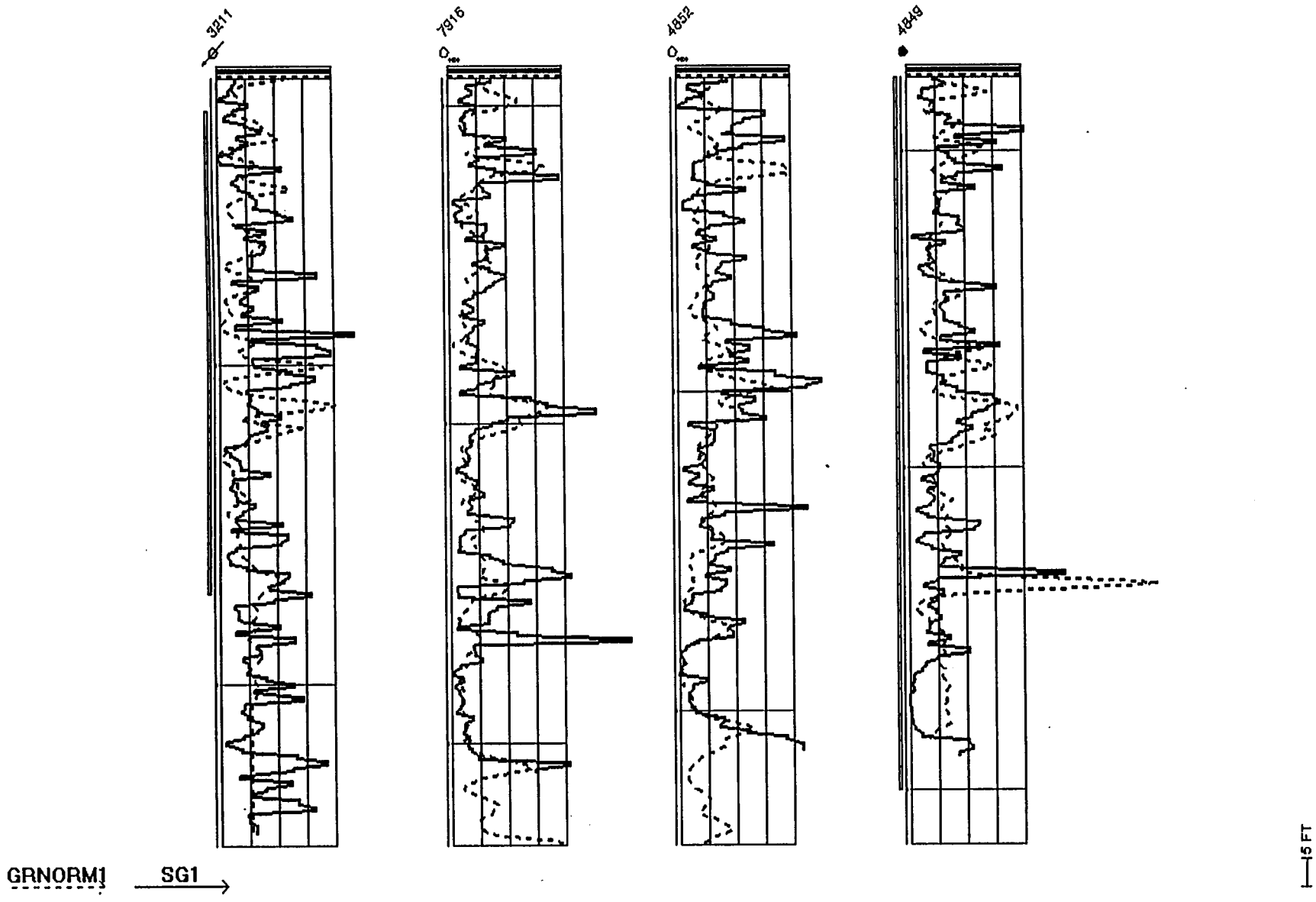

Figure 10-3

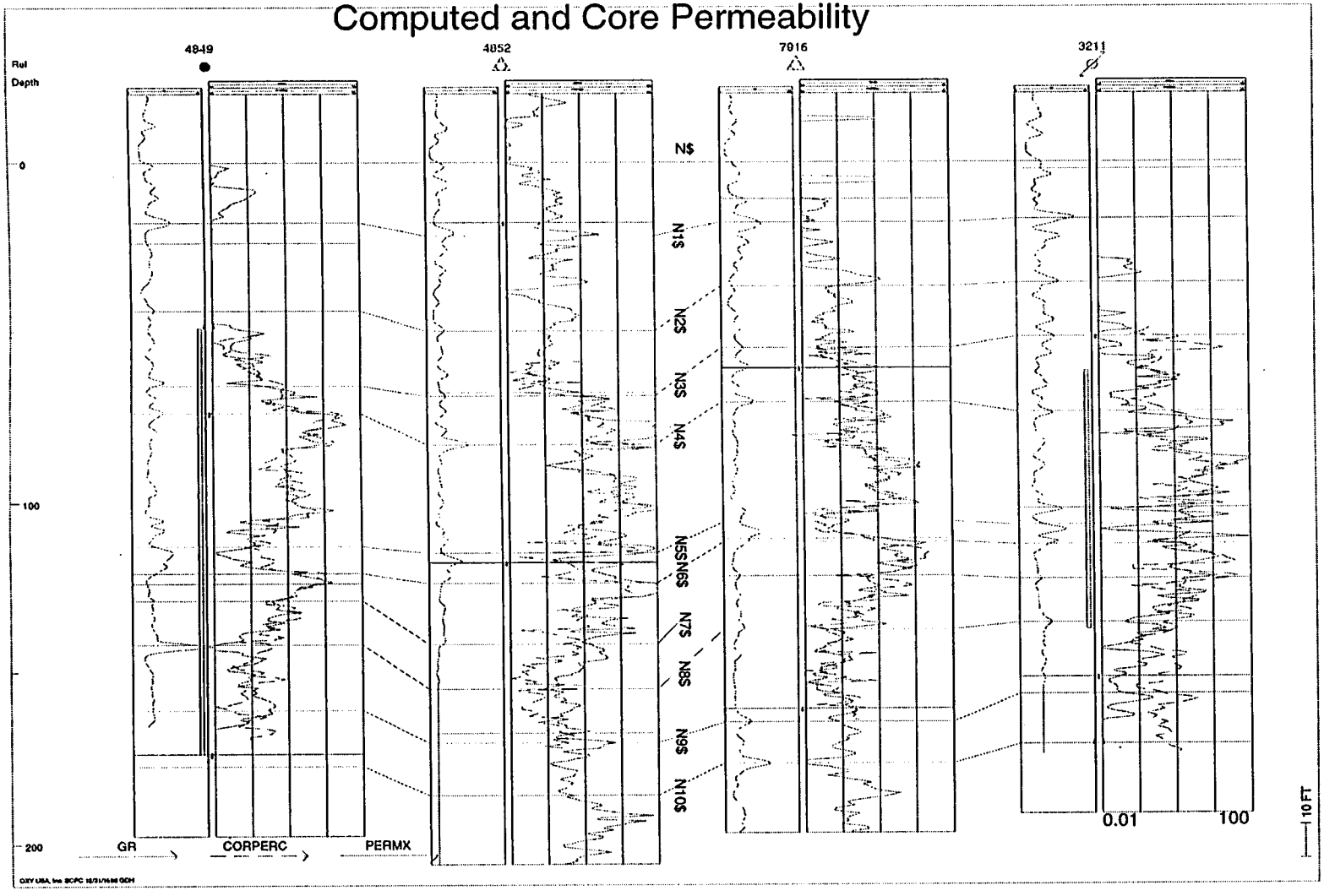
Computed and Core Permeability
Rel
Depth
0
100
200
4849
4852
7916
3211
N$
N1$
N2$
N3$
N4$
N5$
N6$
N7$
N8$
N9$
N10$
GR
CORPERC
PERMX
0.01
100
10 FT

Figure 11-3

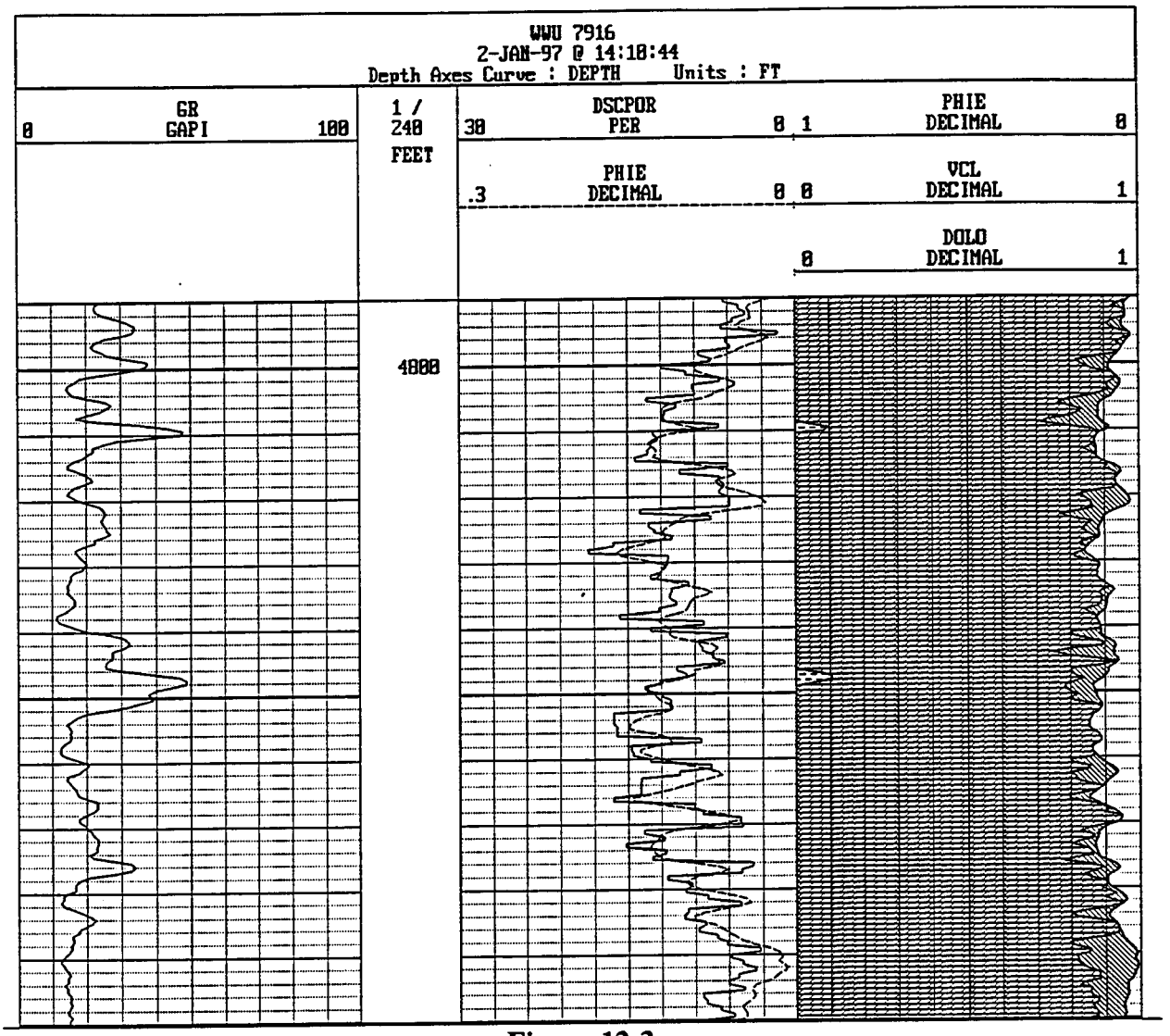
WWU 7916
2-JAN-97 @ 14:18:44
Depth Axes Curve : DEPTH Units : FT
GR
GAPI
0
100
1 /
240
FEET
4800
DSCPOR
PER
30
0
PHIE
DECIMAL
.3
0
1
PHIE
DECIMAL
0
VCL
DECIMAL
1
0
DOLO
DECIMAL
1

Figure 12-3

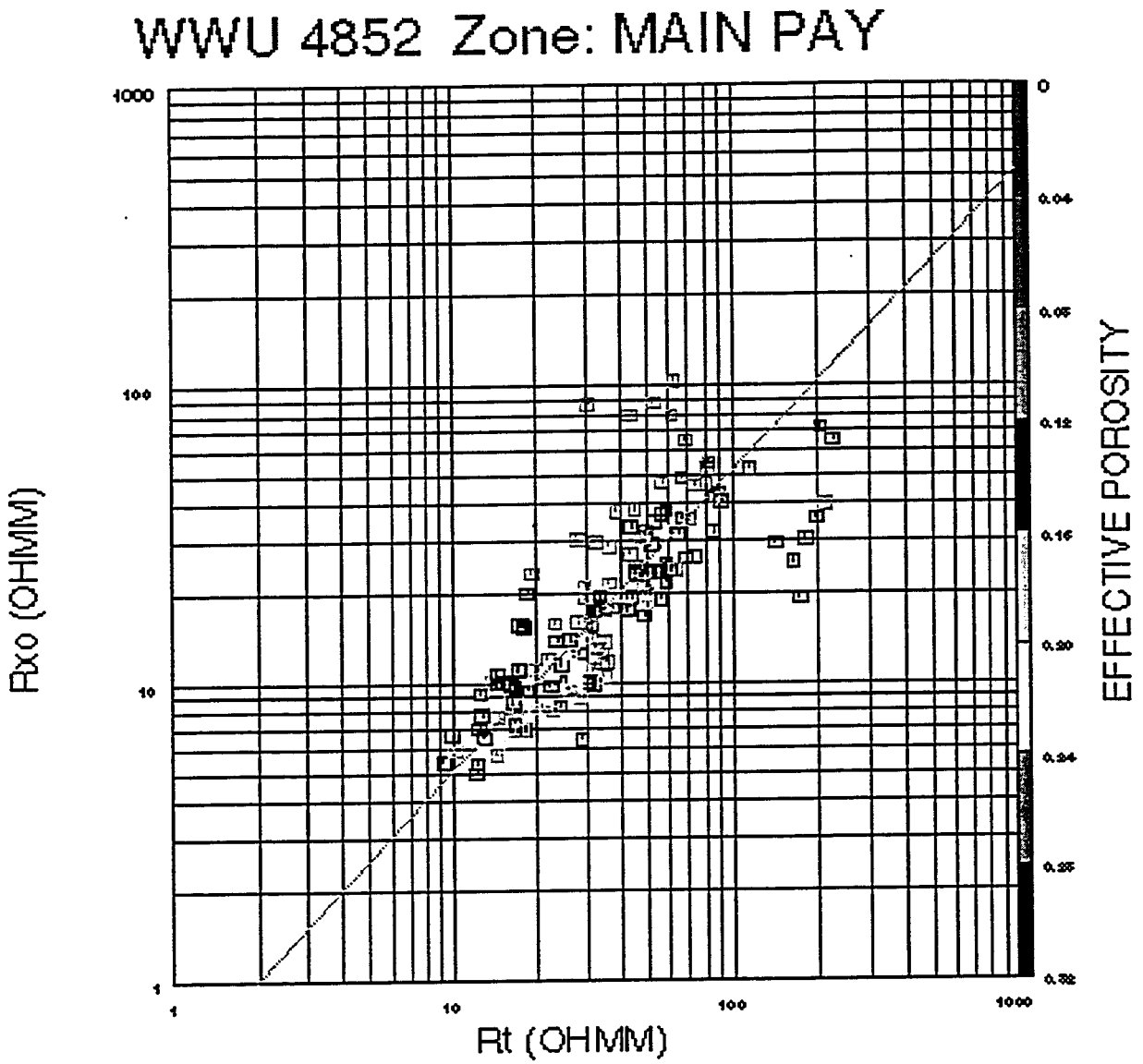
WWU 4852 Zone: MAIN PAY
Rxo (OHMM)
Rt (OHMM)
EFFECTIVE POROSITY
1000
100
10
1
1
10
100
1000
0
0.04
0.08
0.12
0.16
0.20
0.24
0.28
0.32

Figure 13-3

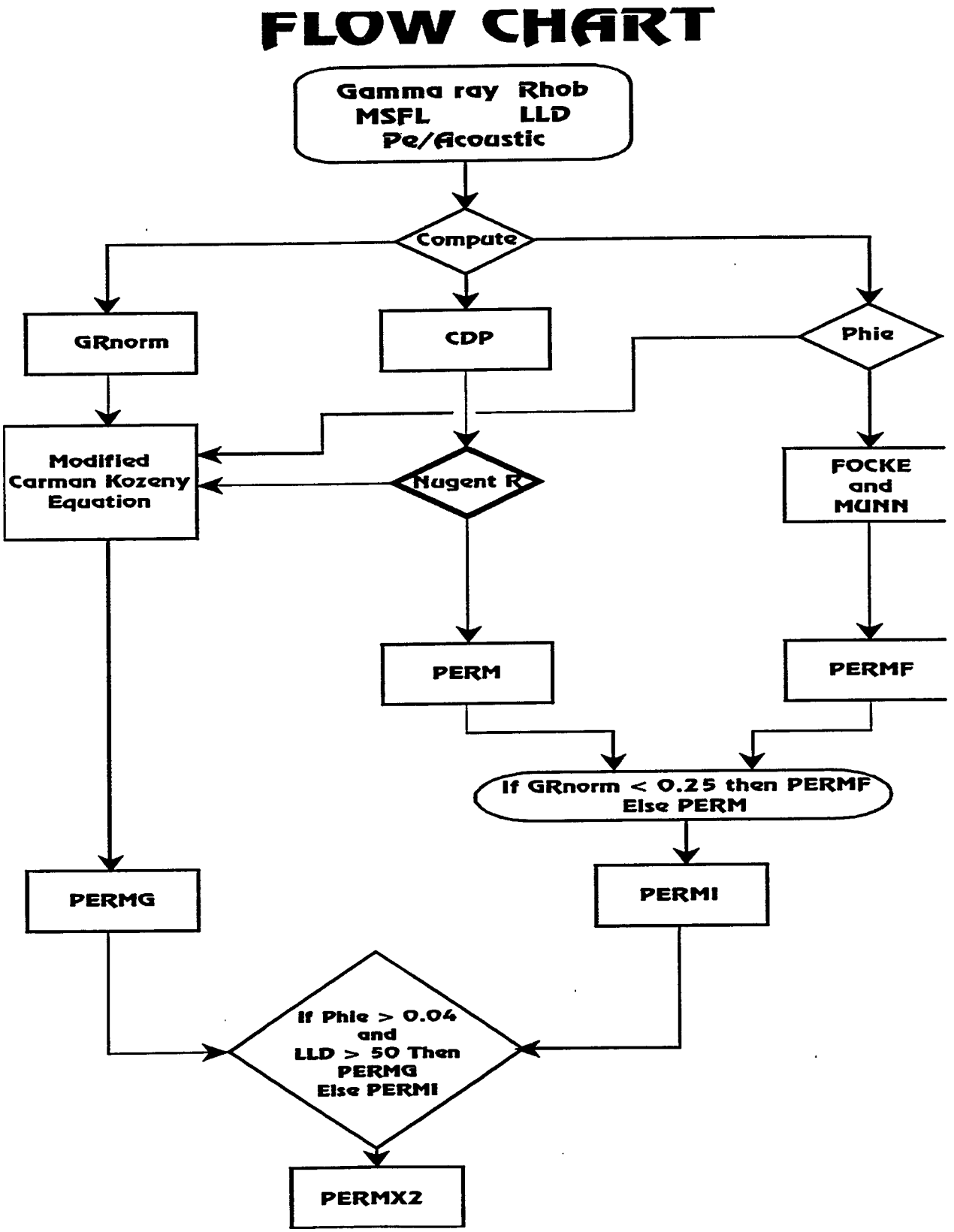
FLOW CHART
Gamma ray Rhob
MSFL LLD
Pe/Acoustic
Compute
GRnorm
CDP
Phie
Modified
Carman Kozeny
Equation
Nugent R
FOCKE
and
MUNN
PERM
PERMF
If GRnorm < 0.25 then PERMF
Else PERM
PERMG
PERMI
If Phie > 0.04
and
LLD > 50 Then
PERMG
Else PERMI
PERMX2

Figure 14-3

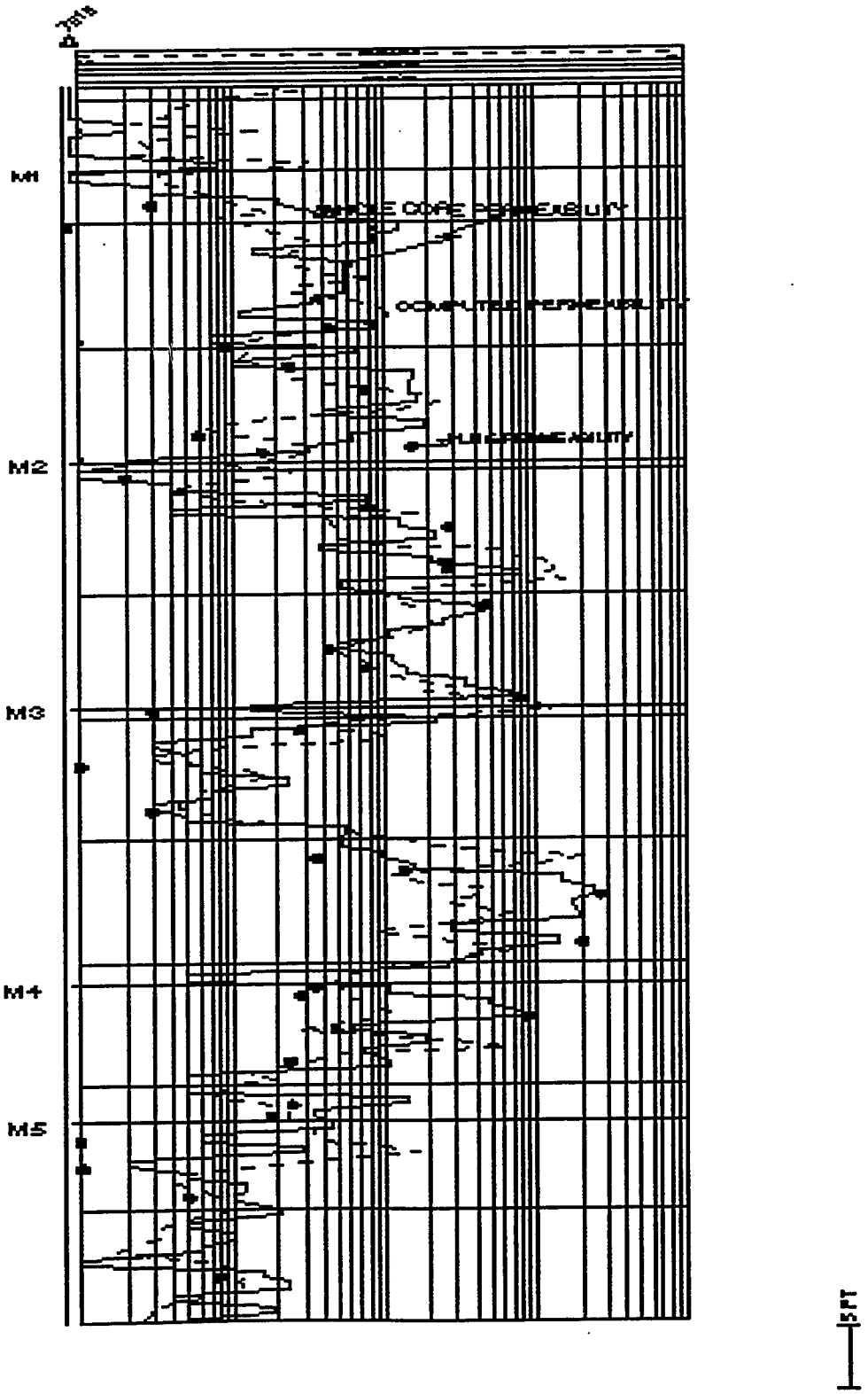

Figure 15-3

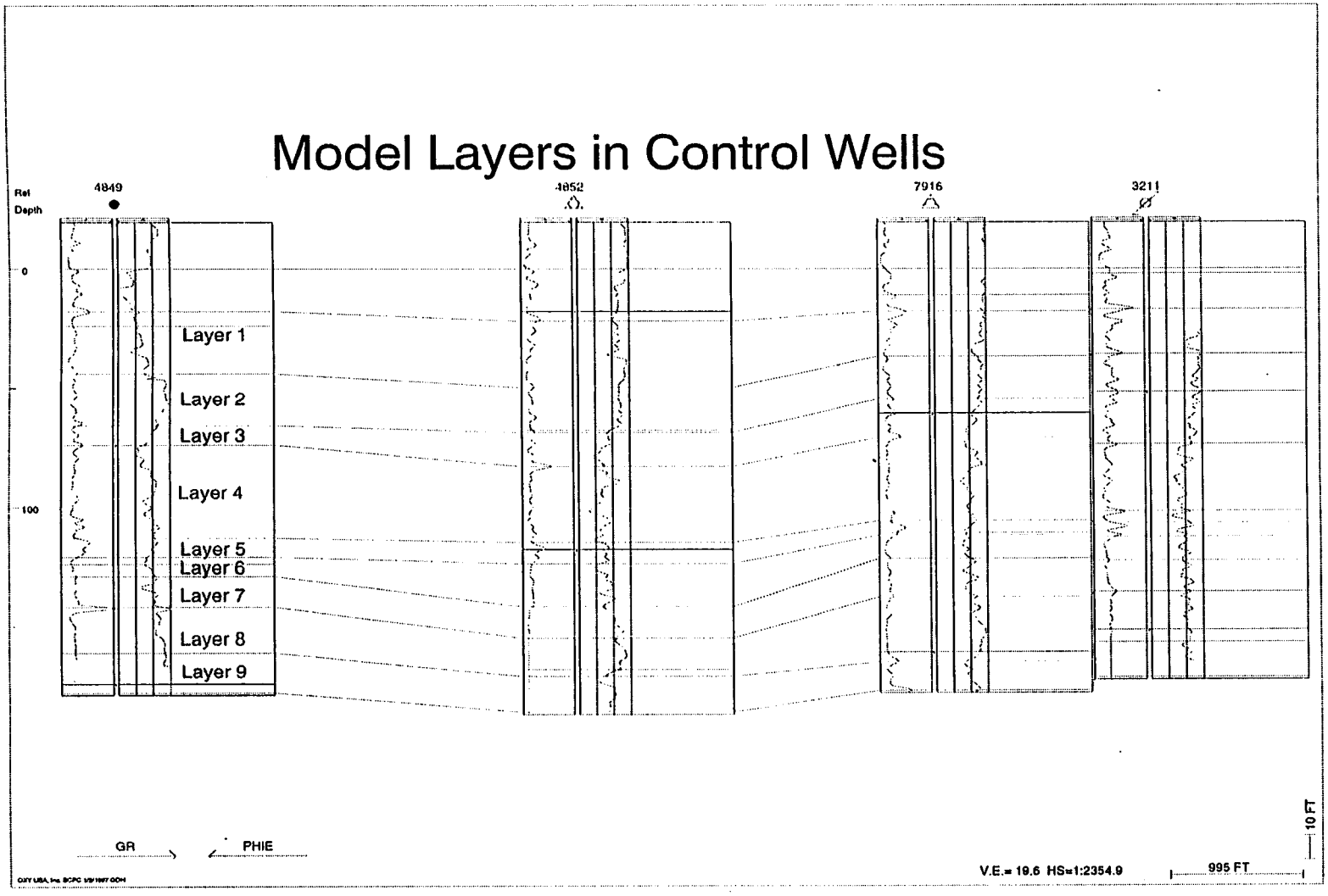
Model Layers in Control Wells
Rel Depth
0
100
4849
4852
7916
3211
Layer 1
Layer 2
Layer 3
Layer 4
Layer 5
Layer 6
Layer 7
Layer 8
Layer 9
GR
PHIE
V.E.= 19.6 HS=1:2354.9
995 FT
10 FT

Figure 16-3

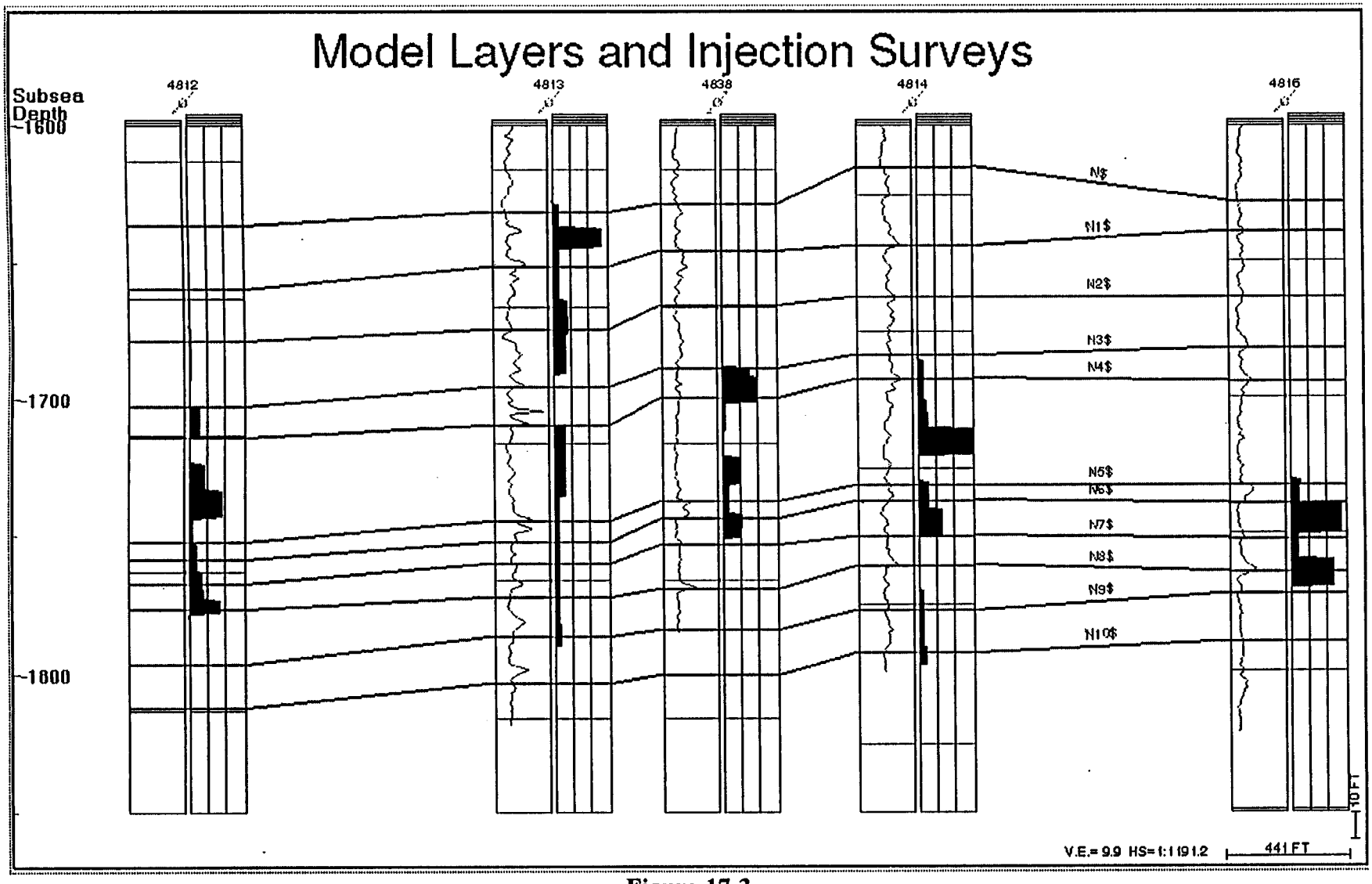
Model Layers and Injection Surveys
Subsea Depth
~1600
~1700
~1800
4812
4813
4838
4814
4816
N$
N1$
N2$
N3$
N4$
N5$
N6$
N7$
N8$
N9$
N10$
10 FT
V.E.= 9.9 HS=1:1191.2
441 FT

Figure 17-3

Chapter 4 - 3-D SEISMIC EVALUATION

Introduction

A 36 square mile 3-D seismic volume was acquired across the Welch field during the first quarter of 1993. The outline of this 3-D volume area is shown in Fig. 1-4. A six square mile area from this volume is dedicated to the demonstration project and is referred to as the DOE 3-D seismic area. Fig. 2-4 shows the spacial relationship of the wells, the wells with modern logs and/or core data (highlighted as large black dots), and the 3-D seismic bin locations within the DOE 3-D seismic area outline. There are 48 3-D seismic bin locations for every one well in the 20-acre spacing configuration and 300 seismic data points for every well with a porosity measurement. Therefore, the reservoir characterization effort depends on surface 3-D seismic methods for horizontal resolution in the interwell spaces. The overall objective of the 3-D seismic evaluation is to translate as much as possible of the well information needed for reservoir simulation to the concentration of 3-D seismic data points using the measurable attributes within the seismic data.

Scope and Objectives of 3-D Seismic Evaluation

The 3-D seismic evaluation is one part of the detailed reservoir description in this project. The evaluation of the 3-D seismic data base as stated in the project proposal is summarized below:

1. **Seismic Structural Interpretation** - Key reflectors will be mapped to establish structural definitions of the reservoir zones. Seismic horizons will be correlated and converted to depth in a conventional manner to create structure and isopach values at each seismic bin location.

2. **Seismic Stratigraphic Interpretation** - Assess seismic attributes to provide spacial pay quality (porosity, etc.) definition and individual flow unit continuity in the interwell space. This will be accomplished with a relatively new technique. Relationships between seismic attributes and log properties will be developed and used to transform the attributes to log properties at each seismic bin location.

3. **3-D Seismic and Tomography Integration** - The reservoir characterization from the 3-D seismic evaluation will be integrated with the cross wellbore seismic tomography data to determine if additional vertical resolution can be incorporated into the 3-D seismic interpretation.

4. **Field-Wide Reservoir Interpretation** - The reservoir characterization interpretation will be extended across the entire Welch field 3-D seismic volume.

This report presents an overview of the structural interpretation and focuses in more detail on the stratigraphic interpretation involving seismic-guided mapping of porosity. The tomography integration and field-wide interpretation are work to be completed in the future during Budget Period 2 of this project.

3-D Seismic Data Base

While the 3-D seismic program was specified to image the shallow (2500 ft) to the deep (15,000 ft) subsurface section, the San Andres pay interval is the focus of this discussion. The San Andres pay is a stratigraphic trap consisting of porous carbonate rocks. The top of the reservoir is approximately 4500 ft below the ground surface. The structural expression of the reservoir zones have monoclinal dip to the south-southwest with a maximum dip of less than two degrees. The isopach thickness of the main pay interval ranges from 60 ft along the northern edge of the Welch field to 120 ft on the southern side of the South Welch Unit. The net pay thickness is a wedge expanding from zero in the north to 100 ft in the southeast. The average porosity for the main pay interval ranges from 10 to 16 %. The sonic log data indicate interval velocities varying between 15,000 and 17,000 ft per second within the main pay interval and 18,000 ft per second for the beds overlying and underlying the main pay.

A previous report outlined in detail the design and field acquisition of the seismic program based on concepts described by Stone[1]. The initial processing was also reviewed step-by-step in the previous report and drew heavily from definitions acquired from Yilmaz[2].

Field Data Acquisition

Data acquisition operations for the Welch 3-D seismic volume commenced in December 1992 when Universal Seismic Acquisition arrived in the field. The shooting and recording was complete by February 1993. The field acquisition parameters are summarized in Table 1-4.

Data Reprocessing

The interpretation of the original data volume revealed artifacts in the migrated amplitudes. These artifacts were suspected of being the result of spikes, large erroneous values, in the data set. The artifacts were above the San Andres Main Pay zone and did not appear to effect the interpretation effort. The presence of these artifacts added an element of uncertainty to the interpretation. By the time the initial seismic interpretation (110 ft by 165 ft bins) was complete and reviewed, the decision was made to describe the geologic model for reservoir simulation on a 100 ft by 100 ft grid. The seismic data were acquired for variable bin spacing: 110 ft by 165 ft, or 110 ft by 82.5 ft. The decision was made to reprocess the seismic data to reduce the

noise and increase the spacial resolution to 110 ft X 82.5 ft which would require very little interpolation when sampling to a 100 ft x 100 ft grid. The field tapes and observer notes were delivered to Geotrace in March 1996 to begin reprocessing the data.

This new processing sequence was similar to the previous sequence. The strategy was to sanitize the data initially through trace editing and to focus on removing noise. A DMO algorithm was also applied as an attempt to sharpen discontinuity boundaries. The processing flow description is listed in Table 2-4. The improvements in the data are shown in Figs. 3-4 and 4-4 comparing the old processing with the new. It is obvious both the signal-to-noise ratio and the temporal resolution have increased considerably.

Seismic to Well Log Calibration

One of the most important and useful tools in geophysics is the synthetic seismogram. It is the bridge that joins together log and seismic data. It puts the log data into a one-dimensional model of a seismic trace where it can be compared to the seismic data. In the Permian Basin, the difference in acoustic velocity between rocks is the dominant factor in determining the reflection coefficients, and density is a secondary consideration. The sonic log data can accurately measure beds of 2 ft thickness or less, but only several inches into the formation from the borehole. The surface seismic data can measure relatively gross features for miles away from the borehole, but have difficulty resolving beds less than about 50 ft thick. These differences, both in dimension and resolution, between sonic log and seismic data present enough uncertainties that multiple synthetic seismograms should be used across a seismic area to obtain absolute horizon identification.

The seismic data were found to require a 90 degree phase shift to attain the best fit with the sonic-derived synthetic seismograms. There are 11 wells with sonic logs in the DOE 3-D seismic area. Fig. 5-4 is one of these sonic logs displayed with its synthetic seismogram showing the positions of the M1, M3 and M5 depositional sequence boundaries. The synthetic seismogram was produced from a 8/12-90/120 Hertz bandpass filter. This synthetic seismogram is inlaid on the seismic line in Fig. 6-4 to show the excellent correspondence between the sonic and seismic reflectivity. Eleven wells provide more than enough sonic data to obtain absolute horizon identification at the San Andres main pay level, and the seismic data were determined to have a vertical resolution of 35 ft at the San Andres level based on the analysis of these synthetic seismograms.

The M1, M3 and M5 horizons are identified throughout the seismic volume as:

	Well Log Pick	Seismic Horizon
1.	M1, Top of Upper Main Pay:	Seismic Peak-to-Trough Crossover
2.	M3, Top of Lower Main Pay:	Seismic Trough
3.	M5, Base of Lower Main Pay:	Seismic Trough-to-Peak Crossover

Seismic Structural Interpretation

The objective of the structure interpretation is to use the 3-D data to describe the structural definition at the reservoir levels at a horizontal resolution 48 times greater than the 20-ac well spacing. This, in turn, will also provide the thicknesses of the seismically observed reservoir zones.

The three horizons; M1, M3 and M5, were conventionally correlated throughout the 3-D seismic volume using the commercially available Vest 3-DSEIS P.C. workstation software. The 3-DSEIS time structure horizon files were transferred to OXY's proprietary geological P.C. workstation software called the Stacked Curves P.C. System (SCPC). All three time structure files were gridded and mapped. Each of these three time structure surfaces dip to the south-southeast, whereas the subsea structure maps from the well log picks express more dip to the southwest. This dip difference indicates there is a velocity gradient within the overlying geologic section due to lateral changes in lithology.

The average velocity gradient method was chosen to convert the seismic time structure files to subsea depth. With the average velocity method, an average velocity gradient is established from the seismic datum to the zone of interest using well data for depth values and seismic data for time values. This velocity gradient is applied to the seismic time picks to create subsea depth structure values.

The final seismic structure maps for the M1, M3 and M5 horizons are presented in Figs. 7-4, 8-4 and 9-4. The accuracy of the method is analyzed by subtracting the seismic-calculated depth structure values from the measured well log picks. The seismic structure calculations tie to the well log picks with a worst case of 3 ft. The isopach interval values were generated from the final subsea structure values and the isopach maps are shown in Figs. 10-4, 11-4 and 12-4.

Seismic Stratigraphic Interpretation

The method used for this study to convert seismic data to reservoir properties is described in a series of articles by Schultz et al.[3,4]

The seismic-guided estimation of log-determined reservoir properties method is a marked change from the traditional approach to seismic data interpretation.

Historically, one would begin with a theory and make approximations (model) which would lead to a relationship between measurable seismic quantities (attributes) and a rock property. Measurements are made on the data which lead to an interpretation. Both the seismic and log data are only passively used to establish and verify the physical relationships. In practice, particularly with 3-D seismic data, there are many seismic attributes that correlate to rock properties even though there is no obvious physical relationship. The seismic-guided estimation of log-determined reservoir properties method places a higher emphasis on the data, realizing there may or may not be a relationship between a given seismic attribute to a particular log property. Therefore, every measurable seismic attribute is evaluated with respect to every important log property for a given reservoir to fully describe any functional relationship that may exist. The overall objective is to translate as much of the well information needed for reservoir simulation as possible to the concentration of 3-D seismic data points via the measurable attributes within the seismic data.

Schultz's method is a non-geostatistical, data-driven approach suited for 3-D seismic data volumes where data points are uniform, closely spaced, and extensive. The data input are reservoir properties derived from well logs and attributes transformed from 3-D seismic volumes. Every log property is cross-plotted with each seismic attribute. A significance measure, probability of relationship using Kendall's Tau indicator, is applied to each cross-plot to determine how well each attribute relates to a property. Underlying physical relationships between seismic attributes and log properties are important but not necessary in this method. A calibration function is sought to best convert one or more attributes to a property. The coefficients for the fit of an over-determined linear regression solution are computed and applied to the seismic attribute data to estimate the log property. A residual correction is added to the converted property data to insure good ties with the well log data. Confidence estimates are made by leaving selected wells out of the procedure and comparing the seismic attribute-converted values to the log-projected values at the missing well locations.

The Kendall's Tau indicator (Tk) is determined from the slopes of every pair of points on the scatterplot by the equation:

$$Tk = (Np - Nn) / ((Nt - Ni) * (Nt - Nz)) ** 0.5$$

where, N is the number of points on the cross-plot,
Nt = (N * (N - 1)) / 2,
Np is the number of positive slopes,
Nn is the number of negative slopes,
Nz is the number of zero slopes, and
Ni is the number of infinite slopes.

The significance is estimated from the value of Tk and the number of points (N) in the scatterplot through the relationship:

$$\text{Significance} = \text{erf}\ (0.477\ Tk * (9N(N - 1)/(8N + 20))) ** 0.5$$

as a percentage. This significance value is posted above each cross-plot in the SCPC.

The reservoir properties available for this study were developed from core data integrated with modern well logs. The methods of analysis and the distributions of these reservoir properties are summarized in the geological chapter of this report.

The seismic expression of the Total Main Pay (M1 to M5) interval is dominantly a seismic trough as exhibited by Fig. 6-4. Figure 13-4 contains three wells with sonic logs, synthetic seismograms, and average porosity measurements across the M1 to M5 interval. These wells are aligned northwest-southeast where an arbitrary line has been extracted from the seismic volume, Fig. 14-4. The relative amplitude of the seismic trough from both the synthetic seismograms and the seismic data shows a decrease in amplitude as the average porosity decreases. There are also places where isolated seismic peaks are scattered within the M1 to M5 interval which is mostly a seismic trough. The seismic section in Fig. 15-4 illustrates some scattered peaks occupying the M1 to M5 interval between shotpoints 213 and 225. These scattered peaks are more concentrated in the northern half of the DOE 3-D seismic area. A seismic trough reflection that is disrupted with sporadic seismic peaks would produce variations in certain seismic attributes across the Total Main Pay seismic interval. The pay zones in the northern part of the study area thin, become tight due to digenesis, and pinch out in places. Mapping these variations in the seismic attributes can help identify and delineate these kind of changes within the reservoir.

Seismic Attribute Data

Seismic attribute data are commonly associated with the amplitude, frequency, and phase information within the seismic record. More recently, data requiring specialized data processing, e.g. acoustic impedance, spectral ratio, and dozens of other measurements, are referred to as seismic attributes. And for the purposes of seismic-guided estimation of log properties the term is even broader. Seismic attribute data are all measurable quantities extracted from the seismic volume at the reservoir level which also include time (depth) structure and isochron (isopach) values. Log-calibrated acoustic impedance values are not considered seismic attribute data for seismic-guided estimation of log properties. The attribute data must be independent from the log data. The seismic attributes used in this study are described below:

Reservoir Elevation - The subsea depth structure surfaces relate to the San Andres pay zones as follows:

M1, Top of Upper Main Pay (Fig. 7-4),
M3, Top of Lower Main Pay (Fig. 8-4), and
M5, Base of Lower Main Pay (Fig. 9-4).

All three structures are monoclinal surfaces dipping about one degree to the south-southwest. These surfaces express a broad nose or terrace in the center of the map and a broad trough or low area to the northwest.

Reservoir Thickness - The isopach intervals relate to the San Andres pay zones as follows:

M1 to M5, Total Main Pay (Fig. 10-4),
M1 to M3, Upper Main Pay (Fig. 11-4), and
M3 to M5, Lower Main Pay (Fig. 12-4).

All three isopach maps have a tabular external form with slight thickening in the center and to the south of the mapped area.

Relative Amplitude - The relative amplitude associated with the M3 horizon, Fig. 16-4, is directly proportional to the average porosity between the M1 and M5 log picks as shown in Figs. 13-4 and 14-4 above. This M3 relative amplitude map generally expresses negative amplitudes which increase to the south. There are areas of positive amplitudes, inside the zero contour (bold lines), to the north.

The Hilbert transform capability within the Vest 3-DSEIS system was used to create seismic attribute files of instantaneous amplitude, instantaneous frequency, and instantaneous phase, each averaged between any two selected horizon interpretations.

Reservoir Amplitude - The instantaneous amplitude files were created by averaging the raw amplitude values, both positive and negative, across the reservoir intervals. The resulting files contain both positive and negative amplitude values which were gridded. The instantaneous amplitude maps are mostly negative amplitudes increasing in value to the south. There are also areas of positive amplitudes to the north similar to those shown on the relative amplitude map.

Reservoir Frequency - The instantaneous frequency files were gridded and mapped. The instantaneous frequency maps express higher frequencies with much variability to the north and lower frequencies with less variability to the south.

Reservoir Phase - The instantaneous phase files were created by averaging the raw instantaneous phase values, both positive and negative, across the reservoir intervals. The resulting files contain both positive and negative phase values which were gridded and displayed for M1 to M5 interval in Fig. 17-4. The instantaneous phase maps express larger negative phases to the south and center of the area with areas of

positive phases to the north inside the bold zero contour lines. And like the frequencies, the phases have greater variability in the northern half of the map.

Statistical Correlations within the Data

The six log-determined reservoir properties available for this study are summarized in the geological chapter of this report. These reservoir properties are listed for each seismic reservoir interval with their average values across the DOE study area in Table 3-4.

The six seismic attributes discussed above were sampled to the well locations. Each log-determined reservoir property was cross-plotted with each seismic attribute for all three reservoir intervals. All cross-plots have a considerable scatter and each was evaluated with Kendall's Tau indicator as a significance measure. The cross-plot displays from the SPCP have the number of points and the Tau indicator value posted above each cross-plot in the upper right corner and the correlation coefficient is found at the bottom. Selected cross-plots for the Total Main Pay (M1 to M5) Interval are displayed in Figs. 18-4, 19-4 and 20-4. Notice the correlation coefficient on these cross-plots is 55% for structure, 77% for relative amplitude and 53% for phase. These correlation coefficients will be referred to again with the multiple linear regression analysis. The number of plotted points, Tau indicator value, and correlation coefficient for each of the seismic attribute vs. log property cross-plots are compiled in quality matrices (Tables 4-4, 5-4 and 6-4).

Porosity - The Tau indicator is required to be greater than 70% to be considered in the development of a calibration function. The average porosity (PHIA) and the porosity feet (PHIH) both have excellent probability of relationship (90's) with structure and amplitude for all three intervals. The PHIH has qualifying (>70) Tau indicators with isopach and phase for the M1 to M5 and M1 to M3 intervals, while the PHIA qualifies with the phase attribute only for these intervals. Both the PHIA and PHIH also qualify with frequency in the M1 to M3.

Permeability - There are 54 cross-plots involving the permeability data and only three have a Tau indicator value greater than 70%. These three Tau values are considered sporadic occurrences and the permeability shows no correlation to the seismic data in this study.

Water Saturation - The 18 water saturation cross-plots have four with Tau indicator values greater than 70%. The amplitude has the most consistent correlations. However, the probability of the relationship for the water saturation to seismic attributes looks weak from the observations in this study.

Calibrating Attributes to a Property

At this point, a calibration function is sought to predict a reservoir property value from an attribute or a set of attributes. The current capability within the SCPC is for multiple variable linear regression analysis. The PHIA and the PHIH are the only two reservoir properties having consistent statistical relationships with the seismic attributes. Both have qualifying relationships with structure, amplitude, and phase. And the reservoir thickness has a qualifying probability of relationship with the PHIH for two reservoir intervals. For this study, the structure, amplitude, and phase were selected to seismically predict the PHIA.

The multiple variable linear regression analysis capability within SCPC was utilized to produce the calibration equation. The PHIA derived from well data was input as the dependent variable while structure, amplitude, and phase attributes were input as the dependent variables. Table 7-4 is a sample SCPC output for the multiple variable linear regression coefficients for the seismic average porosity prediction in the M1 to M5 interval. Recall the correlation coefficients from the cross-plots; Figs. 18-4, 19-4 and 20-4. The correlation coefficient improves to 82% by integrating the three independent variables. The resulting calibration equations are listed below for all three intervals:

1. Total Main Pay Interval (M1 to M5);

$$M1M5PHIA = -28.18268600 - (0.01976901 * M1SUBC) - (0.00077870 * M3AMPS) - (0.00347584 * M1M5PHAZ)$$

2. Upper Main Pay Interval (M1 to M3);

$$M1M3PHIA = -56.58196415 - (0.03637118 * M1SUBC) - (0.0051472 * M1M3AMPS) - (0.02594264 * M1M3PHAZ)$$

3. Lower Main Pay Interval (M3 to M5);

$$M3M5PHIA = -63.14375838 - (0.04068802 * M3SUBC) - (0.00056651 * M3M5AMPS)$$

These equations were applied to the structure, amplitude, and phase attribute values within the seismic bin records to predict a PHIA value at each bin location. The seismic-predicted PHIA values were gridded and mapped. Figure 21-4 is an example of the seismic-predicted PHIA map for the M1 to M5 interval. Because these seismic PHIA estimates were predicted from relationships with less than a 100% correlation coefficient, the seismic predictions do not tie the well data exactly. The seismic-predicted PHIA grids were sampled to the well locations and cross-plotted with the average porosity values from the well data and shown on Fig. 22-4 to demonstrate the lack of agreement.

The seismic-predicted PHIA values were subtracted from the log-derived PHIA values to create a PHIA difference file called PHIA residuals. Figure 23-4 is a histogram plot of the M1 to M5 PHIA residuals which show differences as big as 5%. These residuals were gridded and mapped, shown on Fig. 24-4 for the M1 to M5 interval.

Seismic-Guided Reservoir Property Maps

The PHIA residual grid was added to the seismic-predicted PHIA grid to create the seismic-guided PHIA grid; see Fig. 25-4. The M1 to M5 PHIA map produced from well data is included for comparison on Fig. 26-4. The seismic-guided PHIA grid was sampled back to the well locations. Then the log-derived PHIA values are cross-plotted with the seismic-guided PHIA values, Fig. 27-4, which is to be compared with Fig. 22-4. The standard error of the estimate has been improved by a factor of five by adding the residuals into the seismic predictions. It is obvious the seismic-guided map ties to the well data very accurately. By subtracting the seismic-guided PHIA values from the average porosities derived from the well data, a seismic-guided PHIA residuals file can be created. Figure 28-4 illustrates the M1 to M5 seismic-guided PHIA residuals histogram which should be compared to Fig. 23-4. Figures 29-4 through 32-4 are compiled to show the same results for the M1 to M3 and M3 to M5 intervals. The seismic-guided method has estimated average porosity values for each seismic bin location which tie to the well data to within 0.4 % porosity.

Geologic Model

The rock data within the reservoir simulation model require the following pieces of the data for each reservoir pay zone at each grid node according to Crichlow[5].

1. Elevation (Structure),
2. Thickness (Isopach),
3. Average Porosity across Pay Zone,
4. Average Permeability across Pay Zone,
5. Average Fluid Saturations across Pay Zone,
6. Average Compressibility,
7. Relative Permeability, and
8. Capillary Pressure.

The most common distance between wells with modern log suites and/or core data in the DOE study area is 957 ft with a non-uniform distribution. Therefore, much lateral interpolation is needed to produce a reservoir simulation model at a grid node spacing of 100 ft by 100 ft. The current interpretation of depositional cycles subdivides the Main Pay interval into an nine layer model. This interpretation provides bed thicknesses to as little as 6 in.

The 3-D seismic data were able to resolve bed thicknesses to 35 ft. Therefore, the two major cycles of deposition within the main pay interval are the seismic mappable units. These units are called the Upper Main Pay interval and the Lower Main Pay interval. The 3-D seismic data evaluation has provided reservoir elevation values, reservoir thickness values, and average porosity estimates at a uniform spacing of 110 ft by 82.5 ft across the DOE 3-D seismic area.

Benefits gained by using the 3-D seismic data in the reservoir simulation model are:

1. All the detailed areal variation in the interwell space expressed by the seismic attribute information is contained in the structure, isopach, and porosity interpretations.

2. The structure, isopach, and porosity interpretations tie accurately to the well data.

3. The seismic interpretation reveals extensions of the reservoir beyond the well control in the southern part of the DOE 3-D seismic area.

4. The structure, isopach, and porosity interpretations from the 3-D seismic volume are in a format suitable for input to the reservoir simulation model.

The seismic bin spacing (110 ft by 82.5 ft) supplies approximately 300 additional control points for every well with an average porosity measurement to provide a more complete description of the reservoir continuity. The porosity profile from the well data can be proportioned to match the seismic-guided porosity values at each bin location. This will effectively extend the vertical resolution of the well control to the seismic data volume within the constraints of the seismic-guided porosity values. The final reservoir porosity volume will be consistent with the core, well log, and seismic data.

Summary of Results

The seismic interpretation during Budget Period 1 of this project produced the following major accomplishments:

i. **Seismic Data Volume Reprocessing** - The original data processing was geared toward imaging the deeper structural features. The San Andres level was noisy in places and the spacial resolution needed to be improved to maximize the detail of the interwell variability of the reservoir. The new processing upgraded the bin spacing from 165 ft E-W by 110 ft N-S to 82.5 ft E-W by 110 ft N-S, significantly increased the

signal-to-noise ratio and the frequency content of the data, and improved the vertical resolution to 35 ft at the San Andres level.

ii. **Seismic Structural Interpretation** - Three seismic horizons were tied to San Andres sequence boundaries; M1, M3 and M5. The seismic depth structure calculations tie to within 3 ft of the well log picks. The 3-D seismic bins provide a minimum of 48 data points for every well with a structural log pick. These seismic depth structure surfaces were used to create three seismic isopachs. The following maps and grid files were produced for the geological model:

Seismic Subsea Structure:	Seismic Isopach:
Top of Upper Main Pay (M1)	Upper Main Pay (M1 to M3)
Top of Lower Main Pay (M3)	Lower Main Pay (M3 to M5)
Base of Lower Main Pay (M5)	Total Main Pay (M1 to M5)

iii. **Seismic Stratigraphic Interpretation** - Seismic-guided average porosity (PHIA) values were estimated for each seismic bin location which tie to the well data to within 0.4 percent porosity. For every well with an average porosity measurement there are 300 seismic data points that map the seismic-guided PHIA in the interwell spaces. The following maps and grid files were produced for the geological model:

Seismic-Guided Average Porosity:
Upper Main Pay (M1 to M3)
Lower Main Pay (M3 to M5)

Conclusions

This shallow shelf carbonate reservoir has a very complex porosity system as a result of post-depositional digenesis, primarily anhydritic cementing. Describing barriers to fluid flow in the interwell spaces, such as zones of low porosity, is a formidable challenge in the development of a reservoir characterization model for reservoir simulation. The concentration of data points provided by 3-D seismic volumes contains the areal spacing to meet the challenge. Compressional wave data from a surface 3-D seismic survey have been successfully used to estimate carbonate porosity in this study. The seismic data needed to be reprocessed to reduce noise levels and to obtain greater consistency in the seismic attributes. Bin size reduction, trace editing, and dip moveout provided the most profound improvements on the vertical and horizontal resolution of the data. Horizons were correlated across the top, base, and midpoint of the seismic trough that bounds the reservoir interval. Areas where seismic peaks were encountered within this seismic trough were found to correlate to zones of low porosity within the reservoir. A key element in the interpretation process was the interpolation of the three seismic horizons across these

sporadic peaks maintaining continuous intervals throughout the seismic trough. The structure, amplitude, and phase attributes were integrated through multiple variable linear regression analysis to predict the average porosity. After these porosity predictions were corrected to tie the well data to within 0.4%, the variability of porosity within the interwell spaces was mapped with a high level of confidence.

References

1. Stone, Dale S., 1994, *Designing seismic surveys in two and three dimensions: Geophysics Reference No. 5,* Society of Exploration Geophysicists, Tulsa, OK, 248 pages.

2. Yilmaz, Ozdemir, 1988, *Seismic Data Processing: Investigations in Geophysics No. 2, Society of Exploration Geophysicists*, Tulsa, OK, 526 pages.

3. Schultz, Philip S., Shuki Ronen, Masomi Hattori and Chip Corbit, 1994, Seismic-guided estimation of log properties, Part 1: *A data-driven interpretation methodology: The Leading Edge*, May 1994, p. 305-310 & 315.

4. Schultz, Philip S., Shuki Ronen, Masomi Hattori, Pascal Mantran and Chip Corbit, 1994, *Seismic estimation of log properties, Part 3: A Controlled Study: The Leading Edge*, July 1994, p. 770-776.

5. Crichlow, Henry B., 1977, Modern Reservoir Engineering - *A Simulation Approach*: Prentice-Hall, Inc., Englewood Cliffs, NJ, 354 pages.

Table 1-4

FIELD ACQUISITION PARAMETERS

Welch Field, Dawson County, Texas

RECORDING PARAMETERS	
Recording equipment:	Input/output two system
Channels:	480 with roll along
Receiver lines:	8
Groups per line:	60
Geophones per group:	12 (buried)
Sample rate:	2 milliseconds
Record length:	4 seconds
Low cut filter:	3 Hertz
High cut filter:	120 Hertz
Notch filter:	Out
Pre amplifier setting:	48 decibels
RECEIVER LINE AND GROUP PARAMETERS	
Receiver line interval:	1,320 ft aligned north-south
Receiver group interval:	220 ft
Geophone spacing:	Approximately 9 ft
Geophones per group:	12 in 100-ft linear array
Geophone type:	Mark Products L200 10 Hertz
ENERGY SOURCE PARAMETERS	
Vibroseis equipment:	4 failing Y2400 vibrators on Pelton Advance II electronics on line at all times
Sweep length:	8 seconds
Sweeps per point:	8
Sweep frequency:	8-120 Hertz, nonlinear, 6 decibels/octave
Source line interval:	1,320 ft aligned east-west
Source point interval:	330 ft, staggered between lines
SAMPLING EFFORT	
Variable bin spacing:	110 ft N-S by 165 ft E-W or 110 ft N-S by 82.5 ft E-W
Fold at 4500 foot level:	8-9 (110'x165') and 5-6 (110'x82.5')
Total survey size:	36 square miles
DOE 3-D seismic area:	5.9 square miles

Table 2-4

DATA PROCESSING FLOW DESCRIPTION

Welch Field, Dawson County, Texas

1. Demultiplex/Reformat
2. Trace Editing
3. Geometry Definition
4. Spherical Divergence Correlation
5. Surface Consistent Deconvolution
6. Flexbin
7. CMP Sort
8. 3-D Refraction Statics
9. Initial Velocity Analysis
10. Surface Consistent Residual Statics
11. Second Velocity Analysis
12. Surface Consistent Residual Statics
13. CDP Consistent Statics
14. Post NMO Mute
15. DMO
16. 3-D Migration
17. Spectral Whitening
18. Symmetrical Noise Isolation Process

Table 3-4

Average Reservoir Properties Across Mappable Seismic Intervals

Reservoir Properties	Seismic Reservoir Intervals		
	M1 to M5	M1 to M3	M3 to M5
PHIA - Average Porosity (percent)	9.3	9.0	9.8
PHIH - Porosity Ft (percent-ft)	694	349	353
AK - Arithmetic Mean Permeability (md)	5.3	4.9	5.3
GK - Geometric Mean Permeability (md)	2.8	3.0	2.7
KH - Permeability Ft (md-ft)	382	176	204
SWA - Average Water Saturation (percent)	43.1	39.4	47.0

Table 4-4 - **M1 to M5 Quality Matrix**

Number of Data Points / Kendall's Tau Indicator / Correlation Coefficient

	M1 Structure	M5 Structure	M1 to M5 Isopach	M3 Rel Amp	M1 to M5 Freq	M1 to M5 Phase
PHIA	72/98/55	72/98/55	72/26/12	59/100/77	59/64/24	59/77/53
PHIH	72/99/55	72/99/59	72/84/37	59/100/75	59/63/24	59/71/48
AK	40/31/21	40/44/25	40/66/34	34/16/8	34/52/19	34/50/29
GK	40/19/13	40/29/16	40/43/29	34/6/4	34/70/27	34/69/33
KH	38/49/28	38/58/31	38/74/38	34/10/6	33/52/21	33/62/30
SWA	36/53/31	36/51/32	36/7/7	31/86/48	31/26/11	31/42/16

Table 5-4 - **M1 to M3 Quality Matrix**

Number of Data Points / Kendall's Tau Indicator / Correlation Coefficient

	M1 Structure	M3 Structure	M1 to M3 Isopach	M1 to M3 Amps	M1 to M3 Freq	M1 to M3 Phase
PHIA	47/99/66	47/99/67	47/43/16	39/89/55	39/73/43	39/93/64
PHIH	47/97/59	47/97/64	47/83/42	30/89/52	39/77/45	39/96/65
AK	42/40/17	42/51/21	42/54/27	35/25/15	35/10/3	35/34/26
GK	40/30/14	40/40/18	40/41/30	33/0/10	33/51/21	33/54/31
KH	40/39/19	40/50/25	40/73/50	33/2/4	33/34/7	33/32/21
SWA	36/80/46	36/79/48	36/14/17	31/40/22	31/45/13	31/46/19

Table 6-4 - **M3 to M5 Quality Matrix**

Number of Data Points / Kendall's Tau Indicator / Correlation Coefficient

	M3 Structure	M5 Structure	M3 to M5 Isopach	M3 to M5 Amps	M3 to M5 Freq	M3 to M5 Phase
PHIA	47/98/67	47/99/67	47/6/2	39/96/73	39/41/16	39/30/36
PHIH	47/96/59	47/97/61	47/63/34	39/94/63	39/32/11	39/42/31
AK	38/22/14	38/19/11	38/9/2	33/41/17	33/13/13	33/15/14
GK	39/16/15	39/9/10	39/5/1	33/3/3	33/47/22	33/11/20
KH	39/52/31	39/49/28	39/44/20	33/40/14	33/30/16	33/16/14
SWA	36/9/9	36/11/10	36/25/6	31/82/56	31/5/8	31/18/12

Table 7-4 - Multiple Variable Linear Regression Analysis from SCPC.

SCPC - Multiple Regression Analysis

Number of Wells Fit = 59

For General Form of : Y = A + B*X1 + C*X2 + ...

Coefficients Found:

A = -28.18268600
B = -0.01976901
C = -0.00077870
D = 0.00347584

Equation:

MNP.BESTPHIA = -28.18269
+ (-0.01977 * SEISMIC.M1SUBC)
+ (-0.00078 * SEISMIC.M3AMPS)
+ (0.00348 * SEISMIC.M1MSPHAZ)

Data:

M1SUBC(X1)	M3AMPS(X2)	M1MSPHAZ(X3)	BESTPHIA(Y)	Y(predicted)	Residual
-1689.60000	-7669.10584	-83.97505	8.56150	10.89909	-2.33759
-1678.39000	-5827.31892	-87.22115	9.04020	9.07384	-0.03364
-1656.89400	-4092.92507	-83.89922	8.86100	9.02545	-0.16445
-1725.98000	-5441.69056	-79.54604	8.96970	9.89919	-0.92949
-1754.54400	-4986.31795	-71.79337	8.55830	10.13622	-1.57792
-1765.12000	-8654.73575	-68.81526	9.81710	13.21225	-3.39515
-1692.00000	-5835.65370	-66.69312	9.70910	9.57889	0.13021
-1707.50000	-5236.92594	-79.87577	7.86360	9.37326	-1.50966
-1744.00000	-5355.25255	-69.56759	9.87200	10.22280	-0.35080
-1761.01100	-4421.59125	-69.95526	8.98030	9.83070	-0.85040
-1623.01100	-2834.21509	-55.28083	5.75290	5.91749	-0.16459
-1703.30000	-4793.32196	-52.77434	7.83630	9.03899	-1.20269
-1671.86200	-4246.26456	-74.60853	11.46160	7.91561	3.54599
-1690.30000	-742.44516	3.23003	4.53380	5.82223	-1.28843
-1674.45600	-5242.49147	-64.08776	9.99020	8.77922	1.21098
-1654.80000	-5275.49606	-63.89874	7.07240	8.41700	-1.34460
-1665.90000	-2255.54661	-60.56449	5.25010	4.29639	-1.04629
-1653.84200	-2690.67140	-95.96750	4.57910	6.27379	-1.69469
-1672.60000	-936.00629	-5.70356	7.39190	5.59200	1.69990
-1638.90000	-2201.67875	0.95718	6.34290	5.93451	0.40839
-1676.20000	-5078.18865	-62.43203	9.17220	8.62199	0.55021
-1681.90000	-7096.35339	-55.09067	11.84550	10.40126	1.44424
-1706.18100	-4694.91603	-57.52034	4.08570	9.00282	-4.91712
-1678.50100	-5866.15968	-59.75680	11.93650	9.35989	2.57661
-1679.54700	-7542.07113	-73.31759	11.12420	10.63909	0.48511
-1705.00000	-7501.70156	-74.53884	10.96310	11.10597	-0.14287
-1677.90000	-8586.12688	-65.63134	10.46760	11.37612	-0.90852
-1709.31900	-9104.44334	-70.03806	12.64940	12.45505	0.19435
-1698.70000	-4846.06670	-44.23341	11.77120	9.01882	2.75238
-1661.37700	1718.86958	43.84805	4.05090	3.47223	0.57867
-1738.80000	-5391.52591	-50.07601	10.39060	10.21599	0.17461
-1689.40000	-2461.99361	-34.91411	8.18100	7.01087	1.17013
-1684.52400	-7085.15807	-52.92264	11.51980	10.45194	1.06786
-1741.83100	-6725.55080	-75.86991	13.66410	12.78247	0.88163
-1709.31000	-6714.96686	-54.39882	12.51760	10.64855	1.86905
-1735.95500	-4663.95689	-79.18888	10.74870	9.49200	1.25670
-1766.99400	-5677.15054	-89.56402	11.54160	10.85852	0.68308
-1752.30000	-9919.79214	-79.04649	12.13240	13.92812	-1.79572
-1741.70000	-7605.81803	-62.12182	11.09580	11.95573	-0.85993
-1744.90000	-5906.98797	-67.22421	12.18970	10.67837	1.51133
-1741.50000	-4824.48331	-78.40375	11.67060	9.72935	1.94125
-1743.50000	-7404.40155	-85.25206	12.14930	12.06555	0.08375
-1765.80000	-5687.70697	-87.56445	12.11760	10.85009	1.26751
-1763.20000	-6291.71573	-63.03944	11.71680	11.35428	0.36252
-1763.51200	-7145.49419	-67.59366	12.76340	12.00946	0.75394
-1779.10000	-6299.04540	-85.44558	13.39980	11.59643	1.80337
-1654.30000	-5494.16242	-66.89056	7.84740	8.55920	-0.71180
-1727.20000	-5182.41488	-50.66604	9.91610	9.82179	0.09431
-1750.90000	-6509.64997	-69.23675	11.85470	11.25928	0.59542
-1731.90000	-5422.32021	-61.47257	9.62000	10.06395	-0.44395
-1671.47500	-1765.84359	-32.86191	7.71180	6.12155	1.59025
-1704.30000	-3853.23173	-35.65730	7.92990	8.38621	-0.45631
-1712.70000	-6268.40674	-63.51061	10.45030	10.33616	0.11414
-1729.00000	1604.25430	75.33572	3.52560	5.01054	-1.48494
-1655.40000	-5767.19097	-81.81318	6.87590	8.74948	-1.87358
-1698.40000	-3756.18308	-37.54293	5.37780	8.18745	-2.80965
-1662.60000	-3610.98654	-78.34002	6.90200	7.22485	-0.32285
-1680.00000	-8083.25584	-82.31790	11.15110	11.03827	0.11283
-1714.10000	-8649.65341	-66.59135	13.91430	12.20740	1.70690

Goodness of Fit = 0.670087

Correlation Coefficient = 0.818549

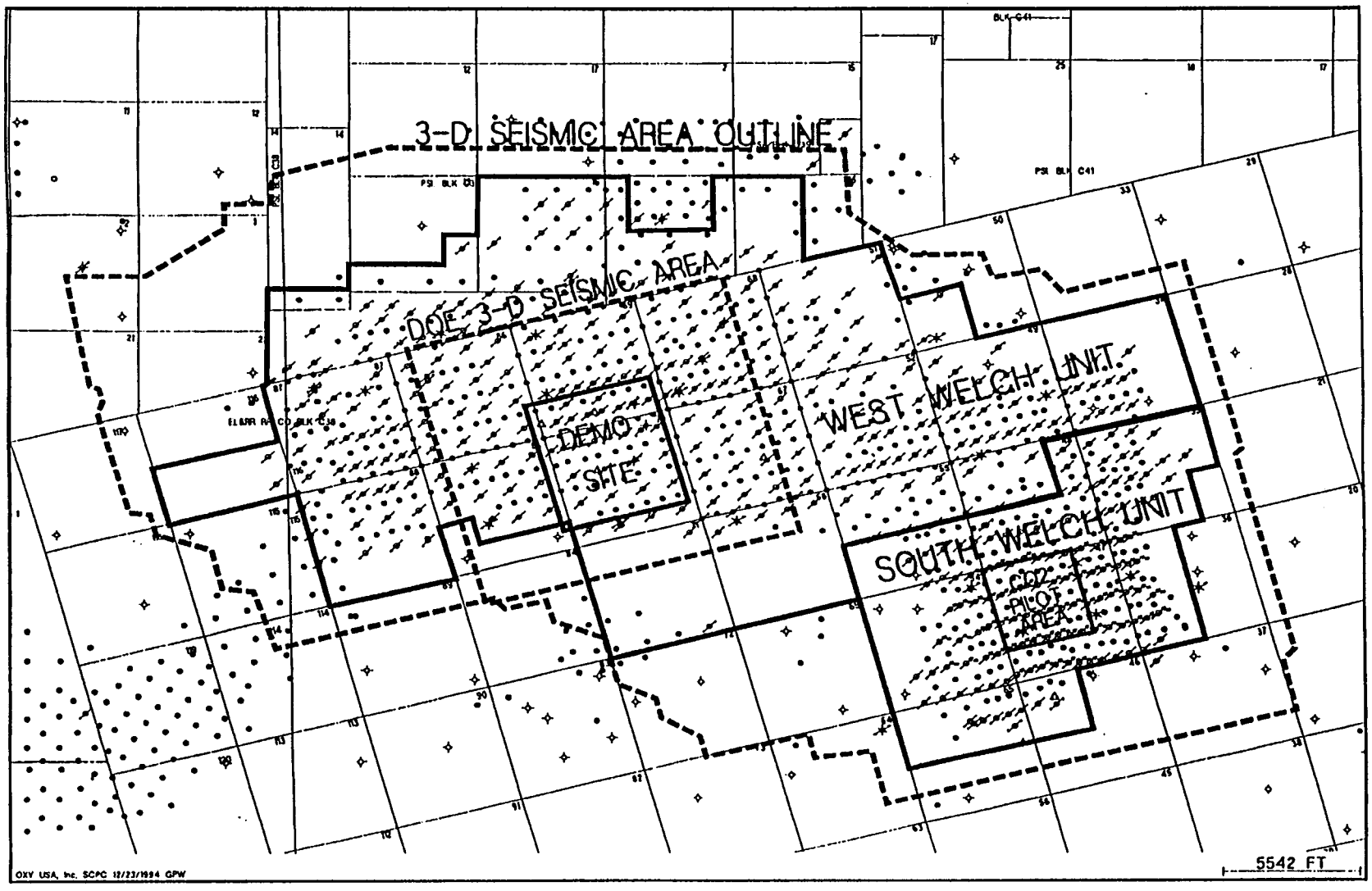

Figure 1-4 - Welch Field showing 3-D Seismic Areas.

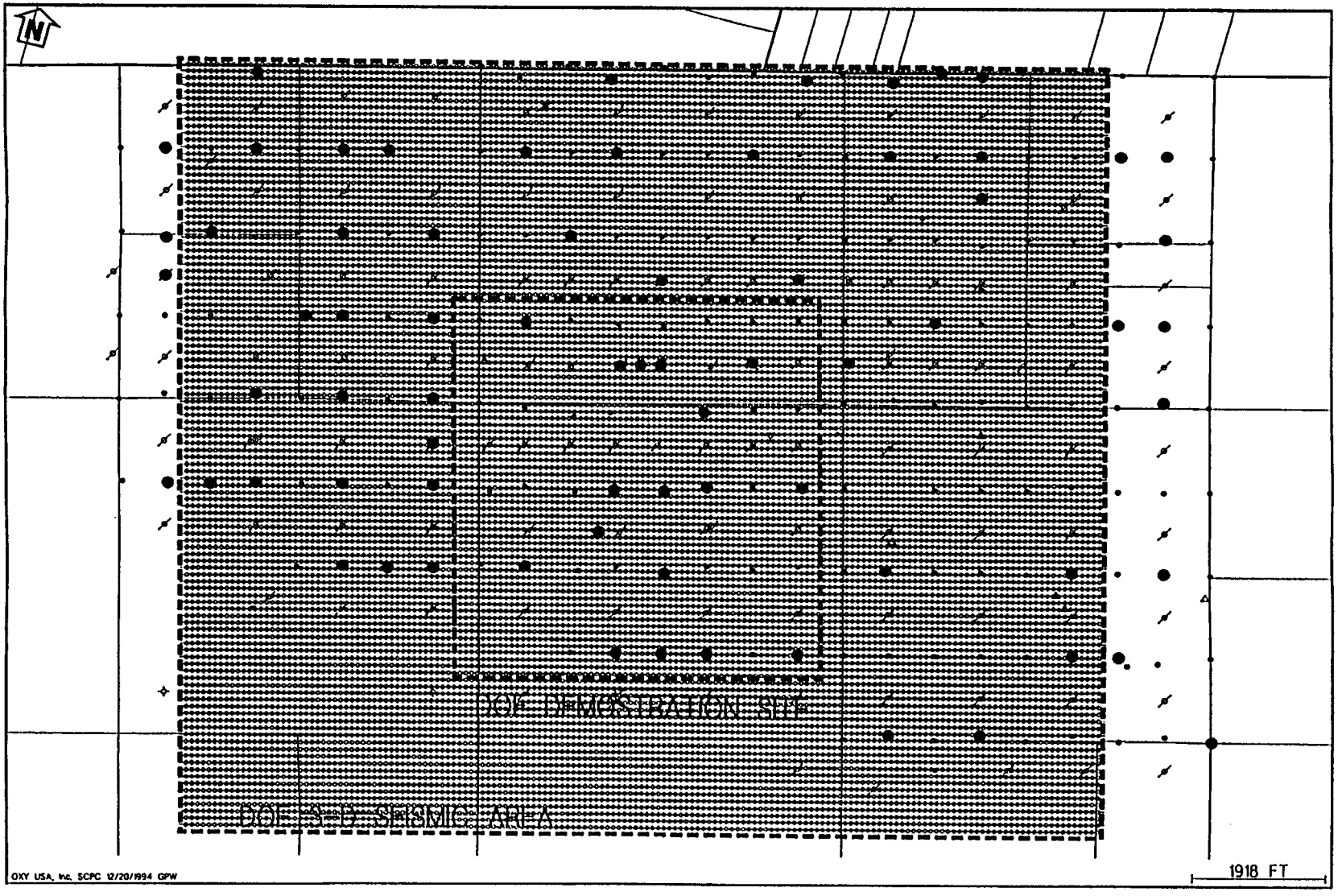

Figure 2-4- Base Map of Wells, Wells with Modern Logs and/or Cores and 3-D Seismic Bins.

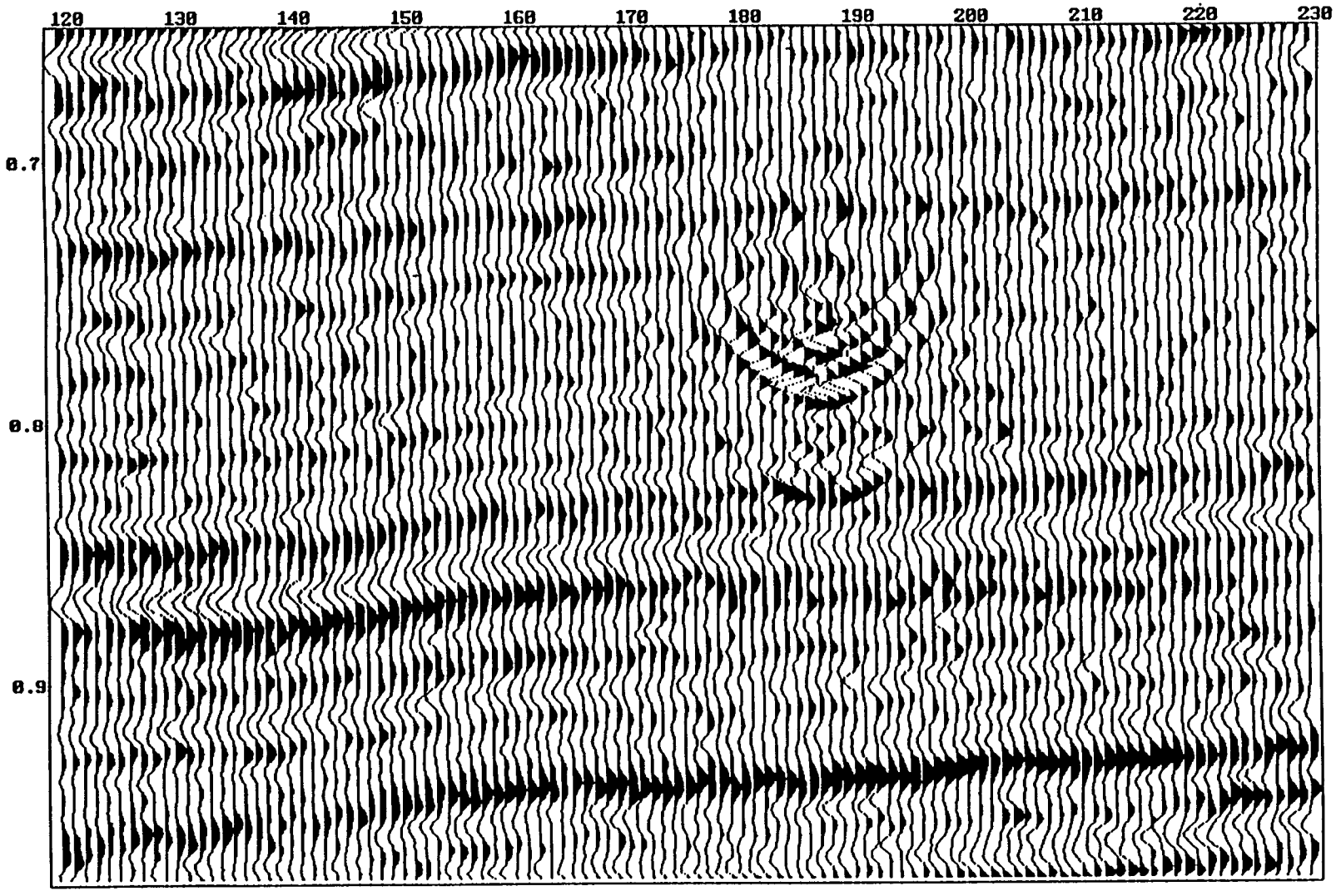

Figure 3-4 - Representative Line from Volume originally processed in 1993.

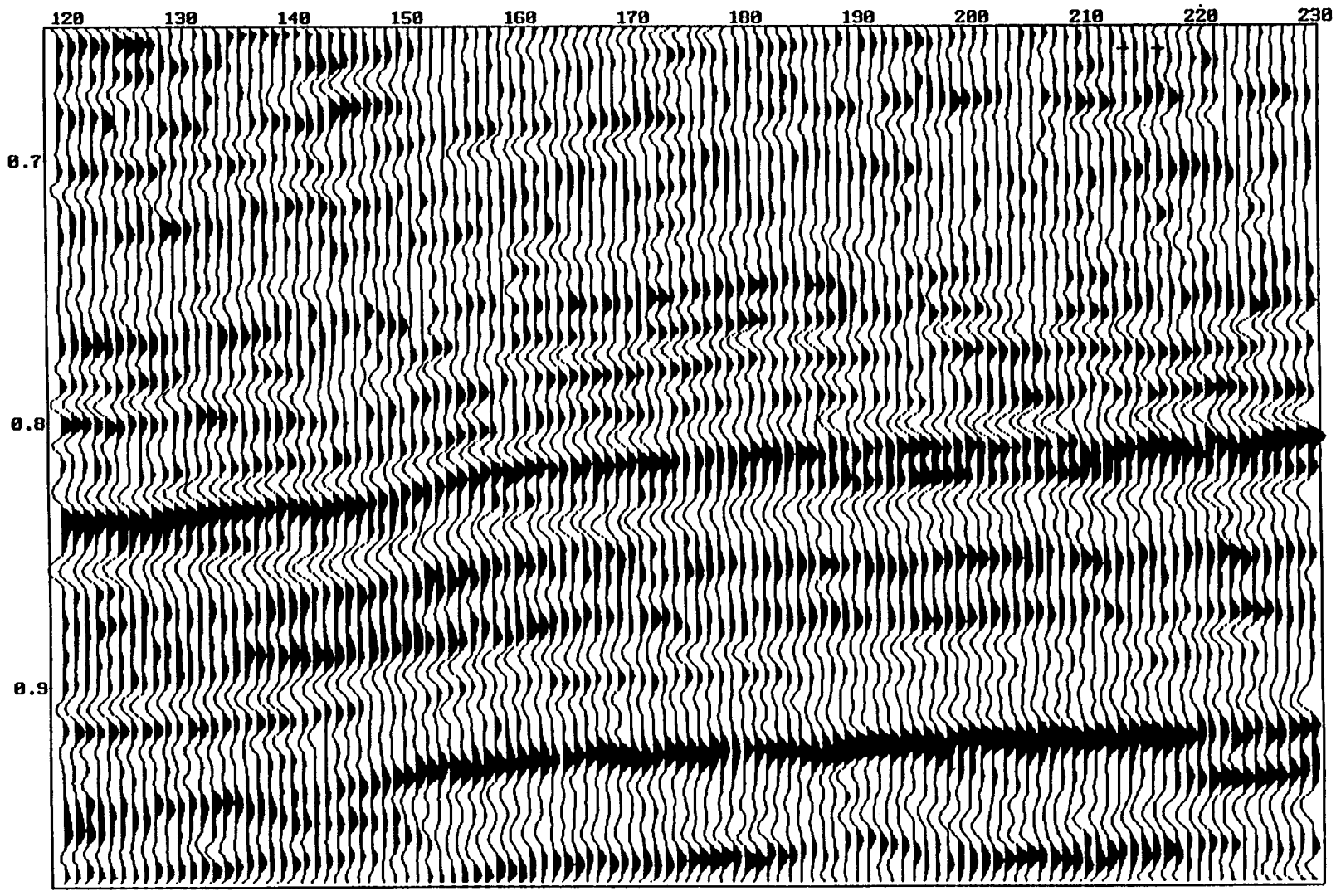

Figure 4-4 - Representative Line from Volume reprocessed in 1996. Same Line as Figure 3.

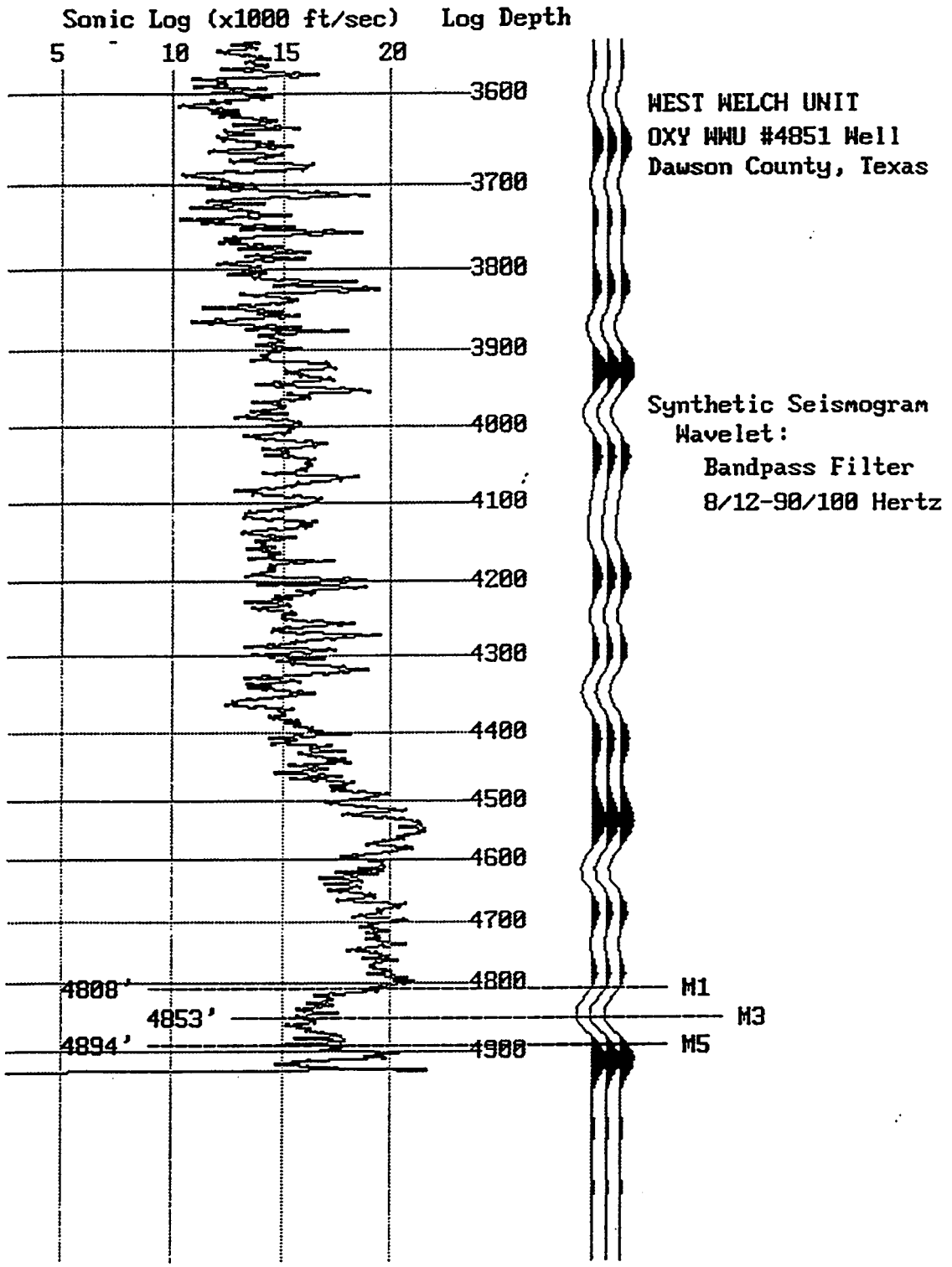

Figure 5-4 - Synthetic Seismogram.

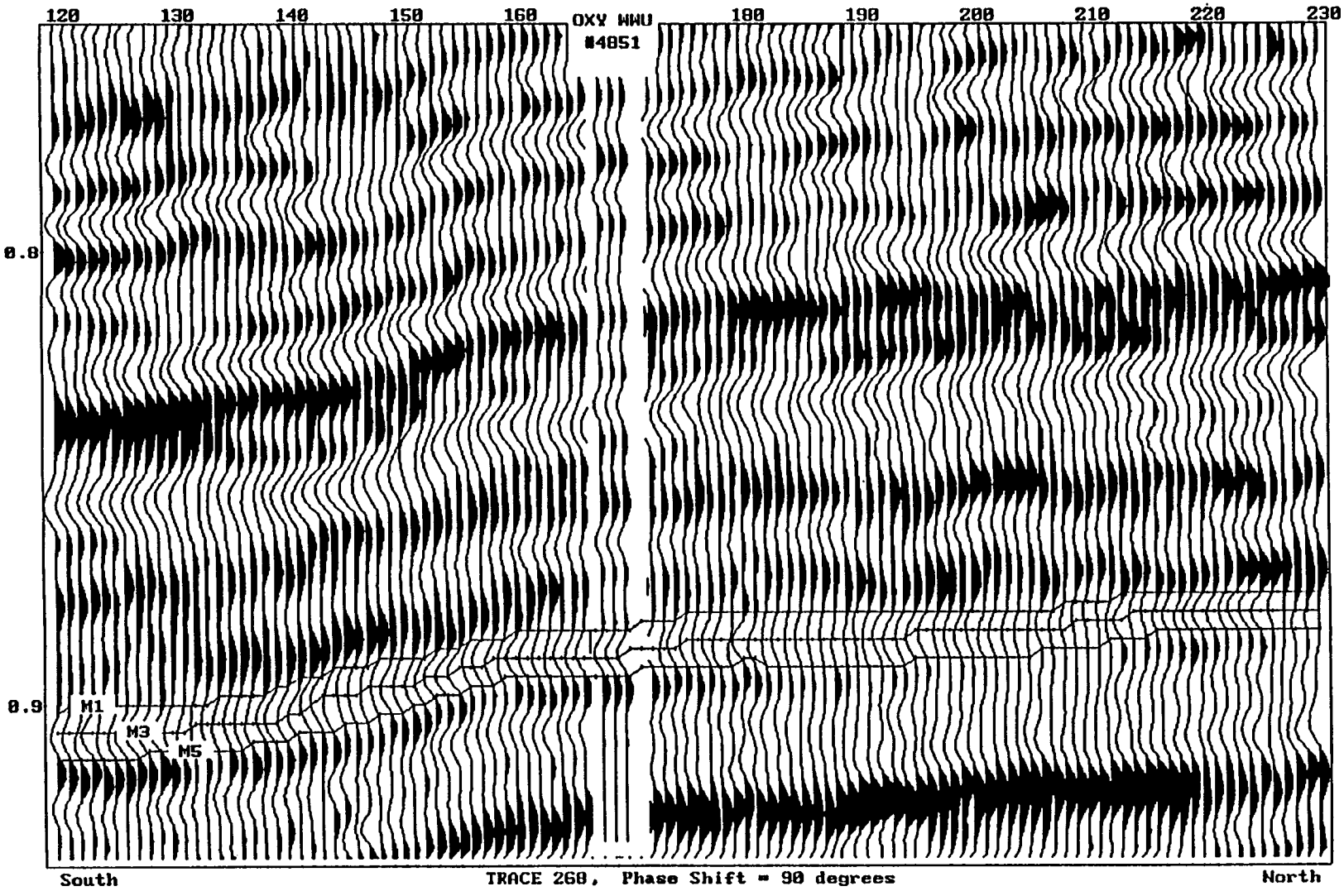

Figure 6-4 - Seismic Line tied to Synthetic Seismogram in Figure 5.

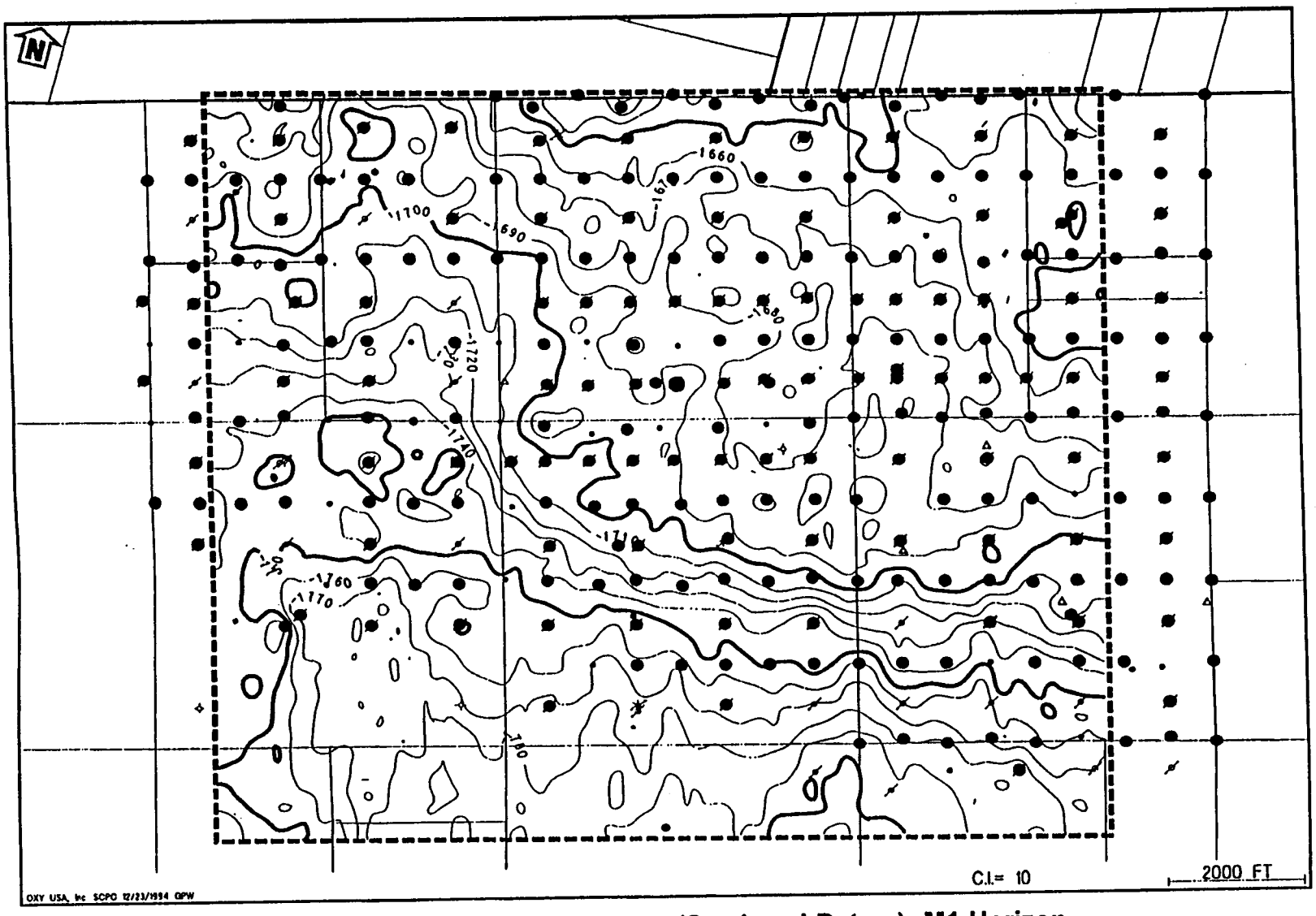

Figure 7-4 - Seismic Structure (Sea Level Datum): M1 Horizon.

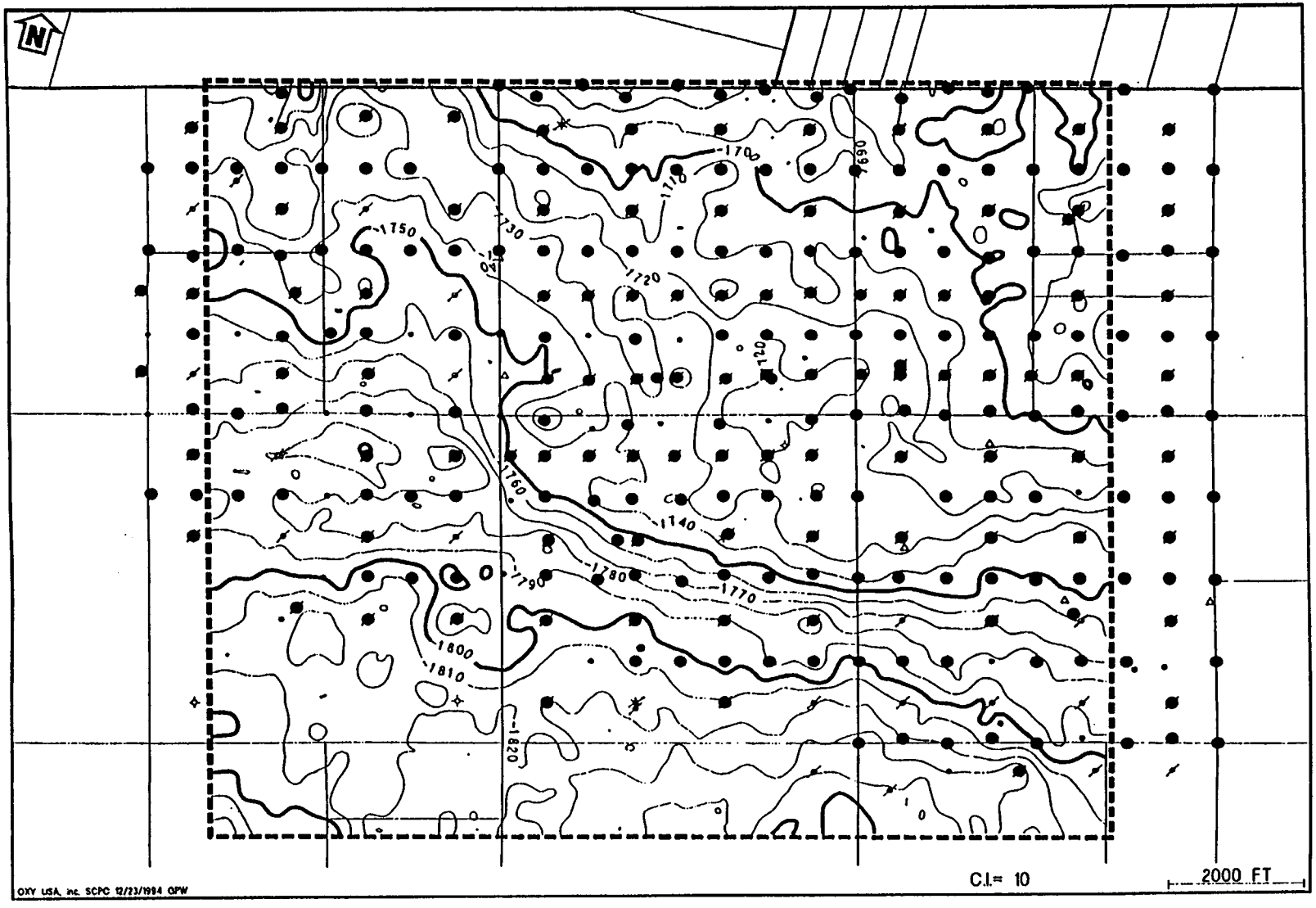

Figure 8-4 - Seismic Structure (Sea Level Datum): M3 Horizon.

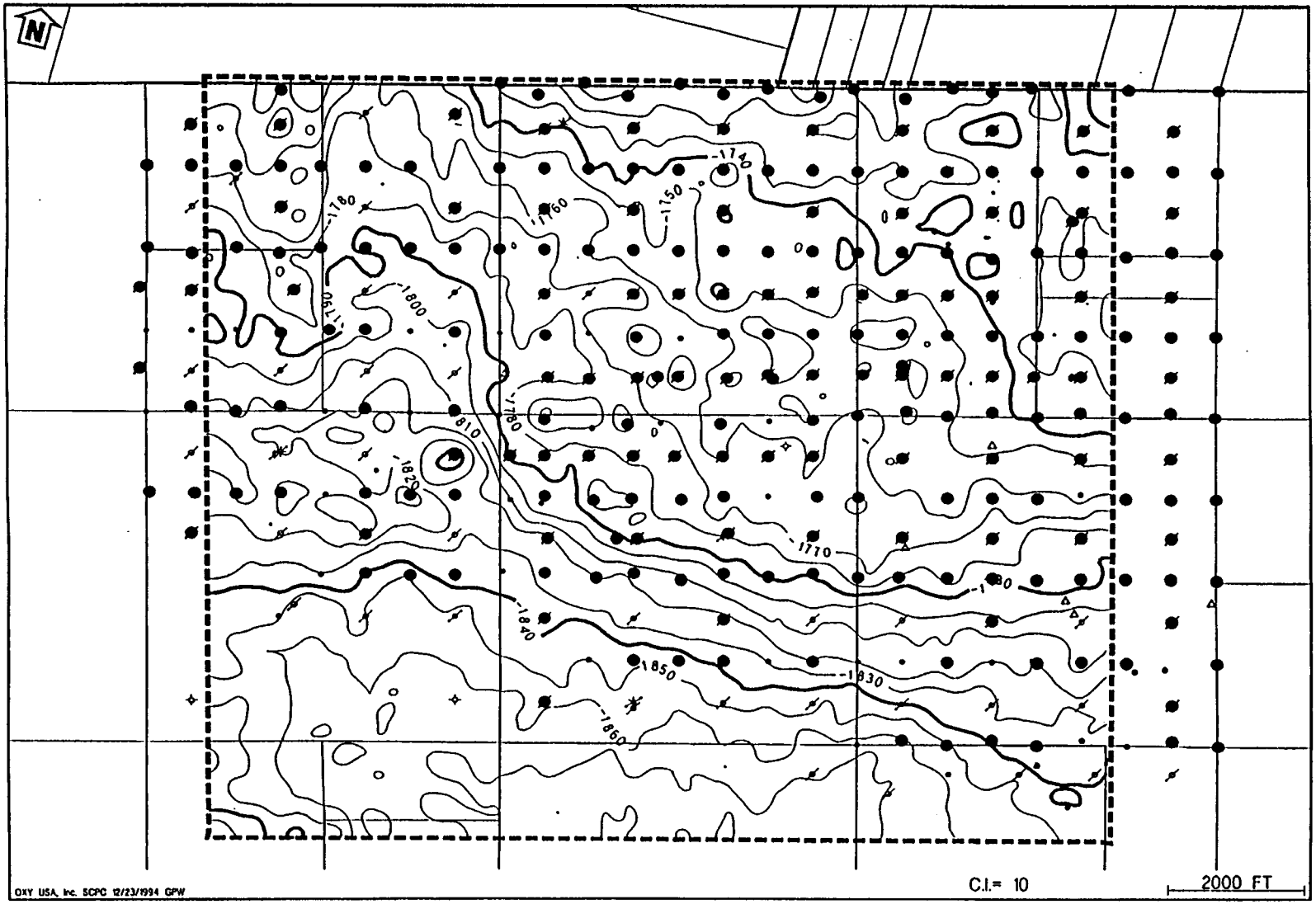

Figure 9-4 - Seismic Structure (Sea Level Datum): M5 Horizon.

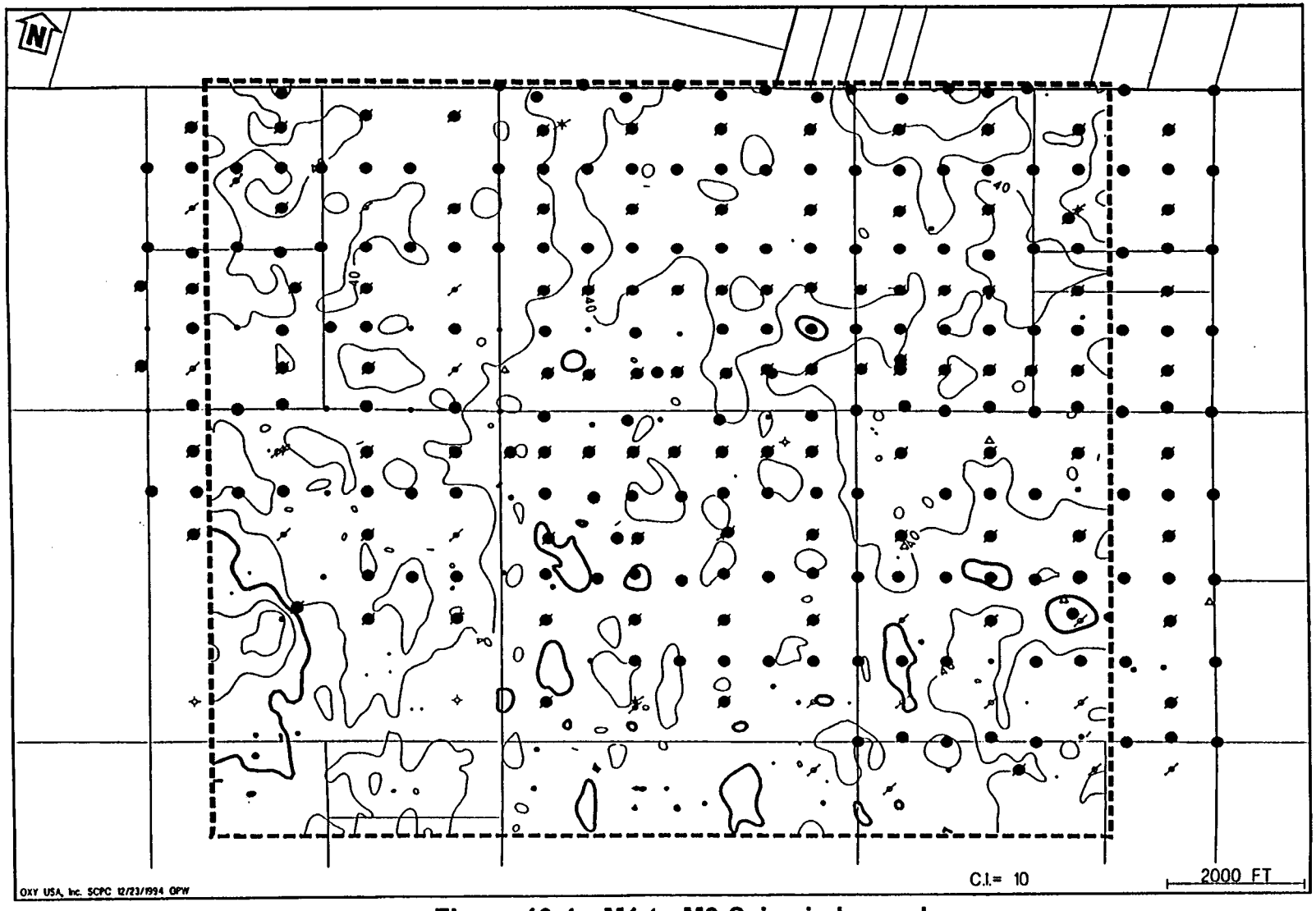

Figure 10-4 - M1 to M3 Seismic Isopach.

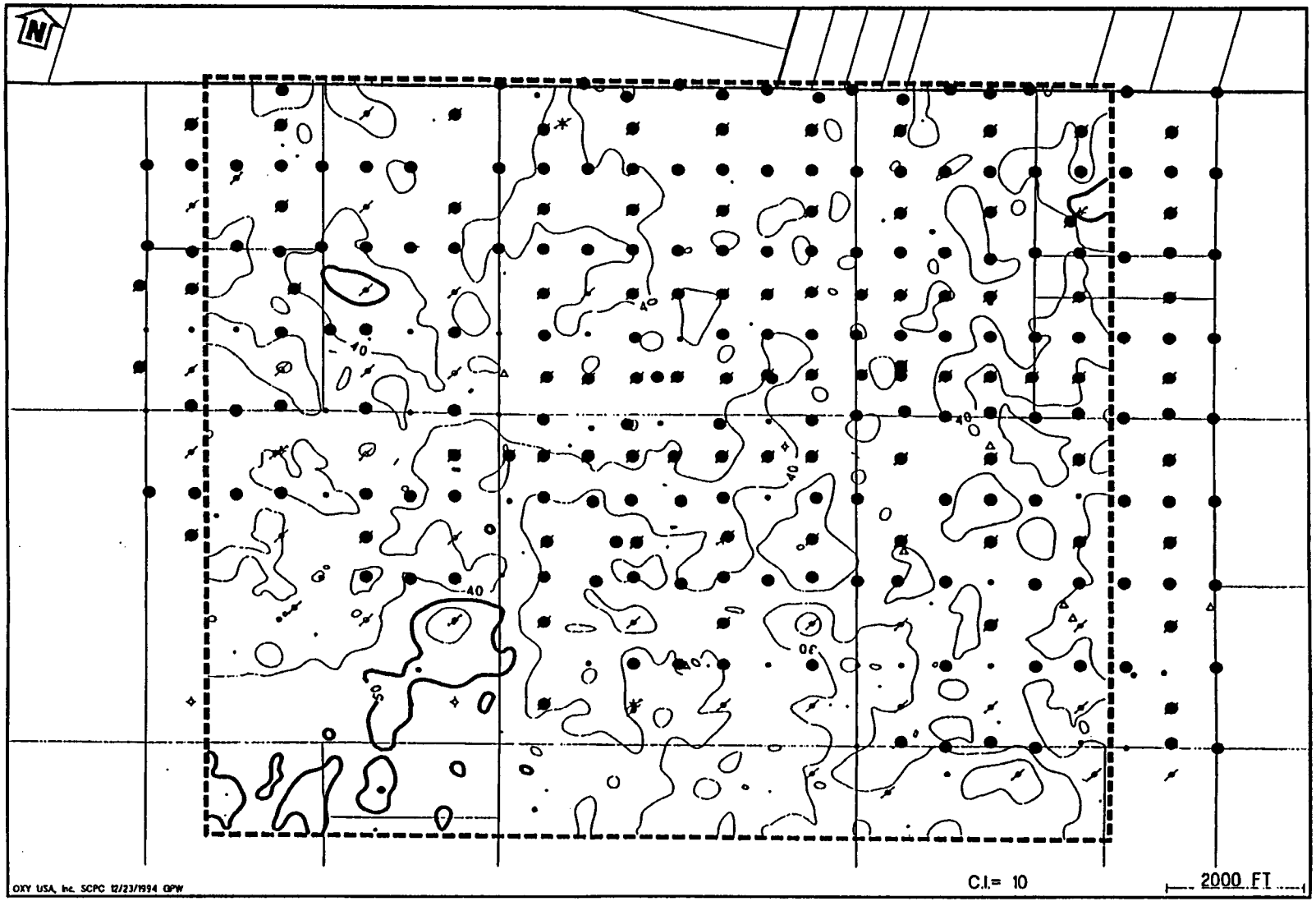

Figure 11-4 - M3 to M5 Seismic Isopach.

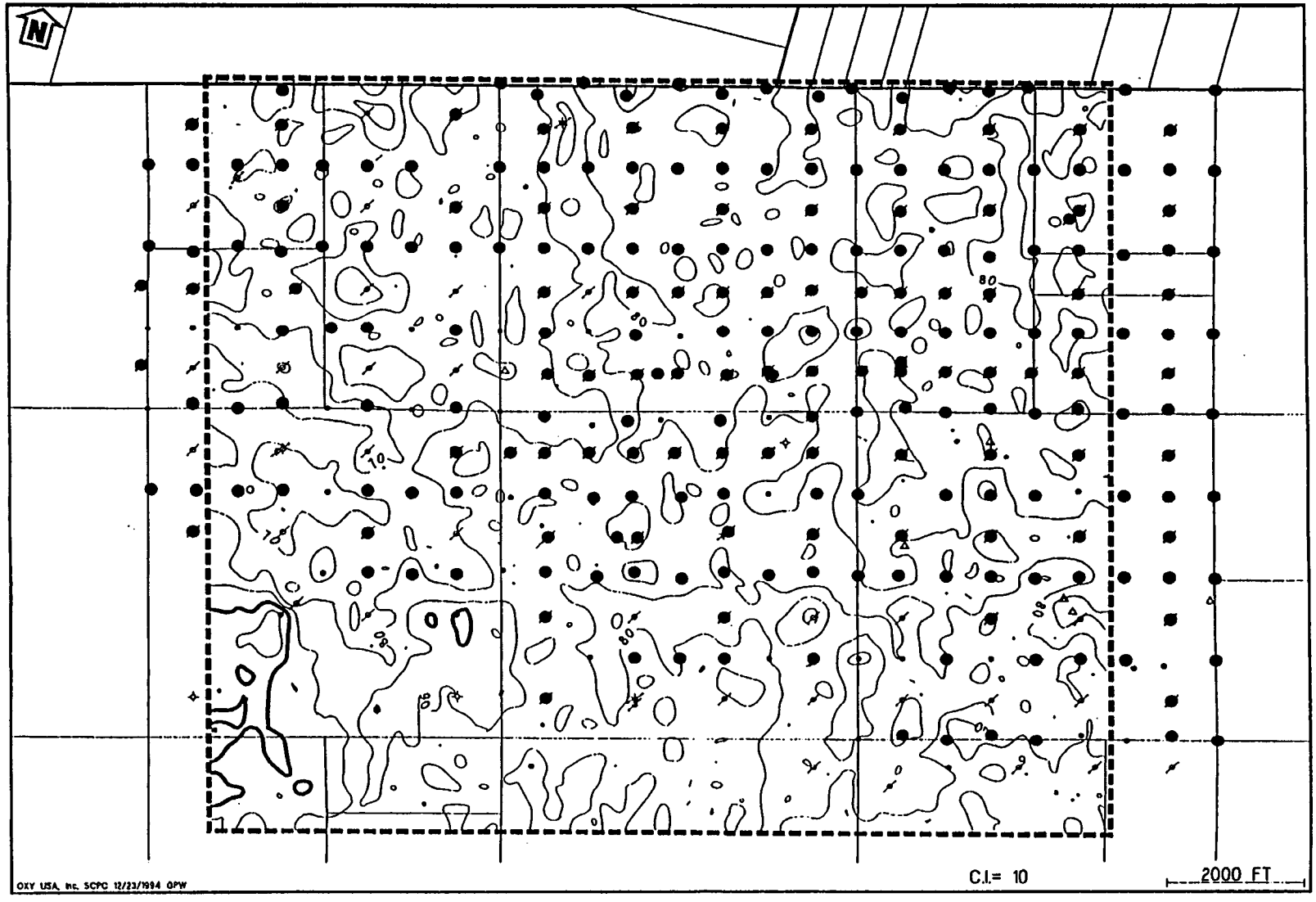

Figure 12 -4- M1 to M5 Seismic Isopach.

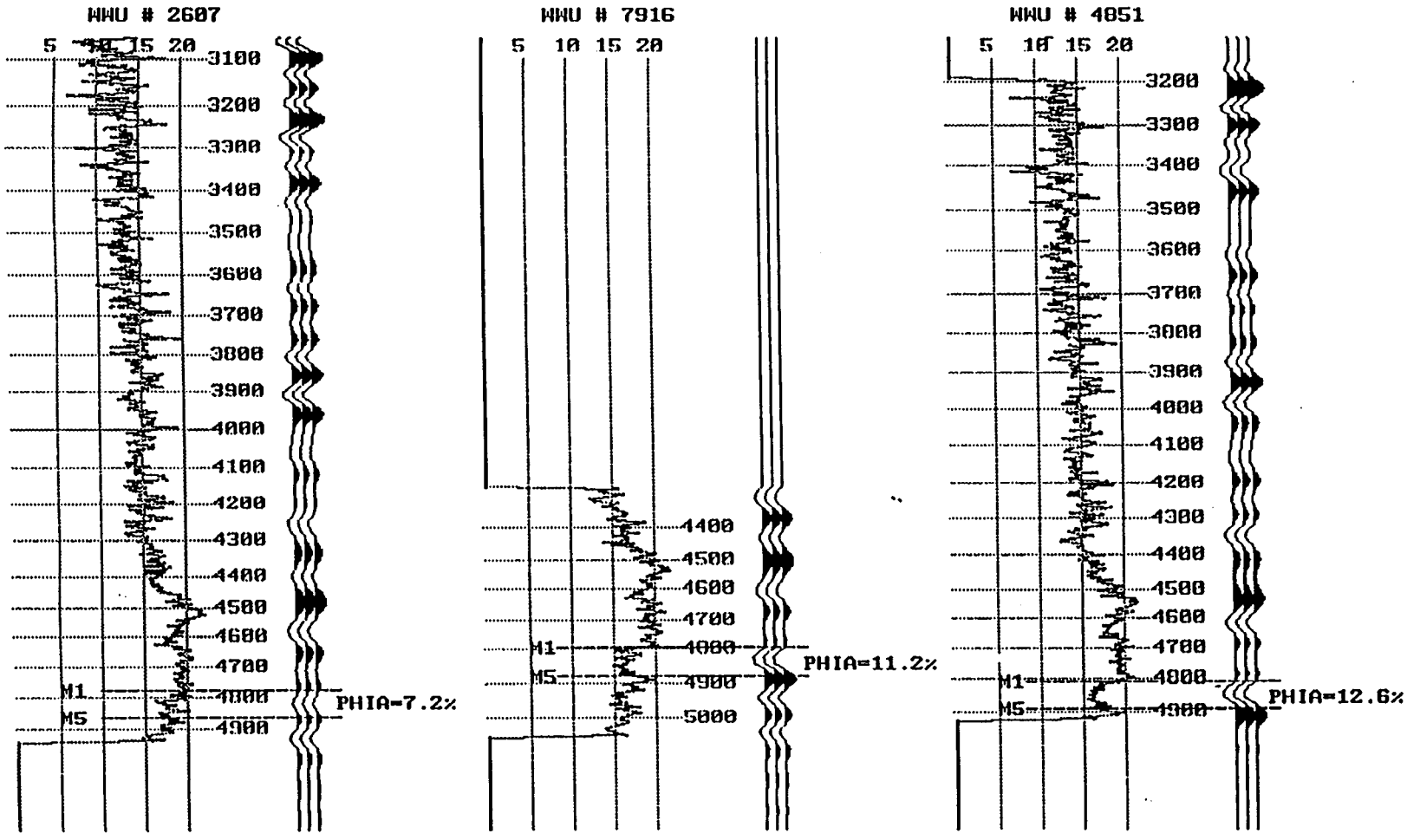

Figure 13-4 - Amplitude from Sonic Reflectivity is directly proportional to Average Porosity.

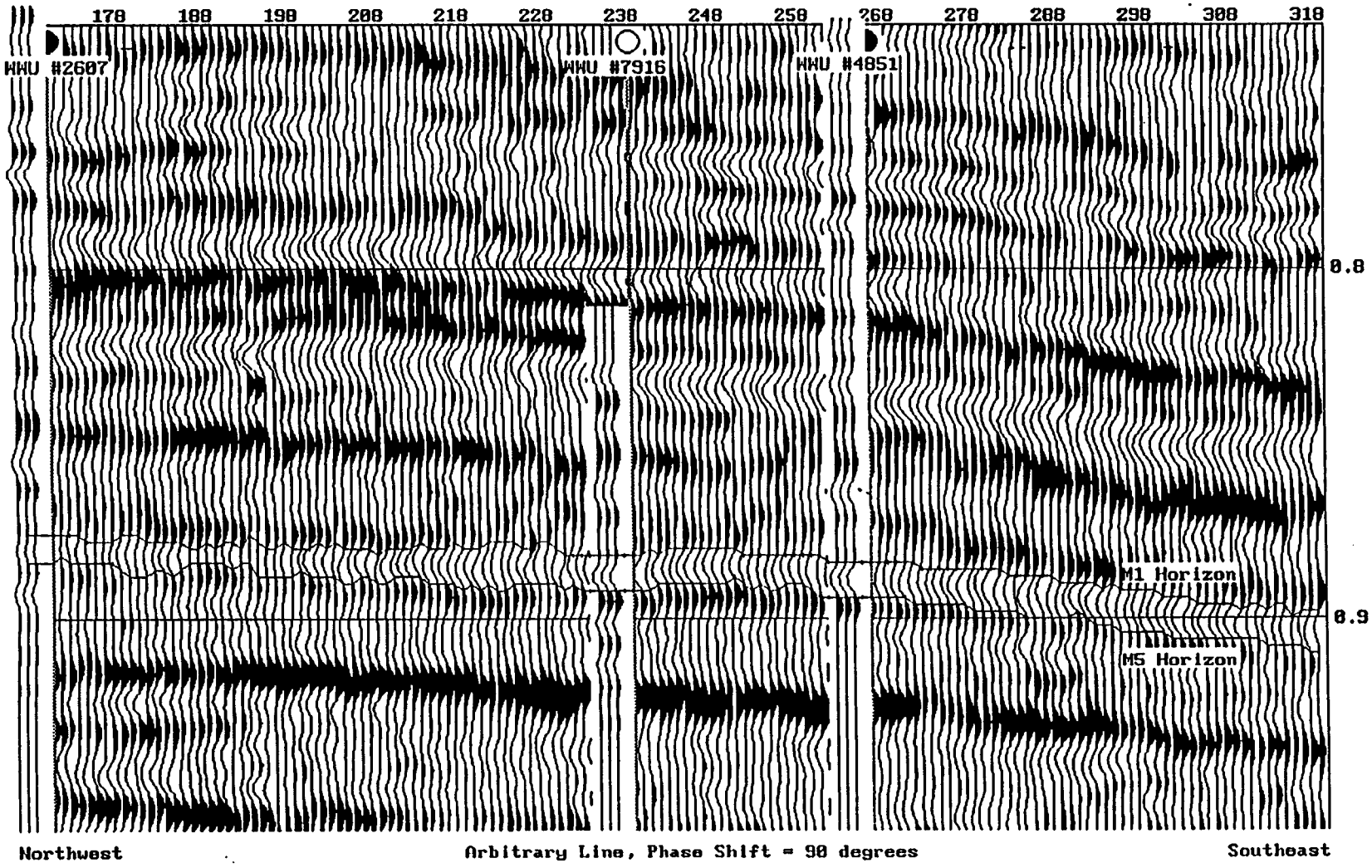

Figure 14-4 - Amplitude from Seismic Reflectivity decreases to the Northwest.

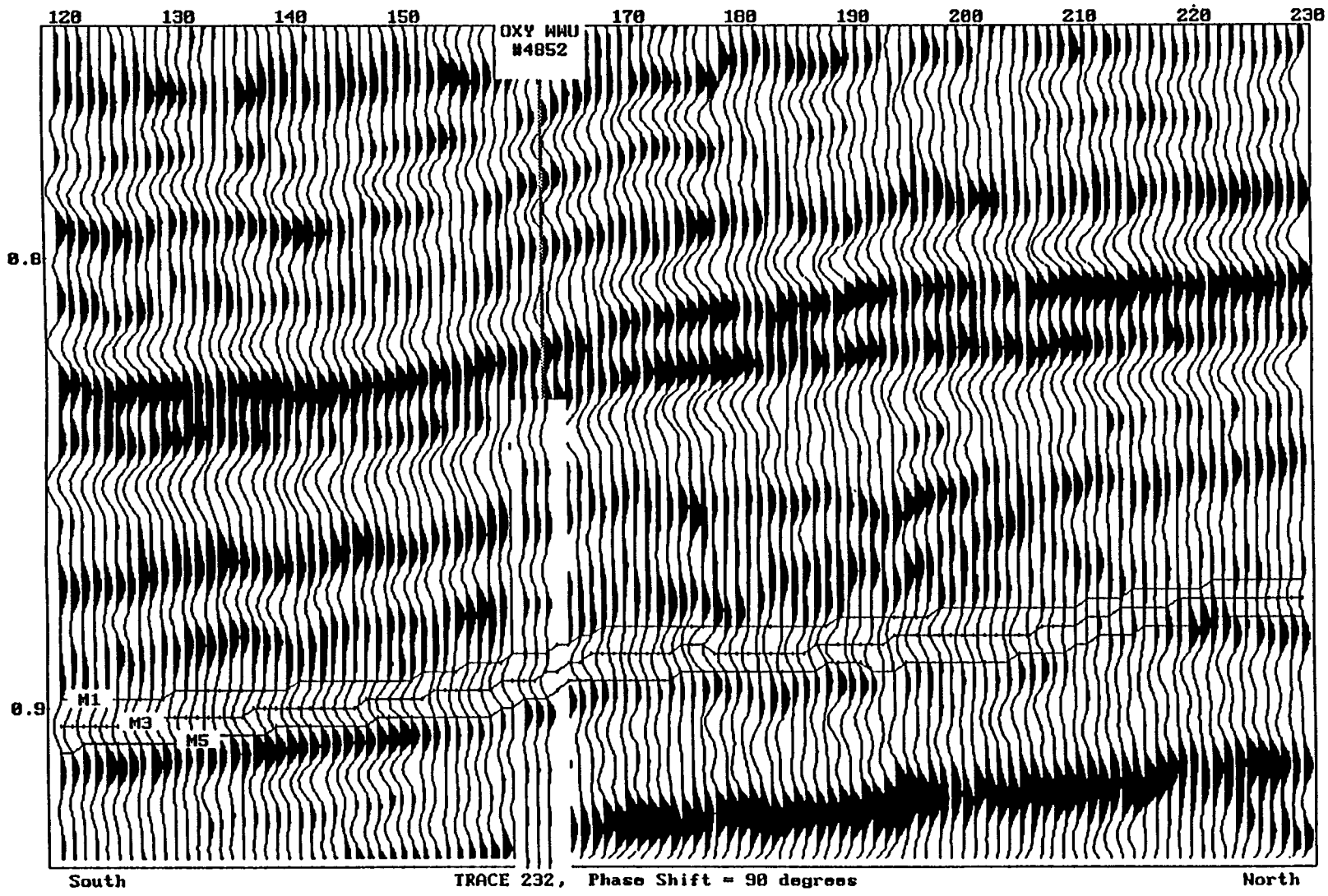

Figure 15-4 - Sporadic Peaks within the Trough bounding the Reservoir Interval.

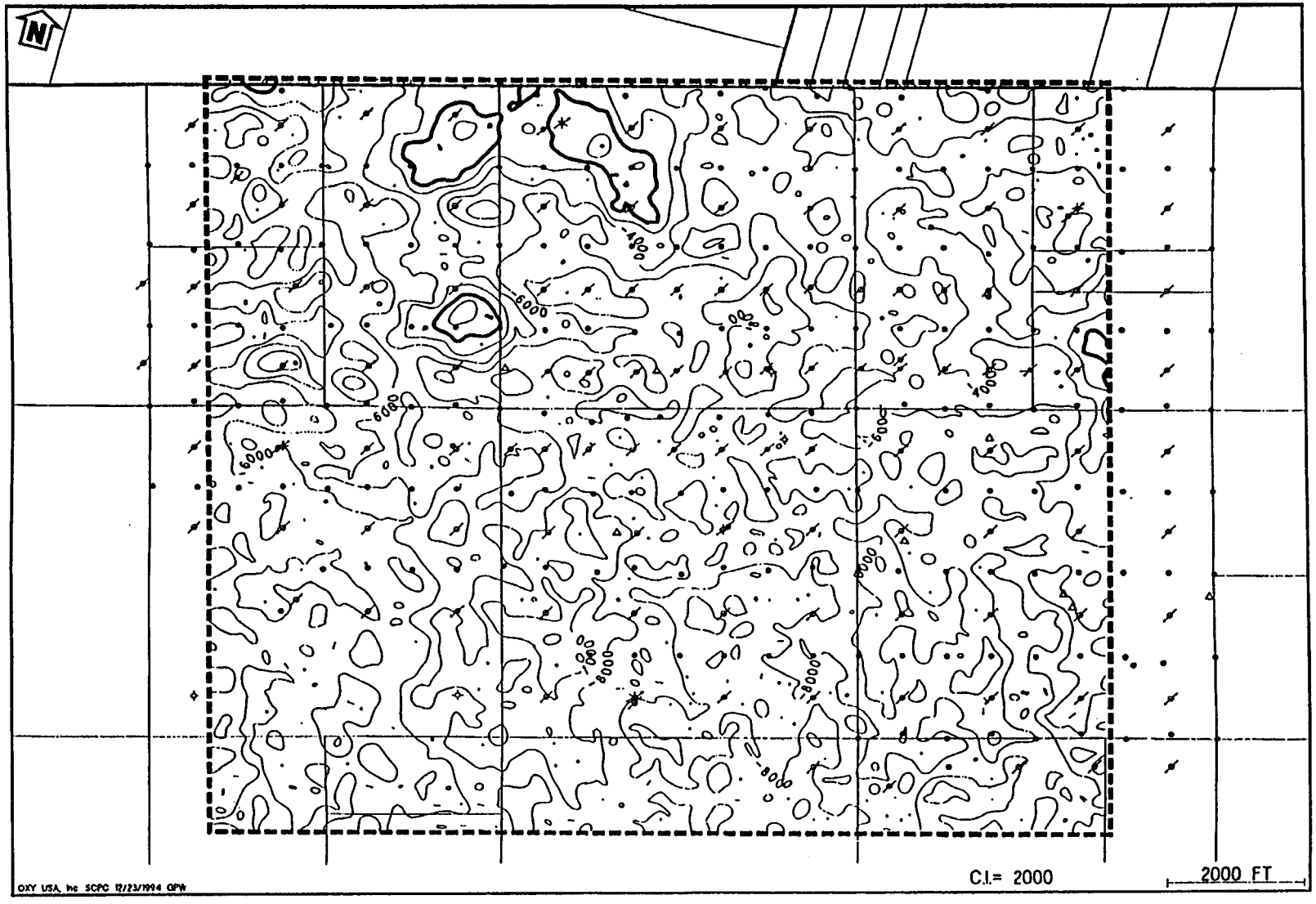

Figure 16-4 - Relative Seismic Amplitude: M3 Horizon.

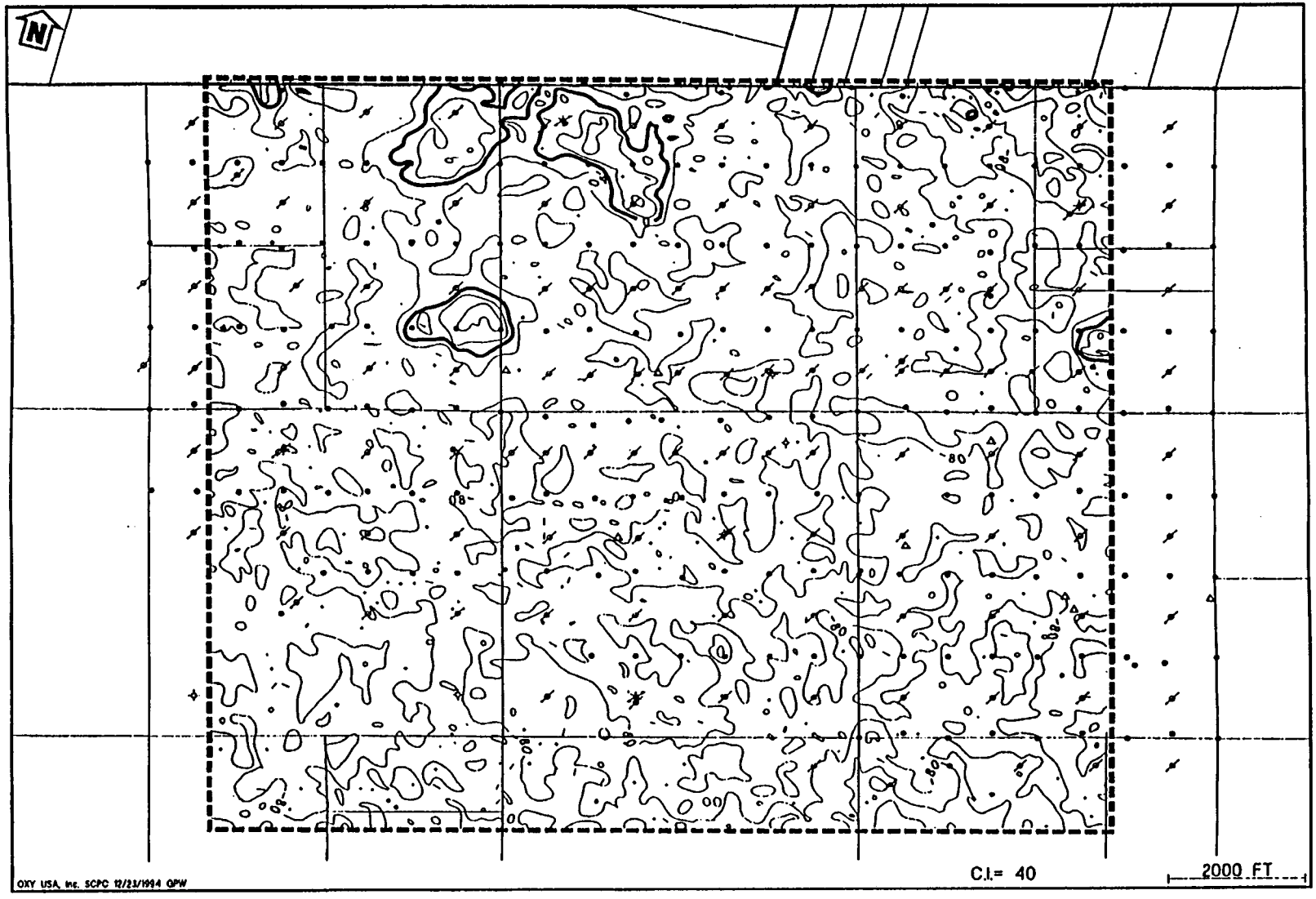

Figure 17-4 - Summed Instantaneous Seismic Phases: M1 to M5 Interval.

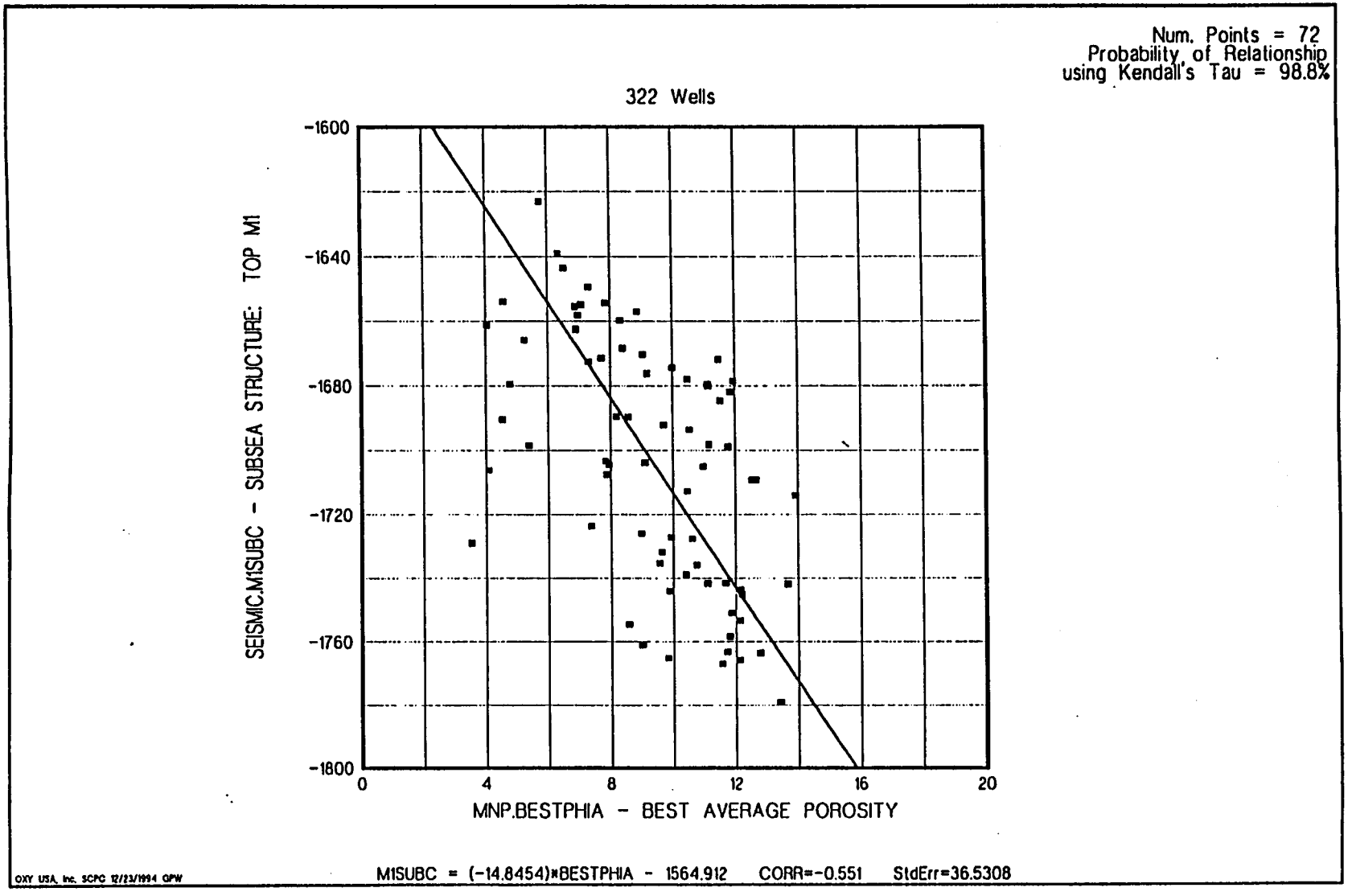

Figure 18-4 - Average Porosity versus M1 Structure.

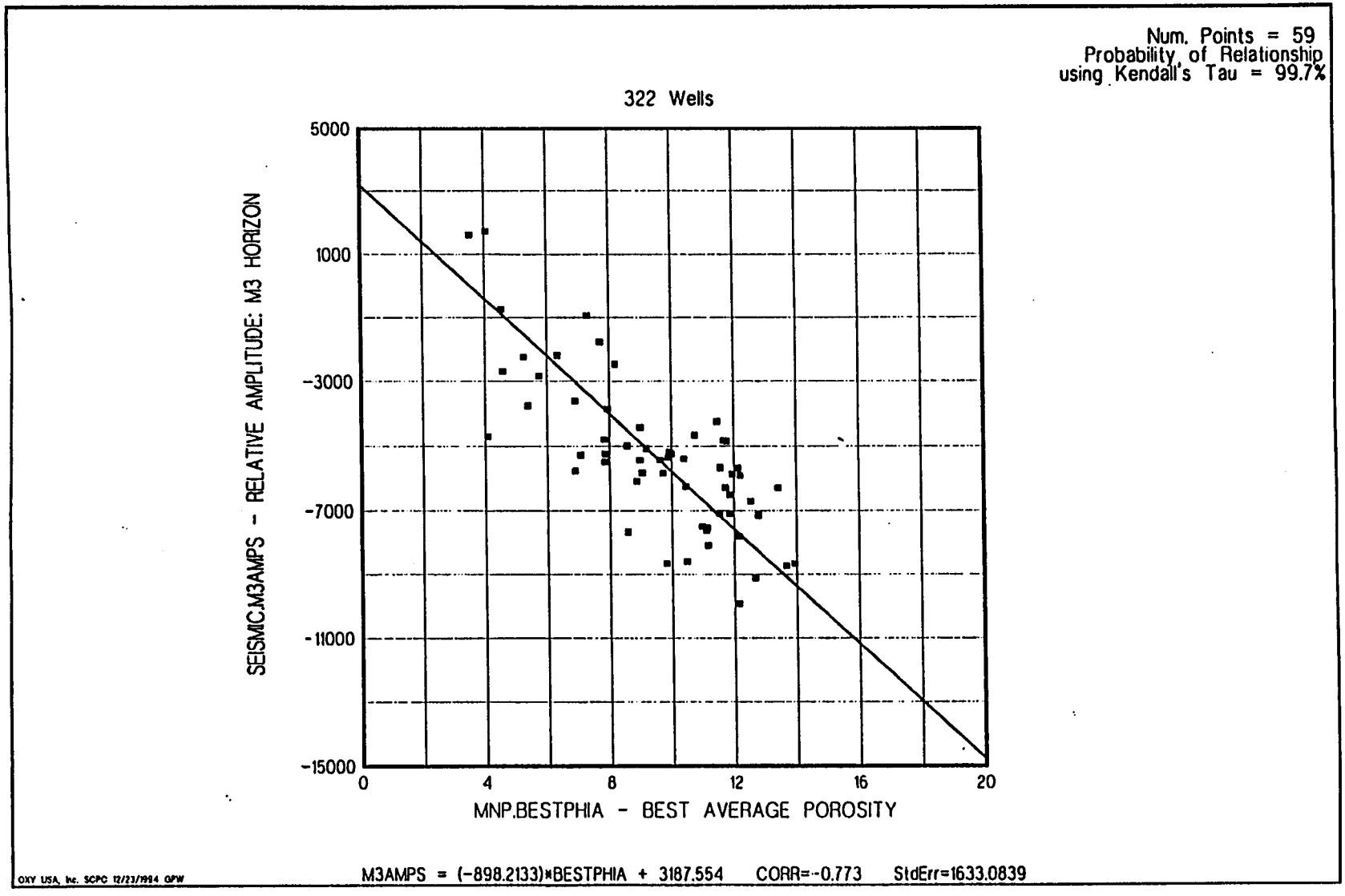

Figure 19-4 - Average Porosity versus M3 Relative Amplitude.

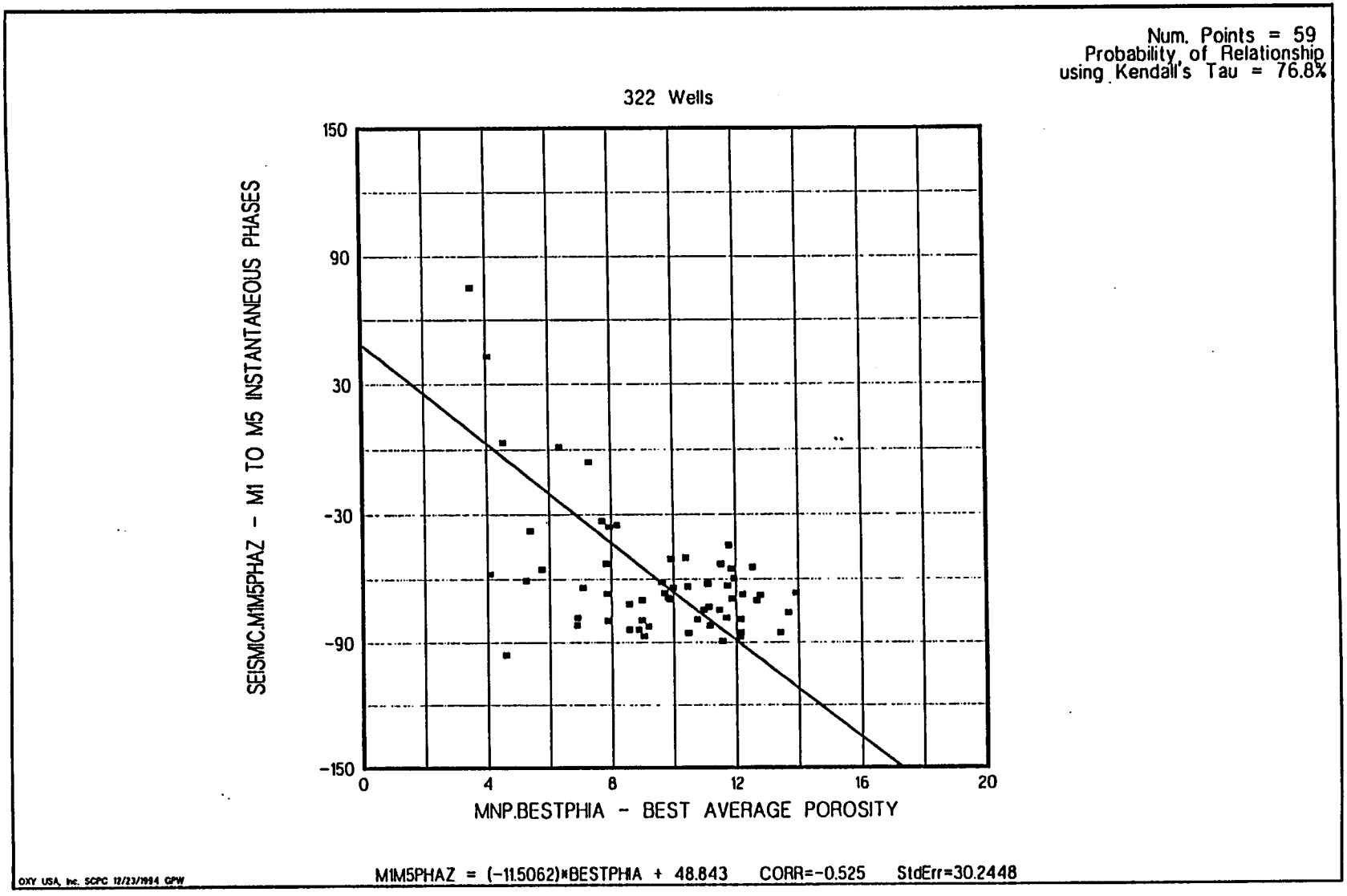

Figure 20-4 - Average Porosity versus M1 to M5 Summed Instantaneous Phases.

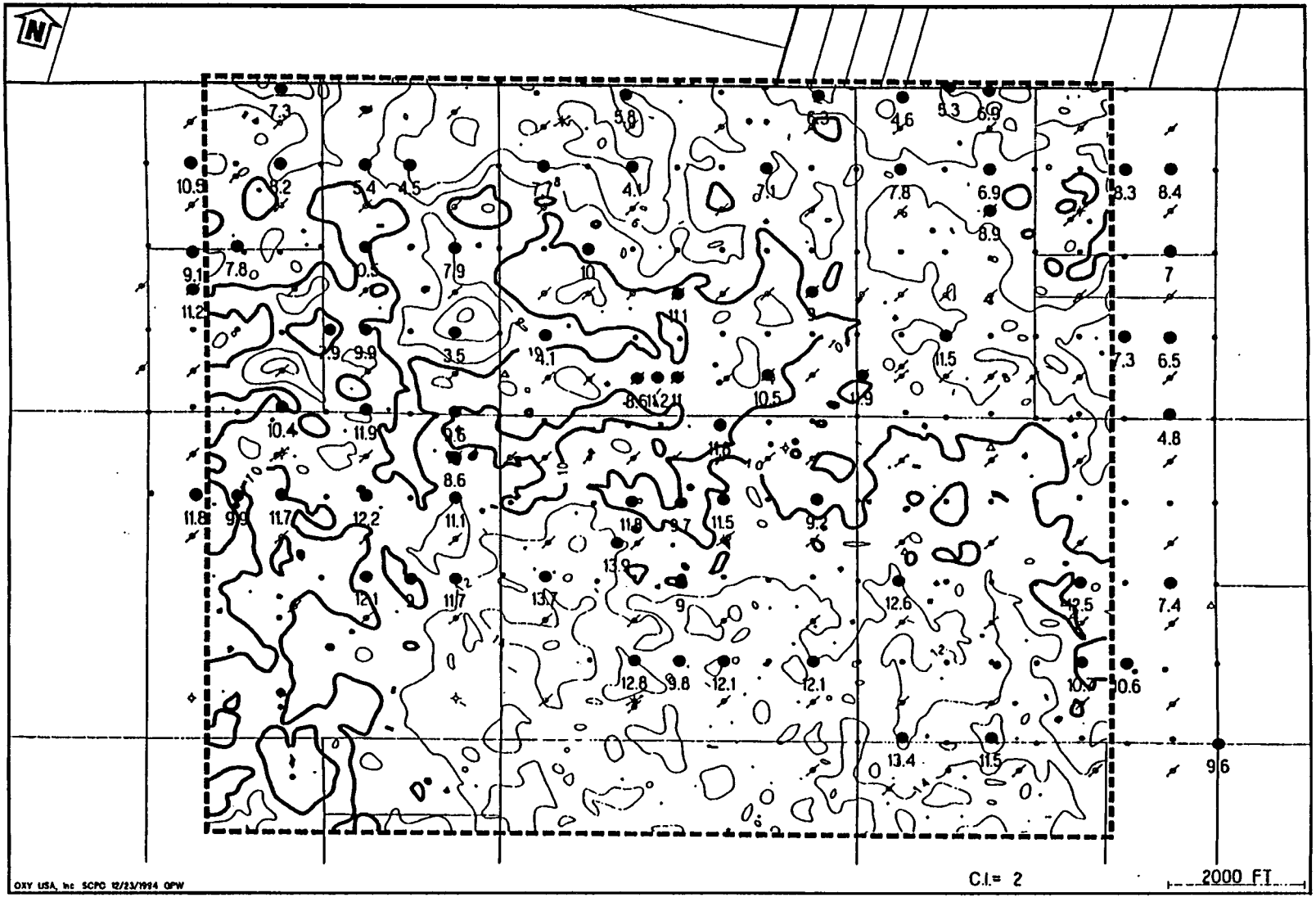

Figure 21-4 - M1 to M5 Seismic Predicted Average Porosity (PHIA).

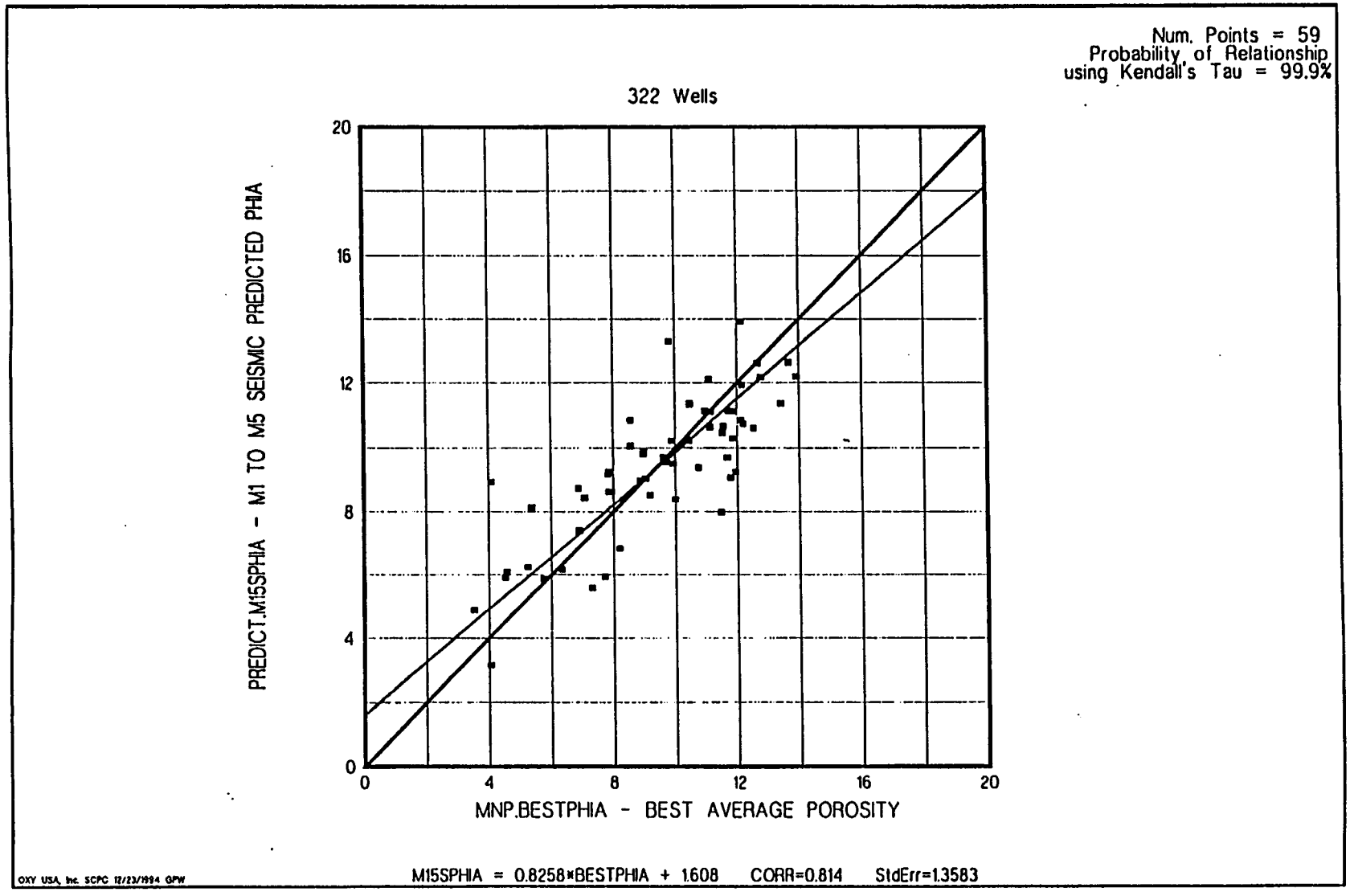

Figure 22-4 - Average Porosity: Well Data versus Seismic Predictions.

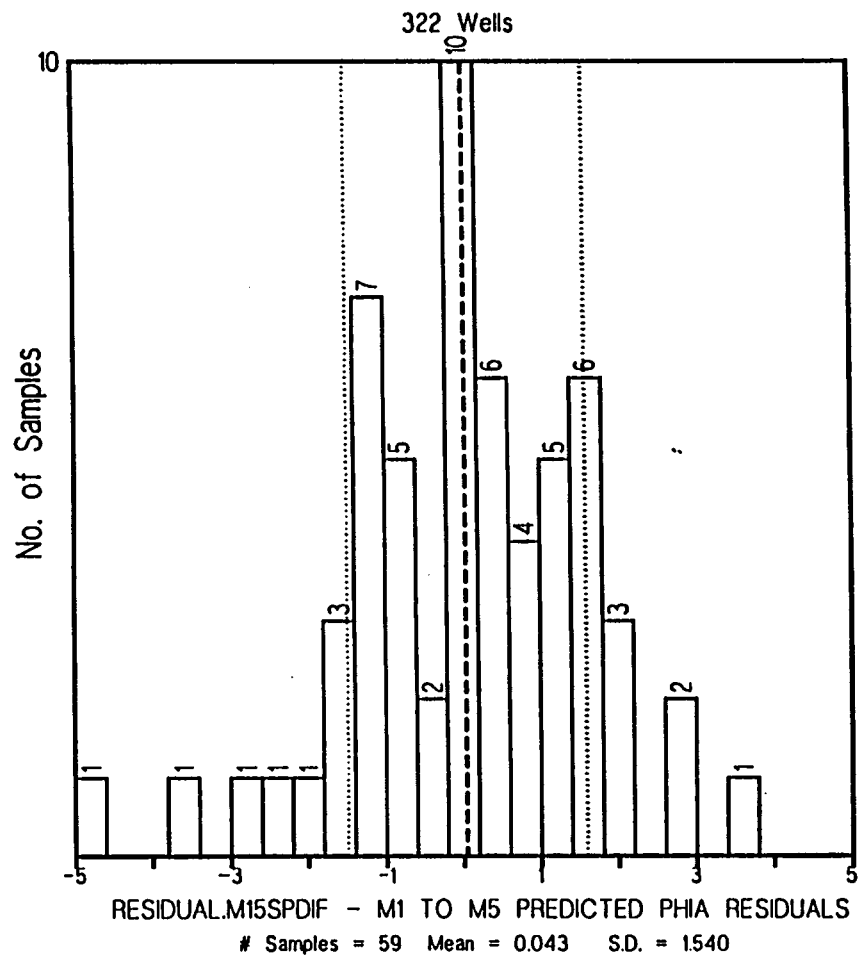

OXY USA, Inc. SCPC 12/23/1994 GPW

Figure 23-4 - PHIA Residuals from Seismic Predictions.

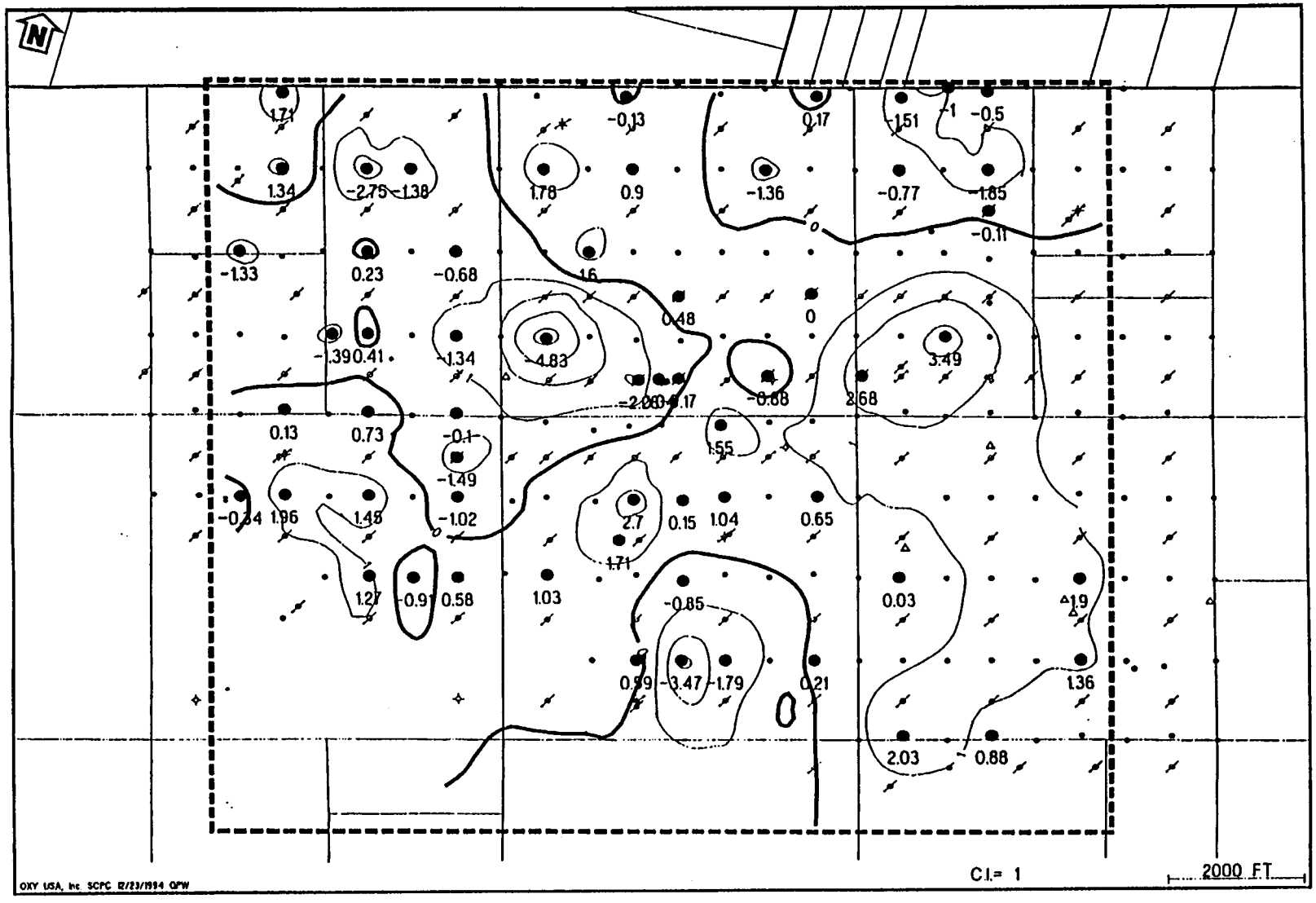

Figure 24-4 - M1 to M5 PHIA Residuals (Well Data - Seismic Predictions).

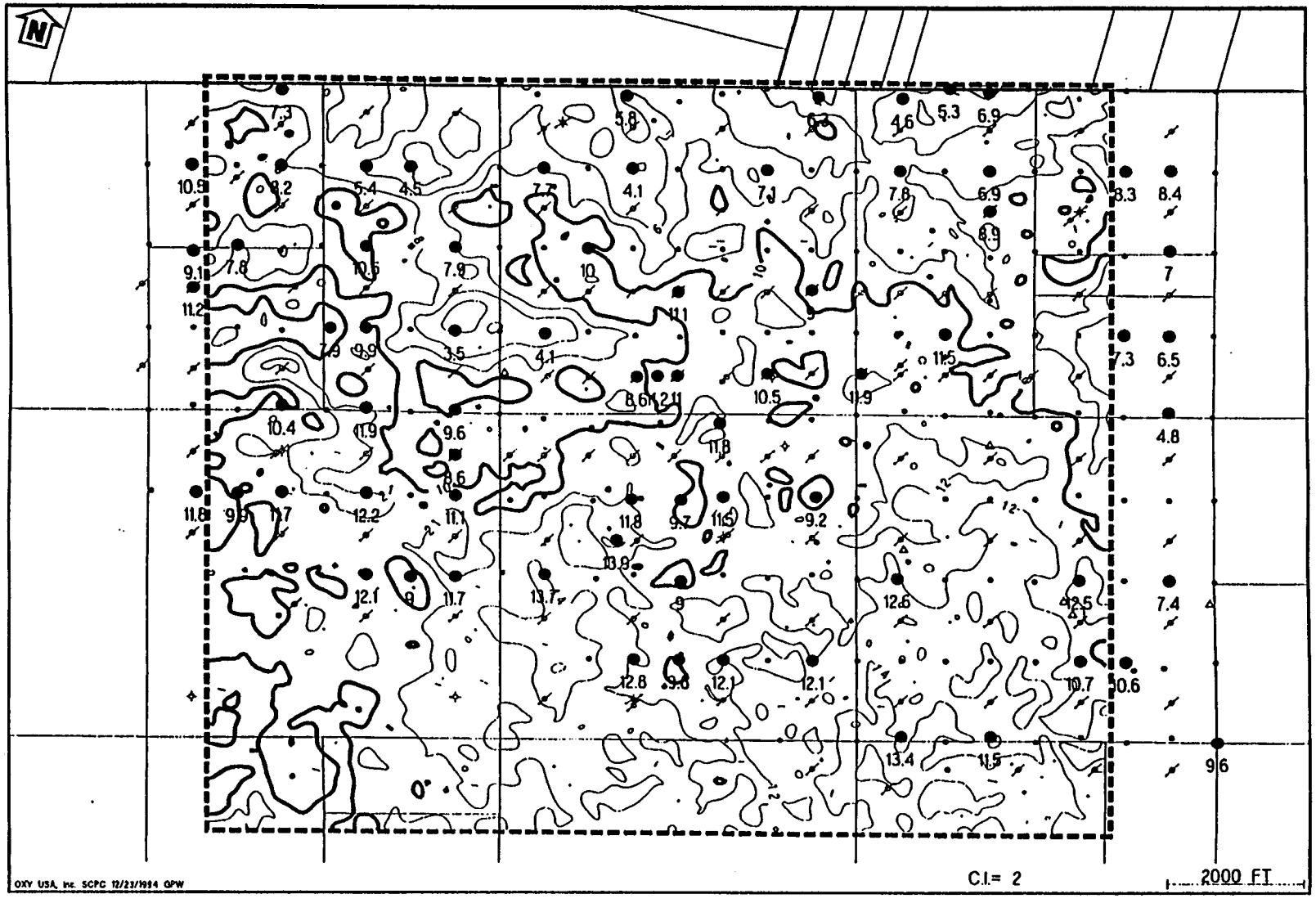

Figure 25-4 - M1 to M5 Seismic-Guided Average Porosity.

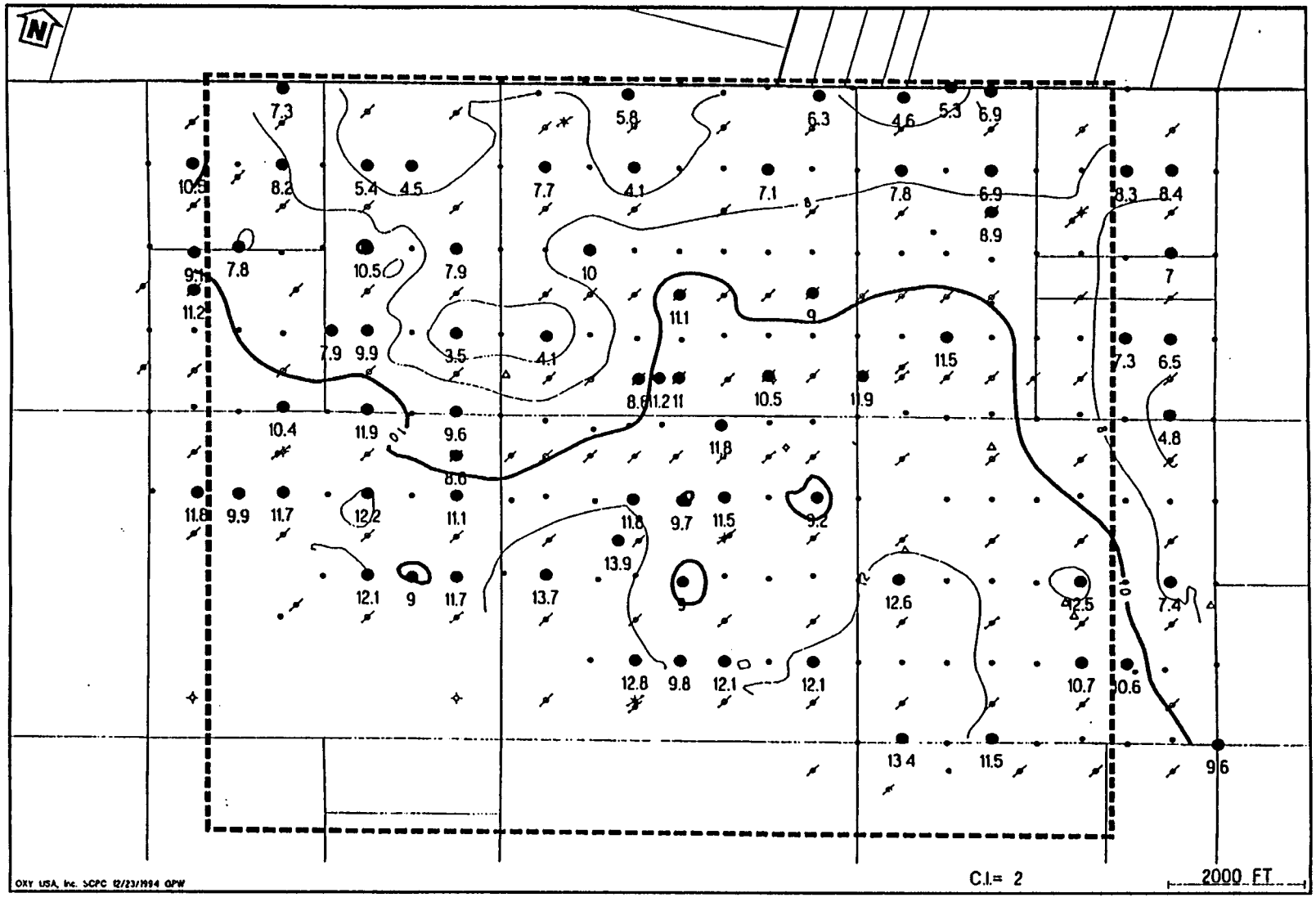

Figure 26-4 - M1 to M5 Average Porosity (PHIA) from Well Data.

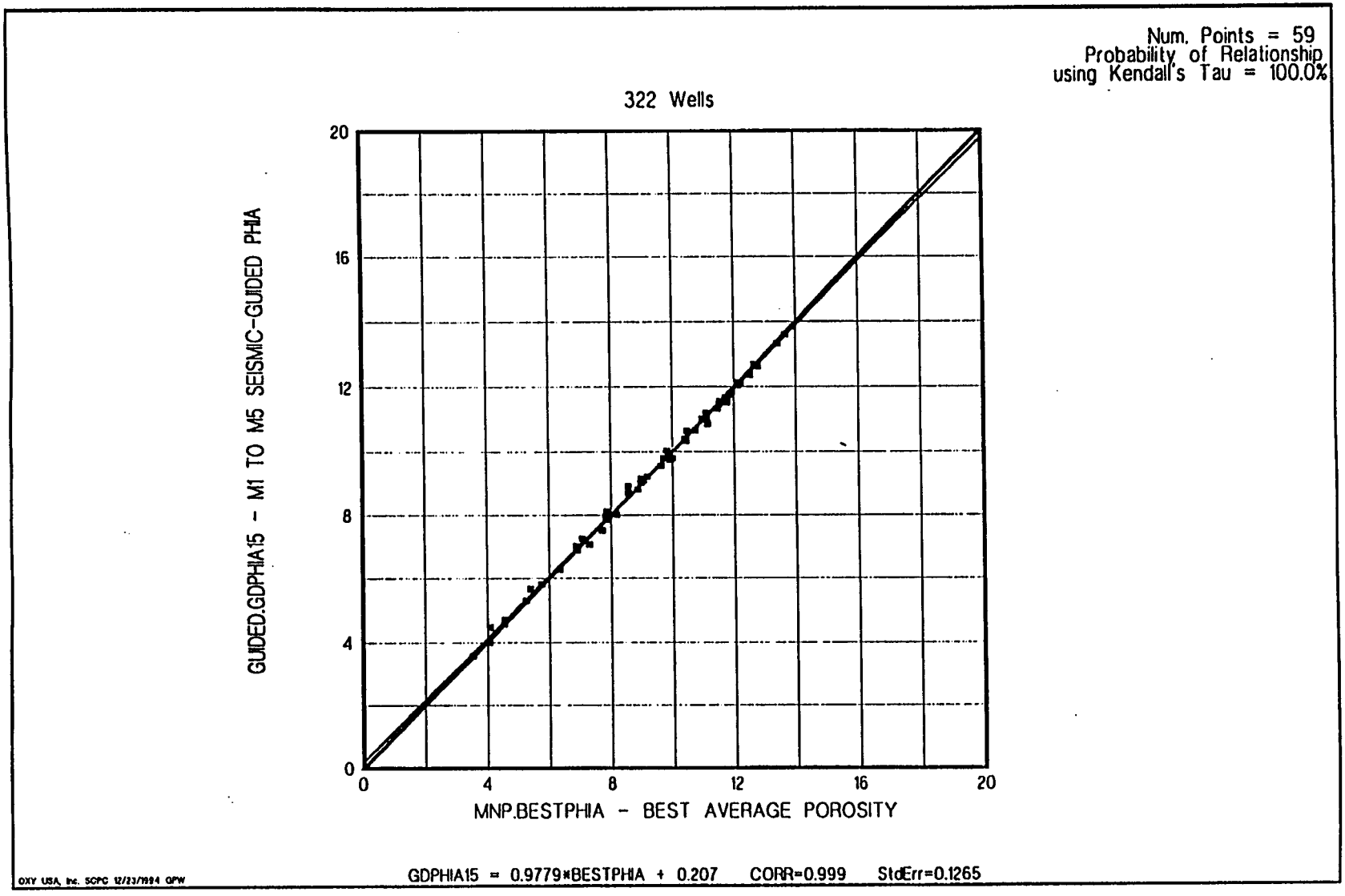

Figure 27-4 - Average Porosity: Well Data versus Seismic-Guided.

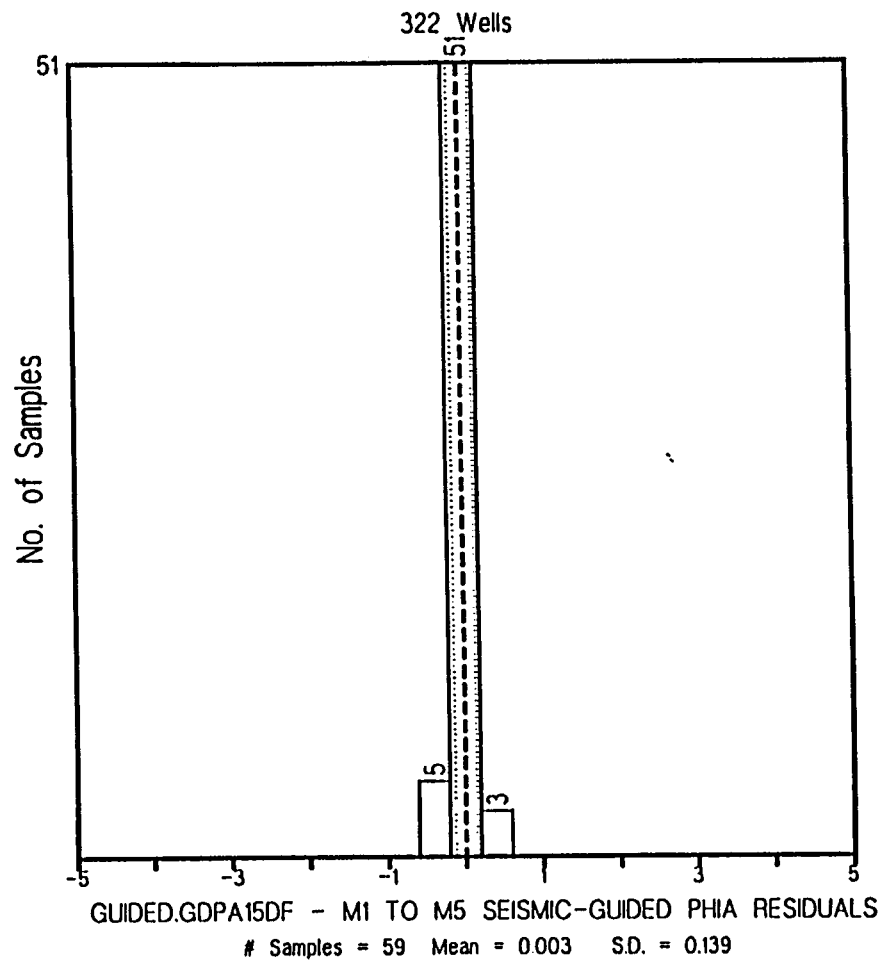

OXY USA, Inc. SCPC 12/23/1994 GPW

Figure 28-4 - PHIA Residuals from Seismic-Guided Values.

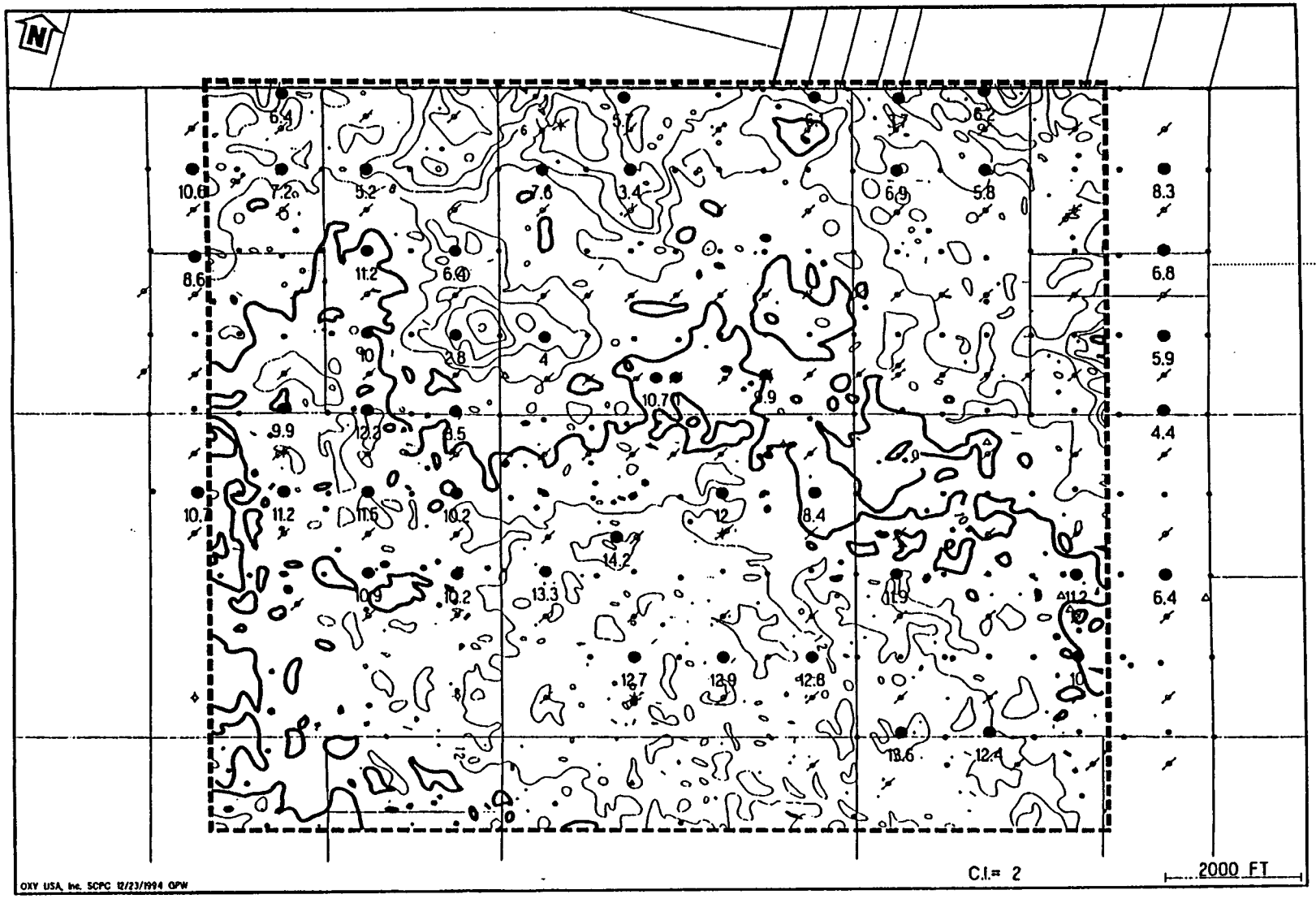

Figure 29-4 - M1 to M3 Seismic-Guided Average Porosity.

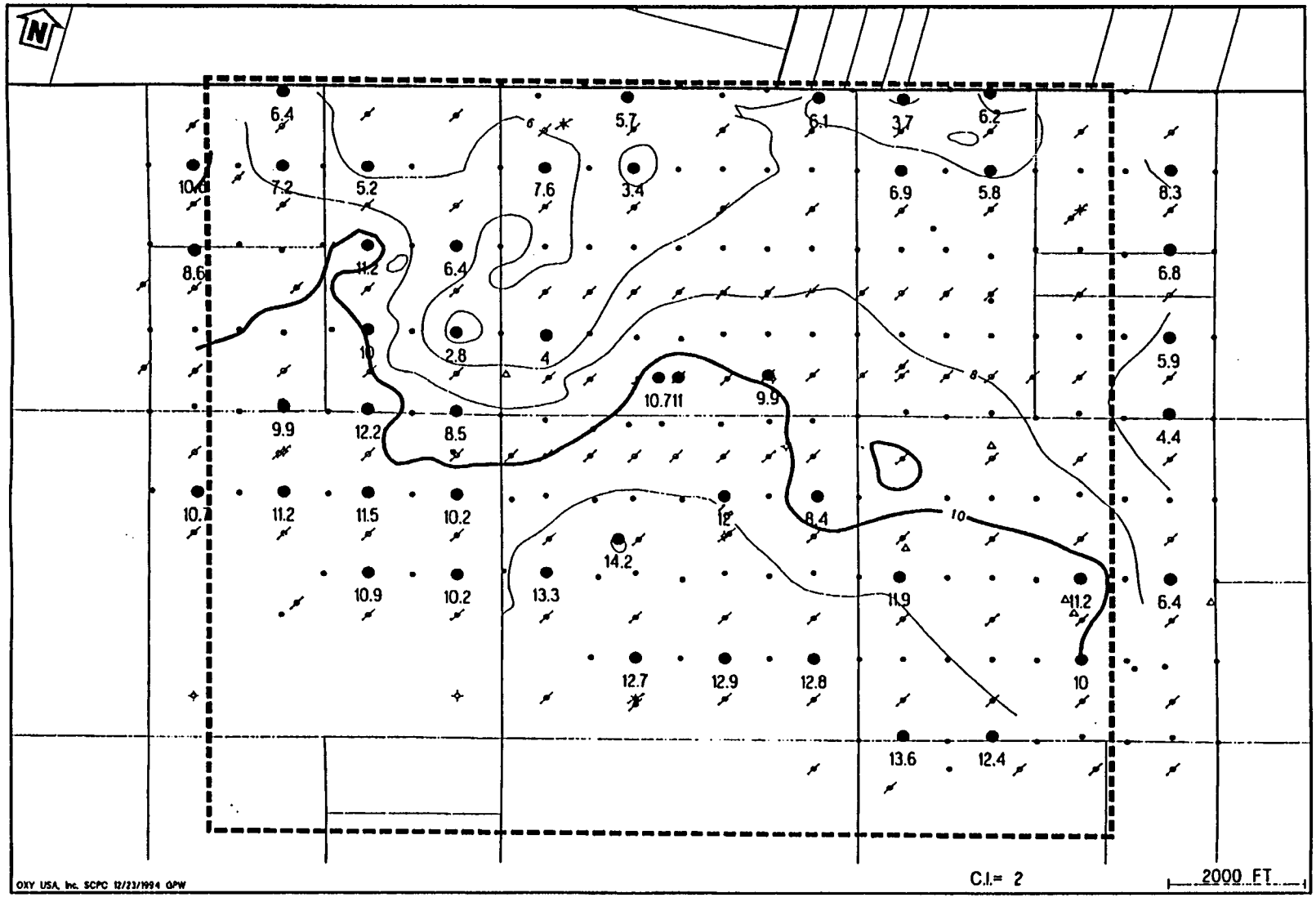

Figure 30-4 - M1 to M3 Average Porosity (PHIA) from Well Data.

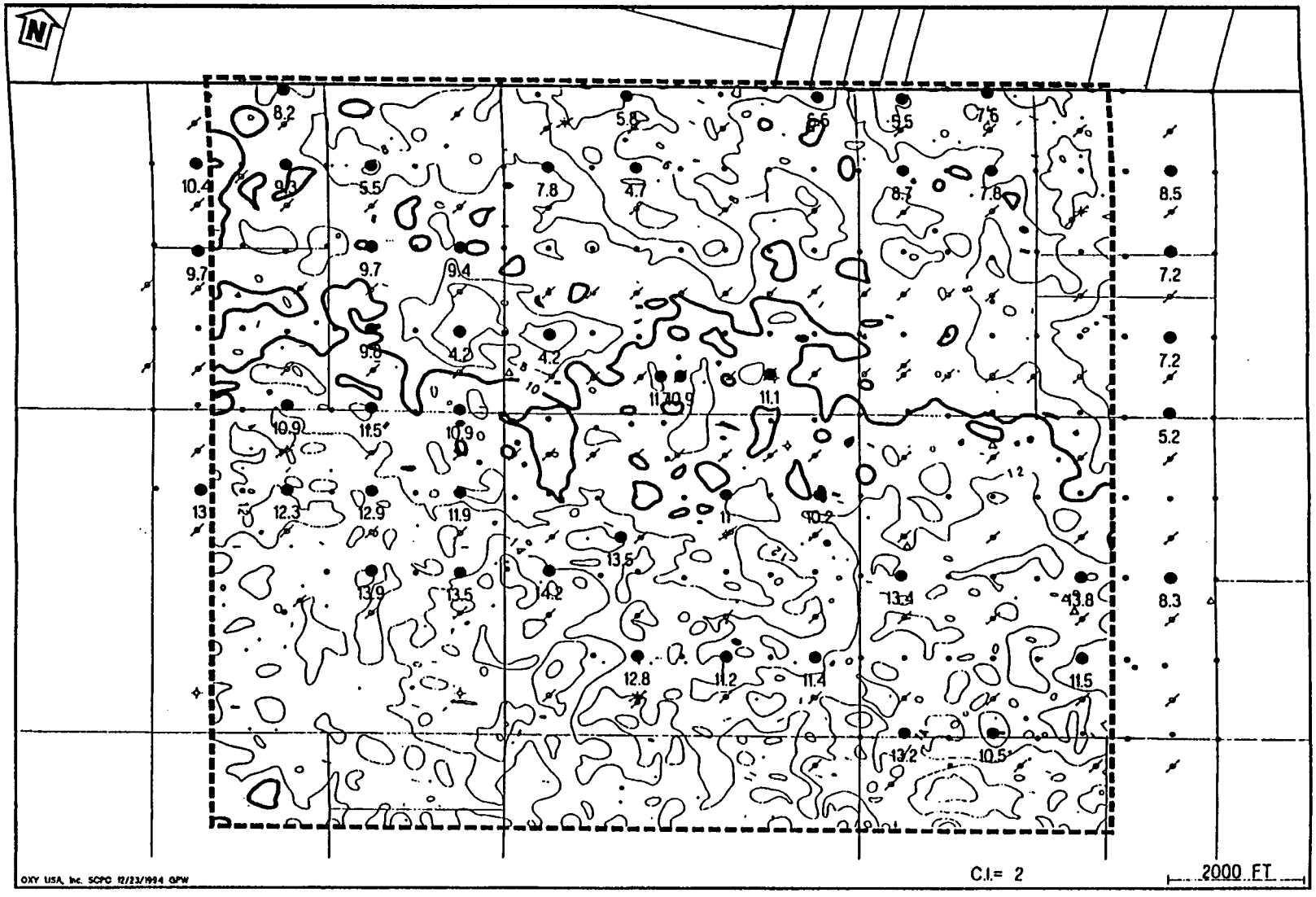

Figure 31-4 - M3 to M5 Seismic-Guided Average Porosity.

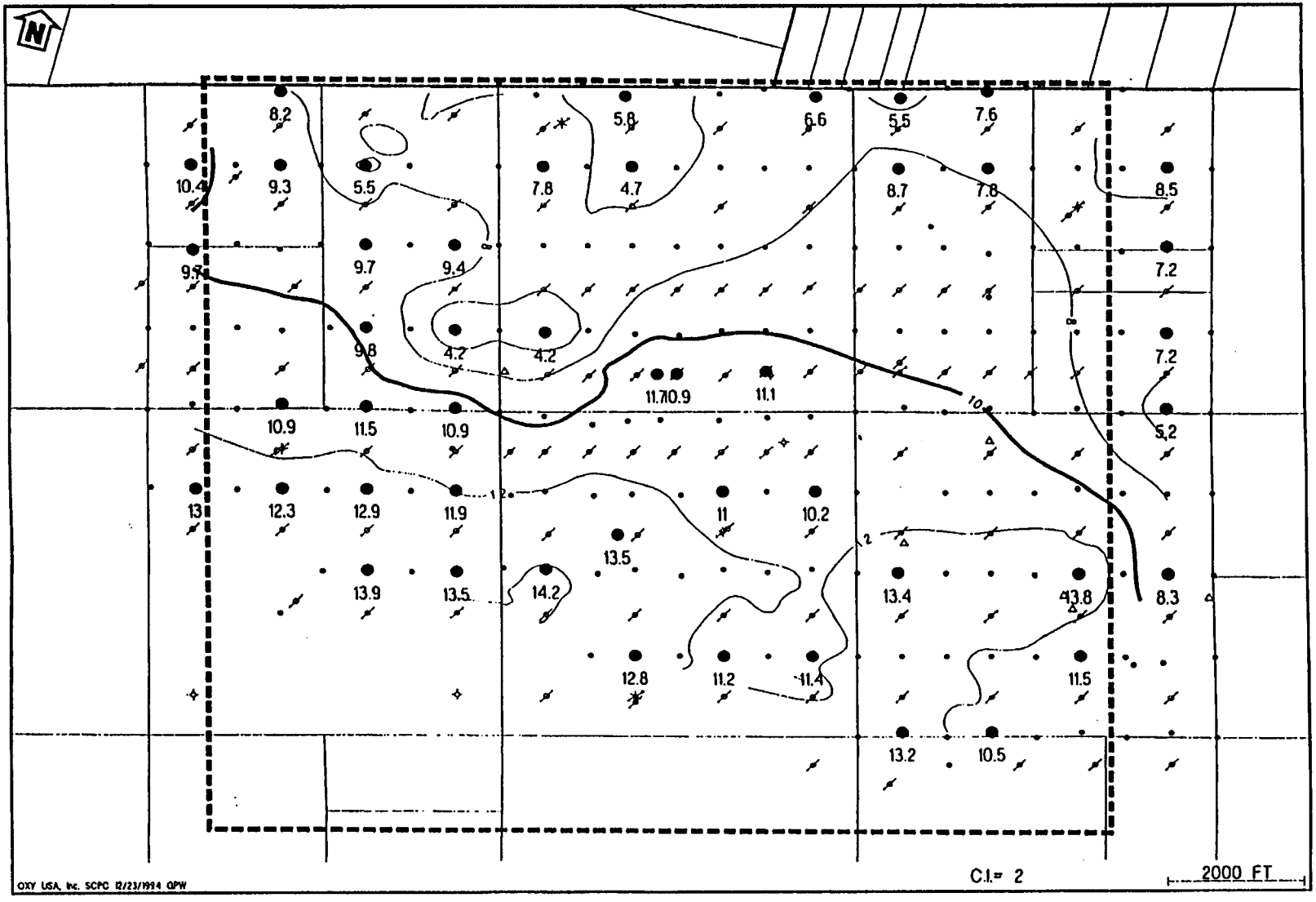

Figure 32-4 - M3 to M5 Average Porosity (PHIA) from Well Data.

Chapter 5 - BOREHOLE SEISMIC PROGRAM

Introduction

The borehole seismic program is based on interwell seismic surveys carried out between one or more pairs of wells, employing seismic source and receivers deployed in separate wells. The main advantage of interwell seismic surveys is that the survey can be carried out in or near the reservoir environment itself. Placing both source and receivers in or near the reservoir eliminates problems associated with propagation through thousands of feet of overlying sediments as well as near-surface weathering problems. The result is that much higher frequencies can be propagated successfully (as high as several kHz) and imaging problems due to complex geology in the overburden are avoided. Interwell seismic imaging offers the potential for providing reservoir information on a scale which is required in many reservoir management or development applications.

There are several different types of interwell seismic surveys which may be carried out; however, only tomography surveys and the interwell VSP surveys were conducted in conjunction with this project. Interwell tomography surveys can provide a relatively high resolution map of the seismic velocity field (both shear and compressional wave) between wells. The interwell VSP survey can provide a relatively high resolution reflection image of the reflecting horizons between the wells, similar to the types of images obtained with surface seismic data.

The carbonate San Andres reservoir under the demonstration area is located at an approximate depth of 4800 ft subsurface and averages about 75 ft in thickness. Detailed analysis of the reservoir interval is given elsewhere in this report, but the reservoir can be viewed as a very finely layered system of flow units. The reservoir is overlain by dolomites and anhydrites of higher velocity than the lower velocity reservoir unit. The lower portion of the reservoir is characterized by relatively high porosity rock which is water saturated. Velocities at the reservoir depth are quite high and range from 14,000 fps to about 22,000 fps with the average about 18,000 fps.

A borehole seismic program was included in this project to demonstrate if interwell seismic surveys could be interpreted with sufficient resolution to bridge the gap between the resolution of surface seismic data and the resolution of well logs. In the proposal for the West Welch demonstration project, borehole seismic was primarily considered as a method to help with the problem of poor sweep efficiency by the CO_2 front due to the heterogeneous nature of a typical shallow shelf carbonate reservoir. The time lapsed interwell seismic surveys should be able to detect the CO_2 frontal advance. This would help validate the initiation of a linear CO_2 front by a row of injectors with their propped fracture wings aligned. The wellbore seismic surveys would cover both the fracture alignment and injection well infill areas for comparison

of the CO_2 frontal advances that occur. The same survey results could potentially describe the injectivity profile allowing optimum profile modification to be practiced.

It was anticipated that the time sequence tracking of the CO_2 fronts would describe the continuous flow units between wells. Even without CO_2 injection, the tomograms were expected to provide a 2-D interpretation of the velocity differences between well pairs. If the velocity differences along the boundaries of the individual flow units are sufficient, it may be possible to identify continuous flow units. Then distribution of the flow unit interpretation between surveyed well pairs across the demonstration area could be attempted using the VSP surveys to provide continuous reflectors that correlate to the tomography interpretations. The VSP data would then be integrated with the 3-D seismic data to determine if variation in the 3-D seismic reflective attributes can be used to map the wellbore seismic interpretation of flow unit continuity throughout the 3-D volume in the demonstration area.

Field work associated with this program began at the site in the West Welch Unit in the fall of 1994. The interwell survey lines were chosen to cross portions of the West Welch site in a radial pattern. The lines emanate from two (seismic) source wells, one in the north of the West Welch study site and the other in the south. Two sets of connecting lines were included between the north and the south patterns. Subsurface lengths of the survey lines ranged from about 700 ft to slightly over one-half mile (2701 ft). One survey line was eliminated because of well bore availability. The final pattern of 15 survey lines is shown in Fig 1-5.

Because of the large contrast in velocities anticipated between the permeable and non-permeable portion of the reservoir when CO_2 is injected, there was a high degree of confidence that the CO_2 front could be mapped by interwell seismic surveys. The determination of flow unit continuity prior to CO_2 injection would be pushing the state of the art, yet the significance of this approach cannot be over emphasized. Seismic techniques represent the only available method for detecting directly the interwell variation in reservoir character. 3-D seismic has proven successful in describing the subsurface environment in detail and accuracy never before obtained. However, the flow units in shallow shelf reservoirs are often only a few feet thick in comparison to the 3-D seismic vertical resolution on the order of 35-40 ft. The approach being proposed in Oxy's West Welch demonstration project is attempting to reduce the vertical resolution of the seismic interpretation to the order of 5 ft across the entire project area.

Interwell Seismic Surveys

Tomography Surveys. The tomography survey can be thought of as similar to CAT (Computer Aided Tomography) scanning which is widely used in medical diagnosis. In CAT scanning, an X-ray source sends X-rays through the body to be imaged at all possible angles (obtained by rotating the source and receivers around the body in a

360 degree circle). Photon detectors opposite the X-ray source record the attenuation of the beam along the different paths it follows through the body. The reconstructed image is an X-ray attenuation map. Since bones attenuate X-rays more than tissue, for example, the two can be distinguished in the resulting computed map or image.

In interwell tomography surveys, seismic (sound) waves replace X-rays. The traveltime of the signal between source and receiver is used in image reconstruction. Typically, the source is deployed in one well and the receiver(s) in another well. The imaging aperture cannot achieve a full 360 degrees as is done in medical imaging due to wellbore availability. The computed image is then a map of the seismic velocity field between the two wells. In computing the image, the same principles are applied, but the problem of image reconstruction is complicated by the fact that sound doesn't propagate along straight lines through the earth. Therefore, both the propagation paths and the unknown velocity field must be simultaneously reconstructed. Although it may be done in other ways, this project used an iterative procedure to solve thousands of simultaneous nonlinear equations required to produce each tomographic image.

To acquire a tomographic survey, source and receiver stations are planned in their respective wells to span a fairly large vertical range of depths. The depth range extends above and below the zone of interest (reservoir) in order to get as much angular coverage as possible through the zone of interest. The source and receivers each occupy a large number of stations distributed over the range of depths to be used in the survey. Data are acquired from every possible combination of source and receiver stations, each resulting in a single multi-component seismic trace.

During the survey, typically, thousands of seismic traces are acquired and the redundancy of the data set will be high. Spatial regions in the reservoir are crossed by many ray paths between various combinations of source and receiver stations. It is the fact that each "small" region in the zone of interest is crossed by many ray paths which allows each such region to be singled out in the imaging process and a velocity computed for it. The size of the region which can be accurately inverted in this way effectively determines the (spatial) resolution of the survey.

Hence, a tomographic image is a computed image. The bandwidth of the data and the density of the ray paths across the zone of interest play an important role in determining the resolution which can be obtained in the imaging. Each of these parameters becomes more difficult to sustain as the survey line length increases, so that, unless compensating measures are taken as the survey line length increases, resolution may decrease. Similar considerations apply to essentially all forms of seismic imaging.

Interwell VSP Surveys. The interwell VSP (Vertical Seismic Profile) is a survey which is carried out in the same way that a normal (surface to borehole) VSP survey is carried out, with the exception that both source and receivers are in separate

boreholes. The only difference is that in the interwell VSP, the source and receivers are very close to the reservoir rather than at the surface of the earth. The data are acquired in the same way as a surface VSP, although much finer station spacing may be used to enhance the resolution of the resulting image. The data are processed as an offset VSP survey.

The interwell VSP survey differs from the tomography survey in that the data are processed in traditional fashion to produce a standard reflection image of the reflecting horizons below the source and receivers. The interwell VSP survey can often image reflectors located thousands of feet below TD in addition to imaging the zone of interest. Because the survey is conducted at or near reservoir level, an increased bandwidth in the data can be expected, which allows the possibility of resolving more finely spaced reflecting horizons than with surface seismic data.

Application of Interwell Seismic Surveys. Interwell tomography surveys can provide a relatively high resolution map of the seismic velocity field (both shear and compressional wave) between wells. The interwell VSP survey can provide a relatively high resolution reflection image of the reflecting horizons between the wells, similar to the types of images obtained with surface seismic data. It has long been known that seismic velocities are sensitive to a large number of physical parameters of the rock, including porosity, pore fluid compressibility, rock type, temperature (in some cases), clay content, cementation, compaction, stress and pressure fields, fracturing, and the list goes on and on. As a result, a seismic velocity image, such as a tomogram, can contain a considerable amount of information about the reservoir environment and changes in that environment. It is of interest to consider briefly how such data can be used in reservoir management.

The most familiar application is the structural mapping of horizons between wells using reflection data such as that provided by the interwell VSP survey. A reflecting horizon is created whenever there is a sufficiently large change in acoustic impedance across an interface in the reservoir. Since acoustic impedance is the product of density and velocity, either parameter can induce a change sufficient to produce a reflection. Almost any technique which can be applied to surface seismic data to interpret changes in the reservoir character can also be applied to interwell VSP data, but often with much higher resolution.

Density changes occur with changes in the pore volume, fluid type in the pores and mineralogy. The rock bulk density reflects this difference and a change in acoustic impedance of the rock may give a clue to this change. Changes in acoustic impedance are often visible in amplitude variations of seismic waves.

A change in pore fluid from oil or water to gas (either hydrocarbon or CO_2)can produce a noticeable change in the acoustic impedance of the rock and can often be detected from amplitude variations of reflected seismic waves. The displacement of

oil by CO_2 in the reservoir often produces a significant decrease in compressional velocities of the rock where the displacement has occurred. Tomographic images of the reservoir before and after CO_2 flooding can be indicative of the advance of the CO_2 flood front in the formation.

Shear wave velocities are typically not sensitive to pore fluid content but are sensitive to fracturing of the rock. The use of shear and compressional images together can provide a powerful diagnostic tool to determine what is actually happening in the reservoir.

These examples are illustrative of some of the kinds of information which can be obtained from interwell seismic imaging. Applications can include identification of sites for infill drilling, monitoring movement of fluids and gas caps, mapping porosity distribution, and preparation of cross sections and reservoir simulation models. The real advantage of interwell seismic imaging is in obtaining data which have sensed the reservoir environment or its nearby surroundings only and to produce interwell images from that data at higher resolution than is possible with other types of seismic data.

Data Acquisition

Surface Field Equipment. Advanced Reservoir Technologies (ART) field equipment consisted of three heavy-duty trucks outfitted for borehole seismic work, as well as two towed mast trailers for managing wirelines at the wellheads. One mast trailer is fitted with a wireline drum and draw-works and eliminates the need for a second wireline truck. The trucks involved in the data acquisition program consisted of a Source Truck Unit, Crane Truck and combination Wireline/Recording Truck.

The Source Truck Unit is a custom-built unit which supports the draw-works for the airgun "umbilical" cable, the air compressor units, and the operator's doghouse. The wireline is specially designed and built for this purpose and consists of an armored cable with internal high pressure air hose and firing control wiring. The cable can support a phased array of borehole airguns. The airguns themselves are essentially marine airgun units scaled down to fit into the borehole. All downhole equipment is designed for use at high temperatures and pressures.

The Wireline/Recording Truck contains a mounted skid with drum and draw-works for standard seven conductor wireline. The interior of the truck has been outfitted with a custom-designed digital data acquisition and control system for the multi-component multi-element downhole receiver arrays. The truck is capable of supporting multiple receiver arrays operating in different wells simultaneously. The operator interface is a custom-designed X-Windows interface operating under the UNIX operating system. This interface provides complete access to tool control and allows querying tool status and performing self-test operations while in use. All operations of the receiver arrays are controlled from this interface, including locking

and unlocking, and commands to acquire, store and transmit digital data. Each tool is individually addressable.

The crane truck is a heavy-duty telescoping crane unit which makes it easy to manage the deployment of the receiver tool string. This string might consist of up to seven multi-component locking receiver units spaced at specified intervals on the wireline. In practice, the spacing of multi-component receiver units was set at 20 ft, which allows actual station spacings of 1, 2, 4, 5, 10 and 20 ft to be easily obtained.

Down Hole Equipment. The Multi-Component Locking Digital Receiver Array consists of up to six multi-component geophone tools, each with locking arm and complete computer circuitry for acquiring, storing, stacking and transmitting data to the surface on command. The digital receiver array is stainless steel construction with an operating range up to about 200°C or about 400°F. It is designed for high pressure/high temperature borehole service from standard seven-conductor wireline The tool was operated with a sample interval of 0.25 ms and record length was generally 0.4 seconds. Paper confirmation records were taken at regular intervals for quality control. Data are transmitted to the surface on command from the observer and are written to hard disk. The data are converted to SEGY format and written to tape for future processing.

Borehole Air Gun Source Array. The borehole airguns are stainless steel construction and operate from a custom-built wireline which supports the necessary firing circuitry and high pressure airhose. Up to three airguns can be deployed simultaneously on the cable and can be fired as a phased array. The air gun source signature is stable and very consistent. The primary acoustic energy is probably generated by the initial collapse of the bubble generated when the gun is fired. The radiation pattern is excellent for interwell seismic work and good shear wave energy is generated by conversion at the casing wall. Shear wave energy can exceed compressional wave energy over certain ranges of angles.

The cycle time for firing the air gun source is typically about 5 to 15 secs. Stacking of data never exceeded eight shots, and was often restricted to one or two shots at each station. There can be very small static errors between firing times on successive shots; however, these were corrected and aligned during processing. As a result, each shot was typically recorded separately to avoid any possible reduction in frequency content. This source unit has been successfully deployed in hundreds of borehole seismic surveys and has never failed to generate usable data over ranges up to the one-half mile span encountered in this project. The air gun source has been used with success in every type of environment from unconsolidated sands in California heavy oil steam floods to the hard, high-velocity rock of the Permian Basin. Although ART has a variety of types of sources available, this source has been the choice for most of the projects to-date.

Survey Design. Survey formats were designed for the acquisition of both tomographic (transmission) and interwell VSP (reflection) survey data. Due to the relatively unknown nature of the subsurface interwell environment and the extreme variability of lengths of survey lines, various experiments were carried out in Budget Period 1 to help determine what would work best when carrying out the repeat surveys which would follow in Budget Period 2. Data were successfully acquired and processed on all survey lines.

Each survey was designed individually in accordance with the survey line length (Fig 1-5). To maintain resolution on longer lines, it was necessary to add vertical aperture. There is a trade-off between the resolution and the cost of acquiring the additional data. Vertical aperture of the surveys ranged from about 600 ft to about 800 ft, depending on the survey line length. Typically, station spacing was reduced above the reservoir level to help to reduce acquisition cost. The data were also processed to multiple levels of resolution. The reservoir zone was the only zone of interest, but data must be acquired and processed on either side of this zone. Processing at a lower level of resolution was applied above the reservoir zone. Station spacing was typically 5 or 10 ft through the reservoir zone, depending on requirements.

On a 1000-ft-long survey line, a hypothetical uniform reservoir with a velocity of 18,000 fps (as might be encountered in the Welch reservoir) will yield an arrival time of 55.5555 ms between source and receiver at the same level. If the source moves up 5 ft, the traveltime changes to 55.5562 ms. If the source moves up 10 ft, the traveltime changes to 55.5583 ms. The change in traveltime resulting from a move of 5 or 10 ft by the source with respect to the receiver in this case is on the order of several microseconds. To accurately detect a change in traveltime of this magnitude would require a bandwidth several orders of magnitude higher than can be achieved in seismic imaging today. Therefore, the spatial sampling used was overkill, but it was maintained to increase redundancy and spatial coverage of the data in the reservoir zone. Station spacing was typically increased to 10 or 20 ft above the reservoir zone in order to obtain broader angular coverage of the reservoir without increasing costs significantly. It is very important to acquire good angular coverage by employing as large a vertical aperture as is practical.

Due to the long lengths of many of the survey lines, it was not clear whether good reflection data could be obtained at grazing angles of incidence provided by the tomography surveys. Additional data were shot on each line with source and receivers at higher levels than were used in the tomography surveys to provide interwell VSP data. This required about a day of additional shooting.

Survey formats were designed for the acquisition of both tomographic (transmission) and interwell VSP (reflection) survey data. Because of the uncertainty about acquiring usable interwell VSP data, various experiments were carried out on

different lines by adjusting the height of source and receivers above the reservoir in an effort to learn what produces the best reflection data. Still, there was no assurance that any reflection data would be obtained. Because of the geometry of the surveys, the very long lines lent themselves to critical refractions rather than reflections at every interface where velocity increases. To completely avoid critical refractions at these interfaces for a practical survey pattern is a challenge.

The interwell VSP data were acquired by placing the source at its station above the reservoir and walking the receivers down to TD at 5 ft station spacing. This allowed the possibility of imaging the receiver side of the reservoir (center to receiver well) with reflection data. A receiver was then stationed at the source depth on the receiver side of the reservoir and the source was walked down at 5 ft station spacing. This allowed the possibility of imaging the source side of the reservoir (center to source well) with reflection data. The two data sets would then be processed separately as offset VSP data and merged to form the complete reflection image.

This proved to be the most practical way to carry out the surveys. The two data sets have slightly different characteristics as would be expected from a common source data set (in the first case), and a common receiver data set (in the second case). There are a number of trade-offs which must be dealt with in planning interwell seismic surveys. The greatest constraint is economic, with limitations on the cost and time which can be spent in acquiring the survey. Many of the requirements which have evolved for the interwell seismic data were not part of the original planning of these surveys. The experience gained from data acquisition during Budget Period 1 will be invaluable in designing future interwell seismic surveys.

Logistics. The initial interwell seismic surveys design included the deepening of wells on the order of 150 ft to allow sources and receivers to acquire data below the reservoir level. This is necessary for imaging the lower portions of the reservoir. Typical depths ranged from about 5000 to 5200 ft subsurface, after deepening, although the actual depth was variable with the well location. Deviation surveys were also run on each well in order to locate accurately the subsurface positions of source and receiver stations.

Original planning for the project called for simultaneous acquisition of survey lines using two receiver arrays simultaneously in separate wells. It had been anticipated that H_2S levels would be tolerable, but higher than anticipated levels of H_2S actually encountered caused one receiver string to be eliminated from the project. The tools eliminated were made of carbon steel (not stainless) and suffered hydrogen embrittlement. Both compressional and shear wave data were acquired using the remaining three-component multi-level digital receiver array. The elimination of one receiver string nearly doubled the anticipated field time and costs required to acquire the surveys.

The original north and south (seismic) source wells were changed to nearby observation wells at the beginning of the program due to high levels of H_2S gas encountered in the original source wells. The north and south observation wells were not open to the formation and presented a much better environment for the seismic source tool and the personnel. However, these wells had not been deepened for the project, so the seismic source depths were typically constrained to levels shallower than the receiver depths with an accompanying loss in survey coverage due to limited vertical aperture.

Field work was carried out on the basis of a 10 to 12 hour work day and about one-half day to one day was required for rig-up or rig-down on each well. The tools performed with great reliability, except for cable connectors leaks, which often required that the survey be shut down while the tools were pulled out of the hole and the connectors resealed. The primary problem encountered was with a single rubber boot which seals the wireline connectors. This, unfortunately, represents state-of-the-art at this time. Down time due to connector leaks was usually on the order of several hours.

Other problems were minimal, although the presence of H_2S gas in the wells in varying concentrations did cause major problems with non-stainless steel tools early in the program. The noise environment on most lines was good, with problems experienced only during nearby drilling operations or when operating near an active CO_2 injection well.

Processing

Some difficulty was encountered in processing the reflection data using a commercially available processing system. These systems are typically not designed to handle the unique geometry associated with interwell reflection data acquired over very long lines with limited vertical aperture.

Variations in flow units on the order of a few feet or less are probably realistic in the San Andres reservoir and this resolution requirement pushes the current capabilities of wellbore seismic technology. The interwell seismic data were processed to a final vertical resolution of about 5 ft, although this may not be fully justified on some of the survey lines, particularly the longer lines. Any additional interwell seismic surveys obtained during Budget Period 2 will be designed in light of what was learned during the initial survey and should come closer to meeting the objective involved.

Sample Interval and Bandwidth. The field data were acquired with a digital sample interval of 0.25 ms. It is possible to record data at smaller sample intervals, but this choice involved several trade-offs, one being the maximum transmission speeds which can be achieved for large quantities of data over seven-conductor wireline. With multiple three-component data sets to be transmitted on a single wireline, an attempt

was made to minimize the data transmission time while still allowing for the maximum expected bandwidth in the data. The 0.25 ms sample interval supports data with a bandwidth up to about 2 kHz, which was believed to be adequate for the original objectives, considering the long lengths of some of the survey lines and the possibilities of frequency-selective attenuation on these longer lines.

Although data were acquired over this bandwidth, the peak spectral response occurred from around 250 Hz and higher, with good spectral energy recorded out to around 750 Hz or more. In processing, some of the data were filtered to about 750 Hz at the high end to eliminate high frequency noise, although much of the processing was done with the bandwidth open to about 1500 Hz.

Gun Static Corrections and Vertical Stack. The data were acquired in SEGY format, with separate auxiliary channels for recording the gun signature and firing time. These auxiliary channels, one for each trace recorded, were used in the first steps of processing the data to remove any possible firing time static from the data before vertical stack. Each firing time channel was picked and hand corrected. The resulting static correction was applied to each individual trace before stacking the data. This was done to insure the best possible preservation of the original bandwidth after stack.

Vertical stacking was used on many of the survey lines for the usual purpose of improving signal-to-noise ratio (SNR). With this objective in mind, each trace was recorded separately and stacking was not done in the field. Data ranged from single shot, which did not require stacking, to as many as eight shots, which were stacked at each level. Normally only one or two air guns were used in the data acquisition, depending on the length of the survey line.

Multi-Component Rotation. Because the receivers can undergo some degree of rotation during data acquisition as they occupy different stations in the borehole, the three channels can change orientation from station to station. As a result, the data were generally rotated in processing to effectively beamform the array. Ideally, one channel of output is oriented in the apparent source direction and the other two channels are orthogonal to this direction after rotation.

Filtering and Deconvolution. In an effort to preserve exact arrival time information in the data, filtering and deconvolution were kept to a minimum and any possible phase shifts in processing were avoided. Processing was done for the most part with the data as recorded in determining first arrival times at the receivers with very little deconvolution of the data occurring.

First Arrival Detection. Using the capabilities of modern seismic data processing systems, the data were zoomed to a scale appropriate for accurate identification of the first arrival time and all first arrival picking was done by hand and written to an output

file. There were no automatic tracking programs employed in the identification of the first arrivals. Data were typically displayed in common receiver format which is a good choice for mixing unwanted information such as tube waves out of the data. Tube waves never presented much of a problem in any of the data sets.

Deviation Surveys. Deviation surveys were run on every well employed in the interwell seismic program. Deviations at the reservoir level from the surface wellhead location ranged from several feet to as much as 80 ft in various directions. Deviations of this magnitude, if not compensated for, would have destroyed much of the ability to image accurately using the interwell seismic data sets. These surveys are considered to be a requirement in conjunction with any attempt to do high-resolution borehole seismic imaging. Corrections for well deviations were entered into the geometry files used in processing the interwell data.

Tomography Surveys. The first arrival times obtained from the processed data sets were written to separate files and used as input to the tomographic data processing program which is a stand-alone proprietary application. All necessary geometry data are also supplied to this program in a separate file which includes the deviation survey data and wellhead elevation corrections.

Traveltime tomographic imaging is computed by reconstructing the subsurface velocity model which generates the best fit to the input traveltime data set. This is effectively a nonlinear optimization code which uses gradient computations to update the current model to one which fits the data better than the previous model in an iterative procedure. The code is unconstrained and the required starting model is normally taken to be a uniform velocity model. Although any model could be input, if desired, only the uniform model was used on the various survey lines. This was done to minimize any possible bias which might be imposed on the output.

Because there can be little confidence in results obtained by applying nonlinear optimization techniques to underdetermined systems of equations, a grossly overdetermined system of equations was solved. This eliminates almost any possibility of non-uniqueness in the results. The only room for nonuniqueness is in the fact that such an extremely large and redundant data set can probably not be fit exactly. Sources of error are wave equation modeling which only approximates the actual propagation of seismic waves through an imperfectly fluid saturated porous, elastic medium and the residual error left when the best fit to the data is obtained. If a good job has been done in extracting the first arrival times from the data, the fit to the data which is obtained will generally be quite good.

To give some statistics to the fit of data on various survey lines, it was generally true that about 70% of the thousands of traveltimes in each survey were fit to within 0.25 ms (the sample interval) and between 90.8 and 99.4 percent were fit to within 0.5 ms. Only two survey lines presented exceptions to these statistics. Since

velocities encountered at reservoir depths were quite high, this still leaves some room for error in the imaging, but only with better data quality (increasing signal-to-noise ratio, for example) could additional improvements be expected.

The tomograms were displayed after processing with a palette of 31 colors assigned to the velocity range in even increments of velocities. As the imaging program runs, various quality control displays pop up in real time allowing for quick identification of possible problems or sources of error. The primary item which is monitored carefully is the accuracy of the wave equation modeling being used, which can generally be increased, if necessary, at an increased cost in computing time. Again, there are trade-offs and the best compromises were usually chosen to guarantee results as close as possible to the required levels of accuracy in the final image. The processor was always mindful of the risk of computing more resolution than might have been actually justified, especially in the case of extremely long lengths of survey lines. In all cases, only a highly overdetermined system of equations was solved, eliminating any non-uniqueness due to solving an underdetermined system.

The goal ultimately set for the imaging was to achieve 5 ft vertical resolution. All lines were computed to this level of resolution, recognizing that high vertical resolution is more likely to be achievable on shorter lines. These levels of resolution may not have always been justified due to different degrees of resolution in the different data sets. However, the overall character of all the processed data is pretty well in agreement. There is some question that a dip of about one-half degree on the strike (north-south) lines was always resolved. This small dip could have been lost to some extent in the small amount of error remaining in the final images after processing. This remaining error is largely determined by the looseness of the final fit of the computed traveltimes to the data. In essentially every case this residual error ranged from zero to 0.5 ms, depending on the individual trace, with most of the error below 0.25 ms. Some of this remaining error could lie in the inability of the computer program to fit the data perfectly, but just as likely it lies in residual small error in the data set itself. Many of the picked traveltimes probably have an error on the order of one or two samples (0.25 or 0.5 ms).

Each type of data set was processed as described above to develop shear and compressional wave tomograms for each line. In addition, these two types of images were combined to produce a Poisson ratio tomogram using the usual equations relating Poisson ratio to shear and compressional velocities. Finally, Vs/Vp tomograms were computed on each survey line which tend to be somewhat similar to Poisson ratio tomograms but display information in a slightly different form.

Figures 2-5-10-5 are the tomograms for three lines representing the best to worst of the 15 lines acquired. As seen on Fig. 1-5, survey line 2 runs east-west out of the northern source well and is 1022 ft long. This line shows the detail present in

most of the shorter lines. Survey line 10 runs east-west out of the south source well and is 1650 ft long. This line represents the worst of the lines believed to be from the noise generated by nearby drilling activities. Survey line 14 runs south-southwest out of the north source line and is 2224 ft long. This is one of the two long lines acquired and passes close to the 4827 well which has a sonic log for comparison. Figures 2-5-4-5 represent compression wave tomographs for interwell seismic survey lines 2, 10, and 14. Although the processed tomograms were designed to be displayed with a palette of 31 colors, the relative variation in velocities is readily apparent in black and white. Variation in the tomogram shading represents only changes in velocity with velocity decreasing as the shading darkens to a minimum of 15,000 fps. The shading changes in increments of 600 fps. The tomograms are not all to the same scale, but sized to fit the page with the aspect ratio being preserved. The vertical span of each tomograph varies, but averages about 380 ft. Only the bottom third, covering the San Andres producing reservoir, was processed in detail. Pseudo acoustic curves, constructed from the wellbore seismic data, are imposed on the tomogram at 50-ft intervals and scaled so velocity is decreasing to the left.

The shear wave tomograms for survey lines 2, 10, and 14 are shown for comparison purposes as Figs 5-5, 6-5, and 7-5, respectively. On these tomograms, the darkest shading represents 7000 fps, and shading changes in increments of 300 fps. Similarly, the Poisson ratio tomograms for the same three lines are shown by Figs 8-5, 9-5, and 10-5. The darkest shading represents a ratio of 0.35, and shading changes in 0.06667 increments.

As discussed, velocity changes can result from variations in rock properties, fluid content and mineral composition. Within the San Andres reservoir being sampled by the tomograms, velocity changes are thought to represent mainly variations in porosity. Therefore, the tomograms are probably characterizations of the porosity distribution within the reservoir. However, the linear (layer cake) nature of the tomograms have a somewhat artificial appearance that raises questions as to where the events are actually occurring in space. It was anticipated that the VSP data would help establish the vertical boundaries between events, but to date the VSP data have not proven interpretable as discussed in the next section. In the two instances where the long and short seismic survey lines nearly overlap - lines 4 and 14 and lines 8 and 15 - there is little similarity between the tomograms and the overlapped sections. This could be due in part to the lower resolution in the longer lines. The only other direct interwell data available are the 3-D seismic interpretations, which do not have sufficient vertical resolution to verify the tomograms. In the few instances where there is a wellbore located along a interwell survey line, the well data and tomogram velocities match the gross porous interval even in line 10 which contains noise from nearby drilling. However, the tomography and well data do not have good peak-to-peak correlations other than in source wells.

Interwell VSP Data. Reference was made earlier to the manner in which the interwell VSP surveys were acquired and to some of the considerations which entered into planning and acquiring these data sets. The data sets were processed initially (static corrections, rotation, etc.) in exactly the same manner as previously described. To complete the imaging step of the processing, the data were gathered to emulate a common source or common receiver with the appropriate source or receiver (as source) locations in their respective wells. The data sets were then processed as standard offset VSP data, e.g. as two separate offset VSP surveys, one for the source well and one for the receiver well. The two resulting images were then merged at the mid-point between the wells to form the complete interwell reflection image.

Problems were encountered in using standard commercial VSP processing software with the interwell VSP data sets due to the unique geometry of these data sets. There have been few previous attempts to process such long offsets with such limited vertical aperture and high velocities. Work continues with the provider of the commercial processing system to improve the imaging capability for this type of geometry which would essentially never be encountered in standard (surface-to-borehole) VSP surveys. In order for interwell VSP imaging to develop into a successful commercial product, the unique demands of this type of survey must be recognized and provided for in producing processing systems for this type of data. There is no technical reason why this cannot be done.

Summary of Results

The objective of the wellbore seismic program during Budget Period 1 was two-fold: 1) establish a baseline reference for tracking the CO_2 flood front advance during Budget Period 2 through time-lapsed tomography surveys and 2) attempt to describe the flow units between wells using the tomograms and VSP images.

Interwell seismic data in the form of compression and shear wave were recorded directly between source and receivers along 15 survey lines. These raw data were processed and displayed in the form of compression wave, shear wave Poisson ratio and Vs/Vp tomograms. Reflective seismic information was also recorded between wells along the same survey lines and processed as VSP data sets.

There is a high probability that the tomography surveys can successfully track the CO_2 front. However, the ability of the interwell seismic tomograms to delineate the flow units between wells was not established during Budget Period 1. Emphasis was placed on refining the processing in an attempt to improved results, but the quality of the data gathered in Budget Period 1 imposed constraints. Work will continue on both the tomography and VSP interpretations during Budget Period 2.

Considerable experience has been gained in conducting the field surveys and processing the data. This knowledge will be utilized in designing any interwell seismic surveys conducted during Budget Period 2 to improve the quality of the data.

Conclusions

The resolution of tomographic imaging is a function of the bandwidth of the recorded data and the density of the ray paths across the zone of interest as well as the amount of processing done. Bandwidth decreases as survey length increases. Adequate zone coverage by the ray paths requires positioning both source and receiver above and below the zone of interest. The longer the survey line, the greater the vertical increments required. The greater the coverage, the higher the cost in terms of data gathering expenses and often in well work to create the necessary rat hole below the zone of interest.

The optimum wellbore seismic survey design becomes a matter of trade-off between obtaining sufficient data coverage to meet the objectives and the total cost involved. Processing is also a cost trade-off. Processing cost involved not only the volume of raw data, but the degree of refinement sought. The results during Budget Period 1 argue for less total survey length and more coverage and processing.

The direct ray path tomograms acquired during Budget Period 1 apparently are imaging to some degree the porosity distribution of the formation. The appearance of the tomographic interpretations and the limited validation checks available suggest that the seismic events are not being correctly located in space. The problem may be more in the area of processing than data quality, although the exact location of the receiver and source in 3-D space is an issue.

The reflective wellbore seismic data have failed so far to produce usable VSP interpretations. The problem lies partly with the use of conventional VSP processing software to handle problems associated with the geometry of long interwell lines that don't exist with surface seismic. However, the lack of adequate data coverage may be a factor also due to insufficient vertical aperture.

Wellbore seismic technology holds considerable promise for interwell characterization. Some success has been obtained in sand/shale sequences. It appears that both the field data gathering methodology and the processing procedures will have to be refined to accommodate the higher velocity realms encountered in shallow shelf carbonate reservoirs. In hindsight, chances for success at West Welch would be increased by having acquired more data at higher sampling rates along fewer but more constrained (well control) survey lines with special emphasis on establishing the exact location of the source and receivers.

Considerable progress has been made in demonstrating the use of wellbore seismic in an actual field situation, but the actual success of interwell seismic surveys in characterizing the San Andres reservoir at West Welch will not be determined until Budget Period 2.

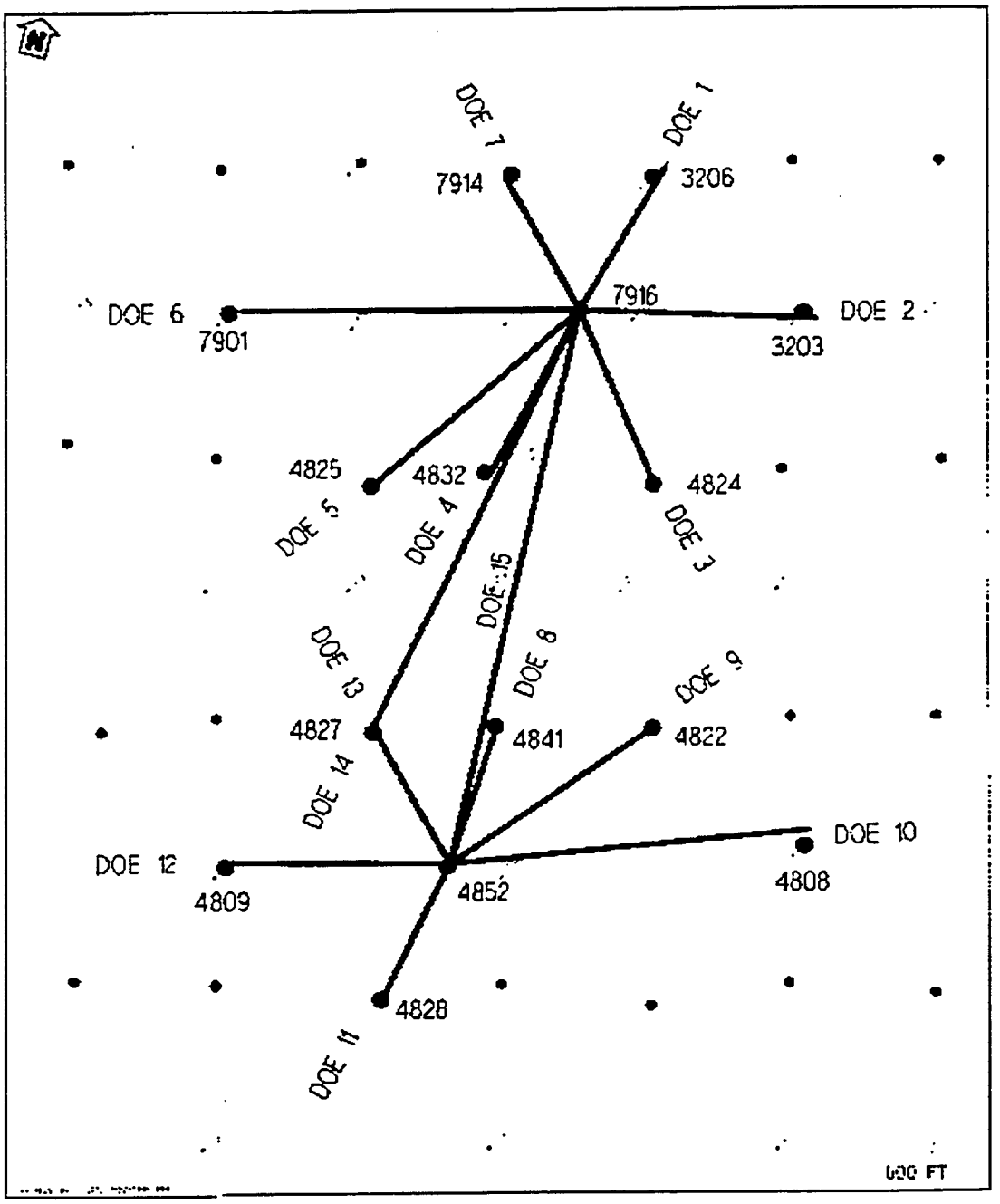

Figure 1-5 Crosswell seismic base lines in project area.

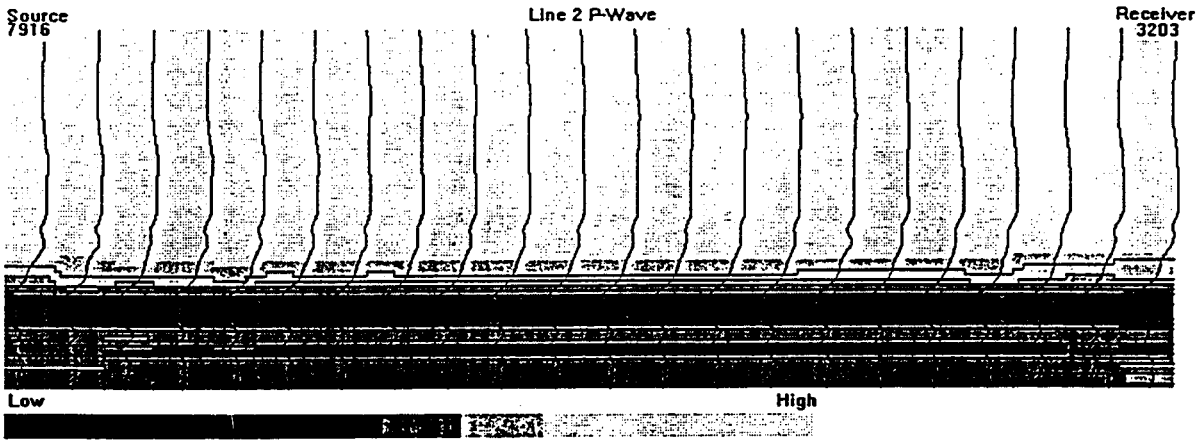

Figure 2-5 Line 2 compression wave tomogram.

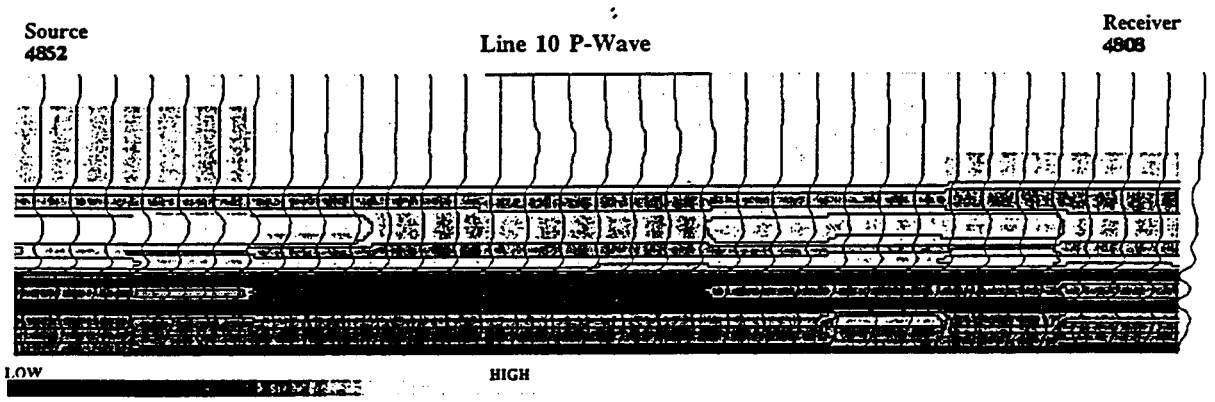

Figure 3-5 Line 10 compression wave tomogram.

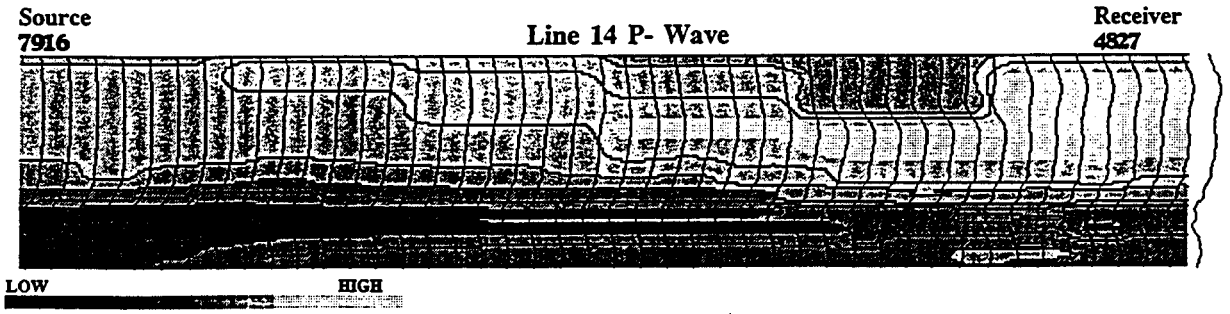

Figure 4-5 Line 14 compression wave tomogram.

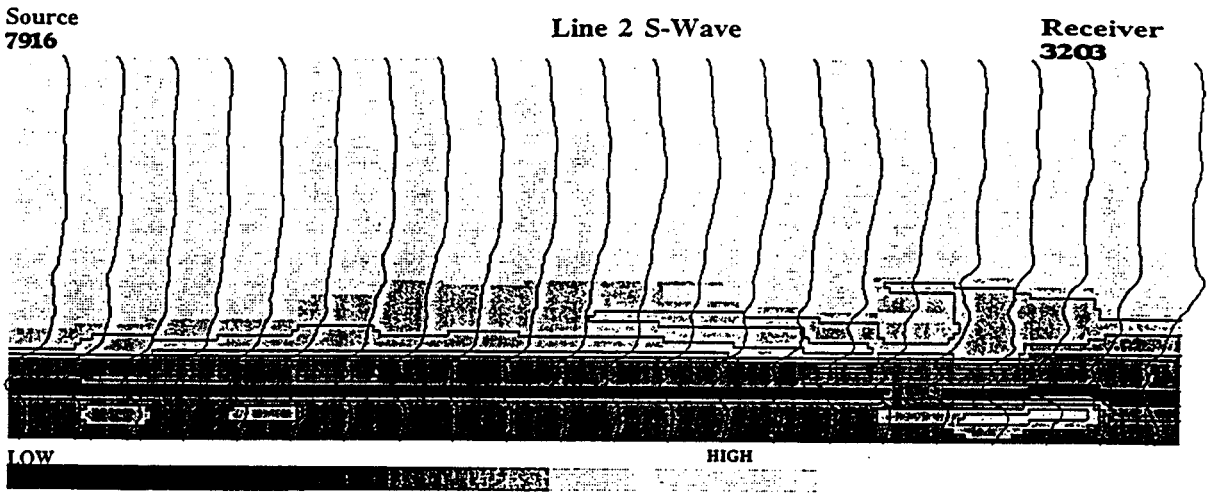

Figure 5-5 Line 2 shear wave tomogram.

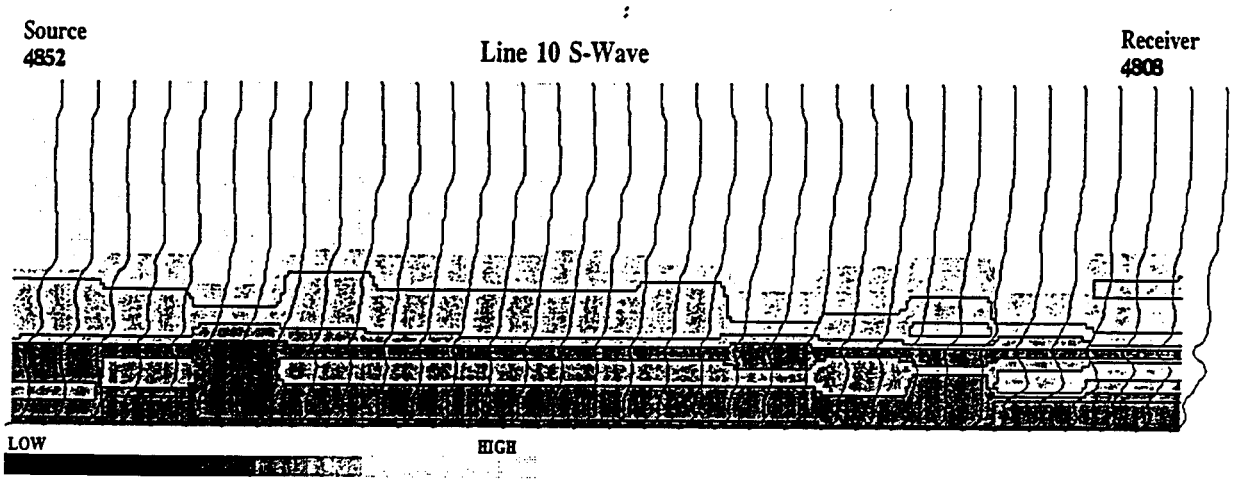

Figure 6-5 Line 10 shear wave tomogram.

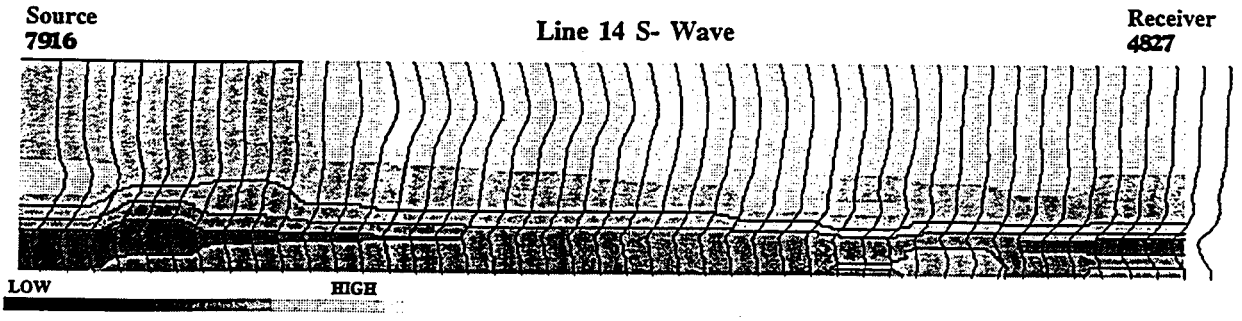

Figure 7-5 Line 14 shear wave tomogram.

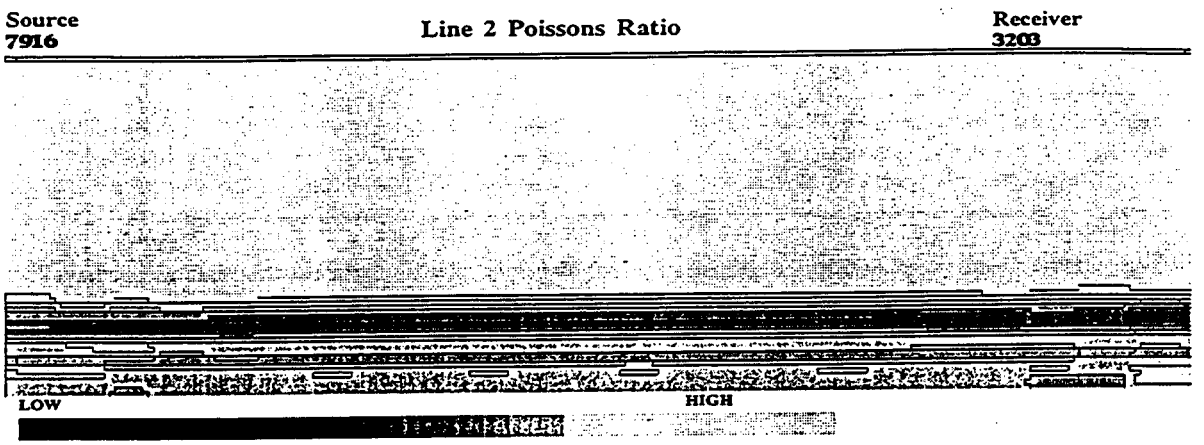

Figure 8-5 Line 2 Poisson's Ratio tomogram.

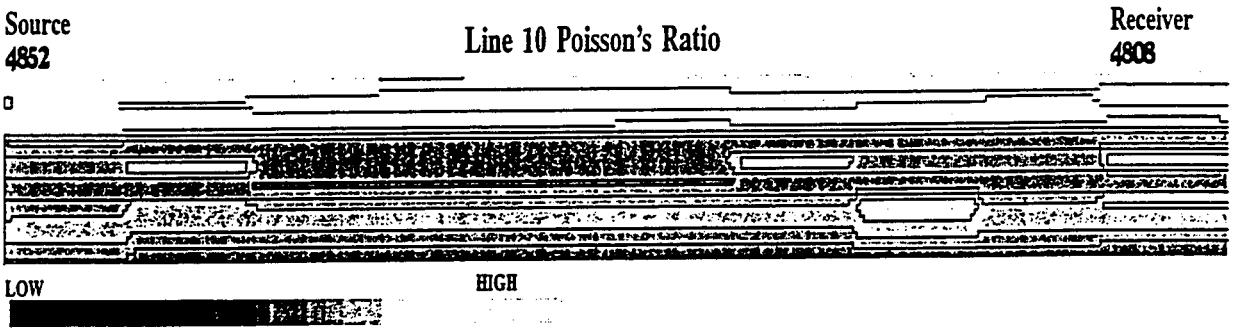

Figure 9-5 Line 10 Poisson's ratio tomogram.

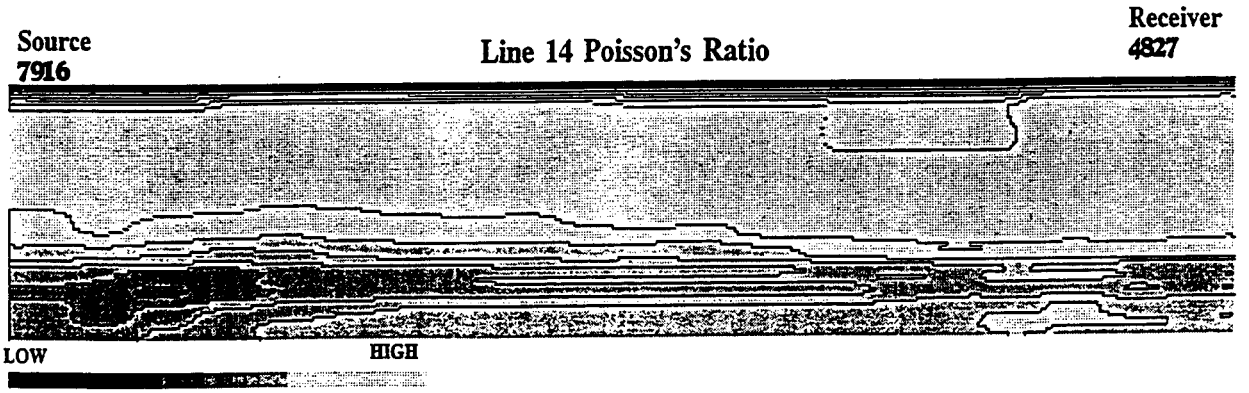

Figure 10-5 Line 14 Poisson's ratio tomogram.

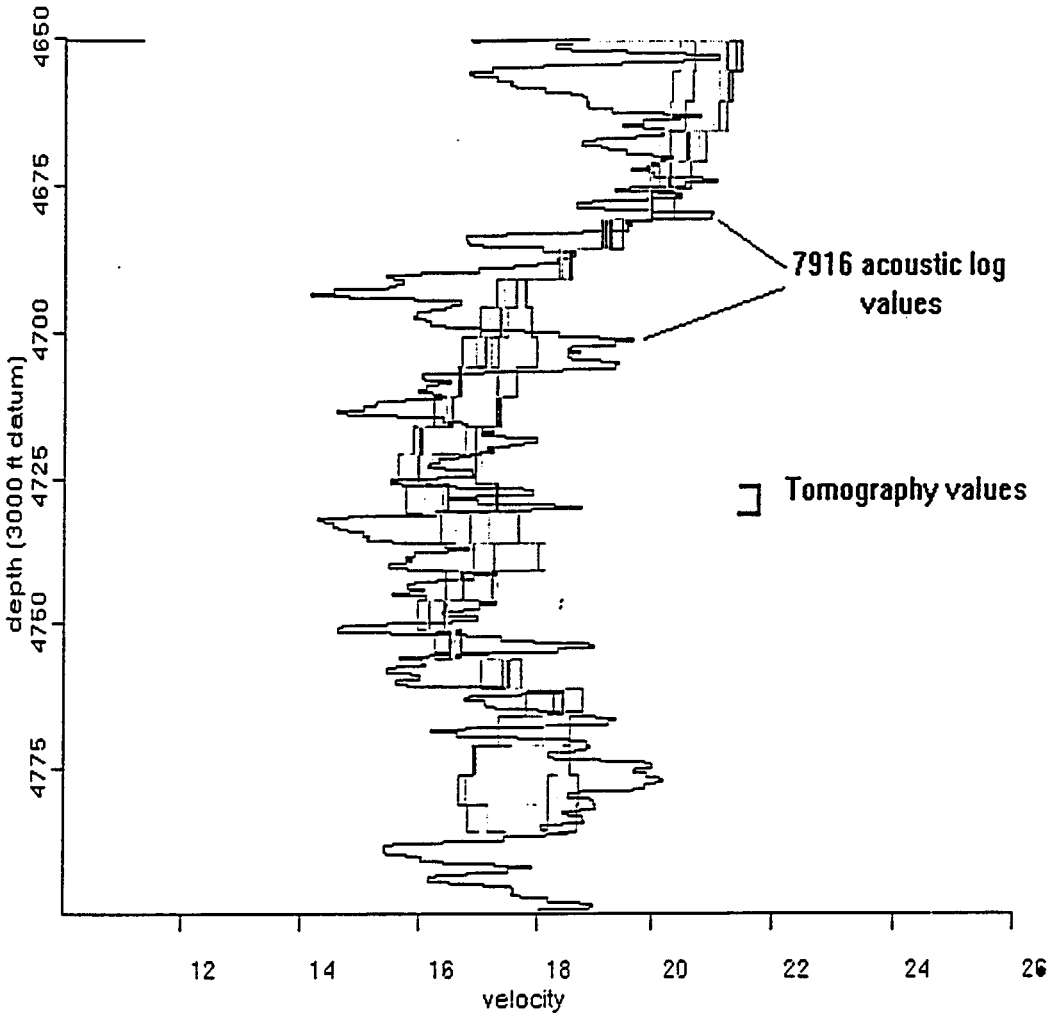

Figure 11-5 Acoustic log and nearby tomography values. Acoustic values have finer resolution.

Chapter 6 - RESERVOIR SIMULATION STUDY

Introduction

The reservoir simulation study had three major objectives during Budget Period 1:

1. Build a reservoir simulation model using a conventionally obtained geologic description of the reservoir (base geologic model) to match primary and waterflood reservoir performance.

2. Use the advanced reservoir characterization technology being demonstrated during Budget Period 1 to revise the base geologic model and repeat the match of primary and waterflood reservoir performance to determine what degree improvement has occurred in the accuracy of the simulations.

3. Use the enhanced simulator to design an optimum CO_2 flood for installation during Budget Period 2.

The first wells in the West Welch area came on production in 1948. The West Welch Unit became effective in 1960. Water injection into the modeling area started in 1955. The simulator project involves the simulation of the entire production history starting in 1948 up to the current time, followed by several forecast simulations. An equation of state (EOS) based compositional simulator, MORE, was used for this study which is commercially available in both PC and UNIX formats.

Fluid Characterization

A fluid characterization developed for the South Welch Unit simulation study was updated for the West Welch. The heptanes plus fraction was split into five fractions, F1 through F5. After satisfactory matching of the experimental data, a procedure was carried out to derive at an 11-component Peng-Robinson EOS characterization for use in the simulation study. The 11 components were obtained by combining some of the original components into pseudo components. Methane and nitrogen were combined into N_2C_1. CO_2, H_2S, ethane and propane were left as single components and the various form of butanes, pentanes and hexanes were combined as individual components, C_4, C_5 and C_6, respectively. The heptanes plus fractions F1 and F2 were combined together as were F3 and F4 while F5 was left as a single component.

Two equation of state characterizations were used in the study. On each, the CO_2 critical properties and binary interaction parameters (BIPs) were reduced to eliminate the occurrence of multiple phases of CO_2 at low temperatures in as many of the model grid cells as possible. The first EOS characterization (wwu 10 EOS) does not

adequately simulate the CO_2 miscible process under the reduced conditions. The slimtube simulations give reasonable values for recoveries and miscibility pressure, but the resulting residual oil saturation profiles and compositions do not match the actual laboratory data. With the second EOS (Mod 11c EOS), the final regression on slimtube data, even with reduced CO_2 critical properties, allows the CO_2-oil BIPs to go back to higher values. This procedure produces the same oil saturation profile (decreasing away from the injection well) expected, and residual oil compositions as found in the multicontact slimtube experiments. In contrast, wwu 10 EOS produces a slimtube oil saturation profile that started at 0% at the injection well and increased toward the producing well. WWU 10 EOS recovers the heavy ends and leaves behind intermediate components to produce the residual oil in the slimtube simulations.

The resulting difference is shown in the project area simulation predictions shown in Fig. 1-6. The wwu 10 EOS produces much higher oil rates at lower CO_2 injected volumes, compared to the Mod 11c EOS which projects similar incremental oil but higher CO_2 injected volumes and flatter oil producing rates. The initial reservoir description and initial waterflood history match were developed using the black oil PVT data generated from the EOS.

Relative Permeability Data

Two different relative permeability behaviors have been identified for the modeling area. The behavior which applied to most of the reservoir occurs in rock type (Type 1) that has a connate water saturation of 20%, a residual oil saturation to waterflood of 40%, and a critical gas saturation of 5%. The second behavior, which applies only to model layers 5 and 7 (see reservoir description below) occurs in a rock type (Type 2) that has a connate water saturation of 25%, a residual oil saturation to waterflood of 30 percent, and a critical gas saturation of 5%.

The hysteresis effect was included in both water and gas relative permeability data for both rock types as shown in Figs. 2-6 & 5-6. The connate water saturation for the water hysteresis curve is consistent at 35% for both rock types while the critical gas saturations are 35% and 25% for rock types 1 and 2, respectively. Data from injectivity tests conducted on WWUI 4816 were used to fine tune the hysteresis curves. A single well radial simulation was run on WWU 4816 to compare the injection bottomhole pressures calculated by the simulator to the values observed in the field tests. The calculated bottomhole pressures compared favorably with the observed values during the water injection cycle but were lower during the CO_2 injection cycle. The gas hysteresis curves for the full area model were adjusted downward slightly to increase the simulator-calculated bottomhole pressures during the CO_2 injection cycle.

Reservoir Description

In sizing the model, an average spacing of 8 gridblocks between adjacent wells

Forecast Simulations

Several forecast simulations have been conducted to project performance under a series of operating scenarios. The forecast simulations were all started July 1997, the expected starting date for CO_2. The base case assumed continuing the existing waterflood to the year 2014. Two CO_2 flood scenarios were projected. In one, a continuous CO_2 slug was injected until January 1998, when WAG operation commenced, to year 2014. The other had continuous CO_2 injection to January 2000 followed by WAG operations until year 2014. Each scenario was run under bottomhole injection pressures of 3300, 3100, and 2800 psia to better understand the impact of injection pressure on performance including out-of-zone CO_2 losses. After several simulations with different WAG ratios, a 1:1 WAG ratio was determined to be the optimum.

The two scenarios were also repeated with 400-ft vertical fractures extending from the injection wells along the injection rows starting with wells 4809 and 4810 (Fig. 6-6). The oil and gas CO_2 rate forecasts from the fractured simulation are shown on Figs. 9-6 and 10-6.

Finally, several forecast simulations with the two different EOS fluid characterizations were conducted to get a range of possible ultimate oil recoveries (see discussion on Fluid Characterization).

Summary of Results

A reservoir simulation model has been developed for the West Welch DOE project area using the basic geologic description. The adjusted simulation model very closely matches the oil and water production during the entire production history. This gives confidence on the simulator's prediction of performance. Several forecast simulations were carried out to determine CO_2 flood performance under various scenarios, which allowed the design of an optimum CO_2 flood for Budget Period 2.

The problems encountered with the interpretation of the wellbore seismic data have prevented upgrading the geologic model as planned. This effort will continue into Budget Period 2.

Conclusions

The reservoir simulator with the basic geologic model, after being calibrated by the history matches, is capable of making reasonably accurate projections of future performance of the demonstration area under secondary and tertiary recovery scenarios.

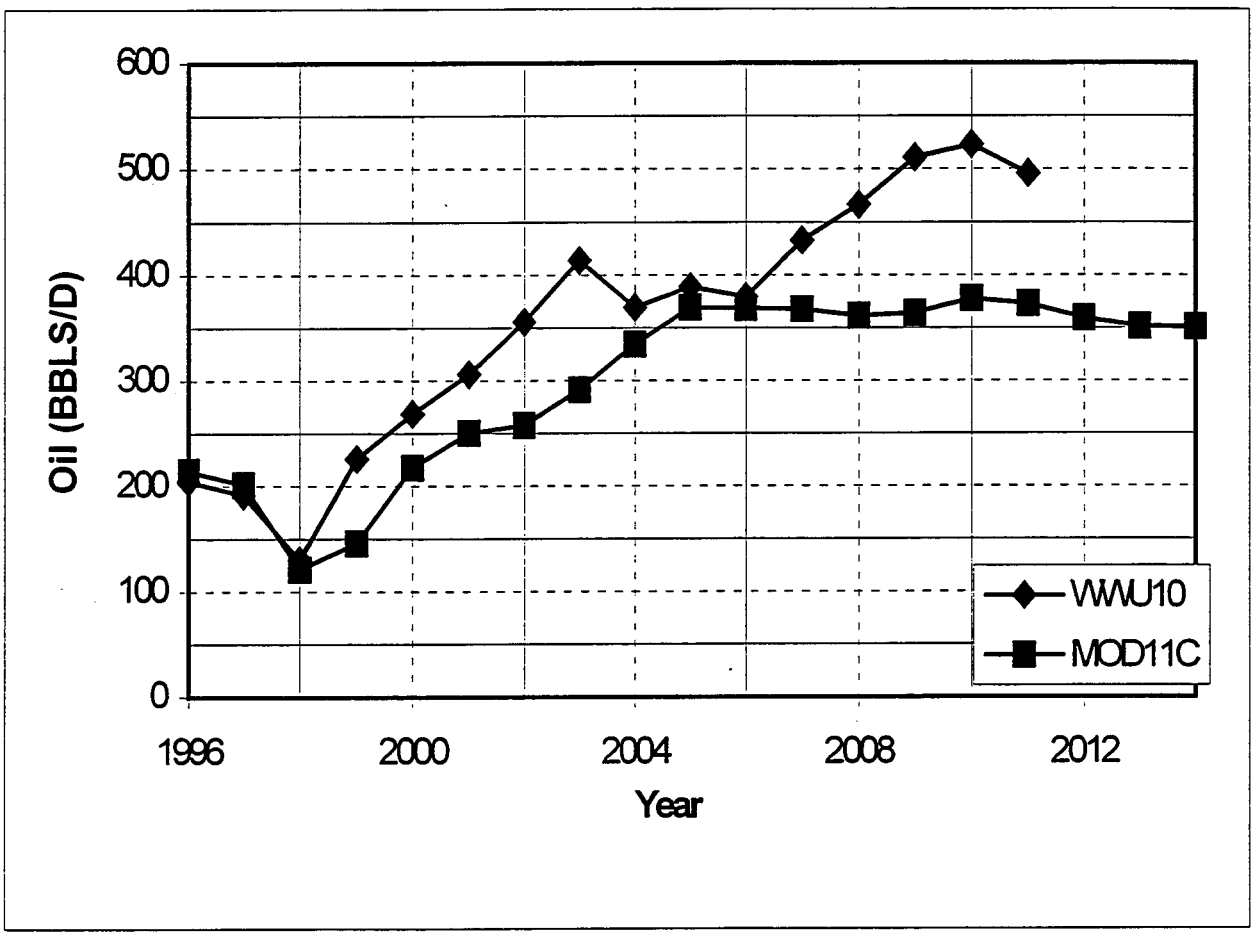

Figure 1-6 Comparison of CO2 flood oil response using the two equation of state characterizations.

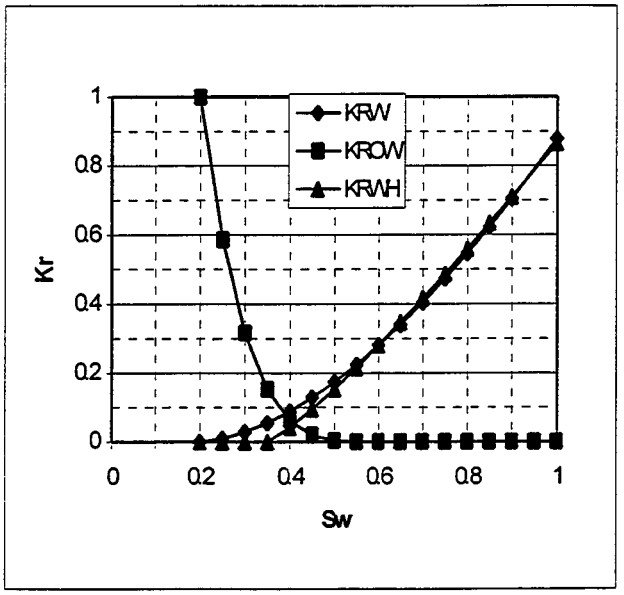

Figure 2-6 Type 1 water-oil relative permeability curves with hysteresis.

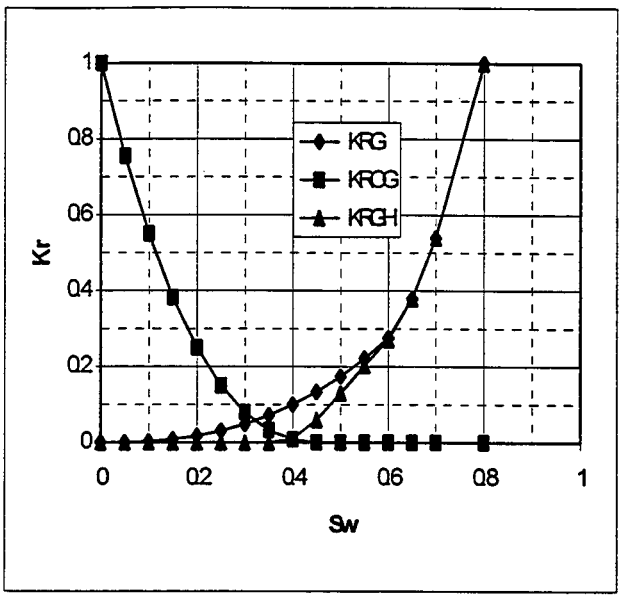

Figure 3-6 Type 1 gas-oil relative permeability curves with hysteresis.

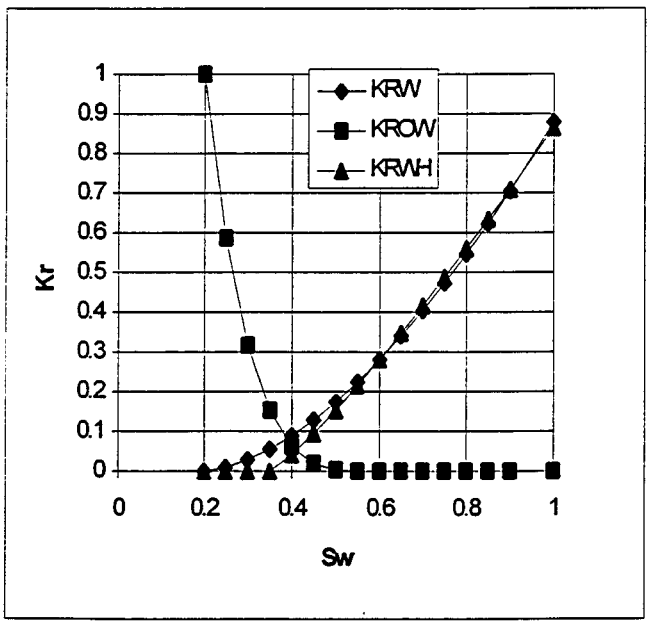

Figure 4-6 Type 2 water-oil relative permeability curves with hysteresis.

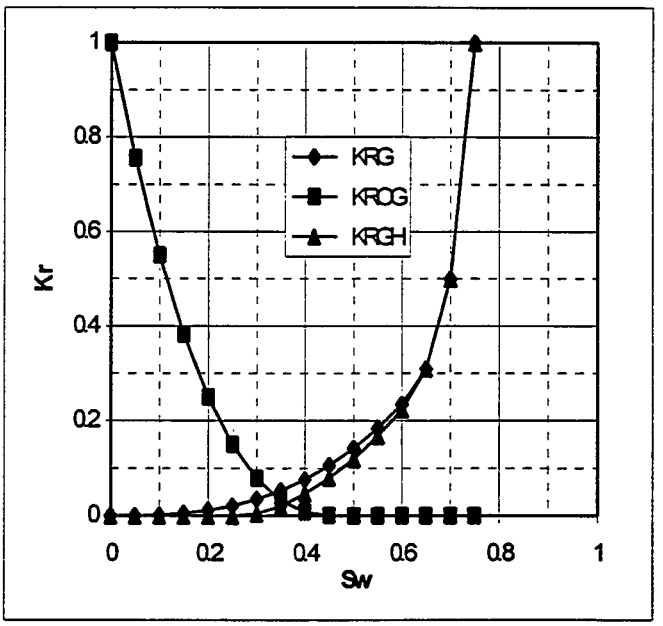

Figure 5-6 Type 2 gas-oil relative permebility curves with hysteresis.

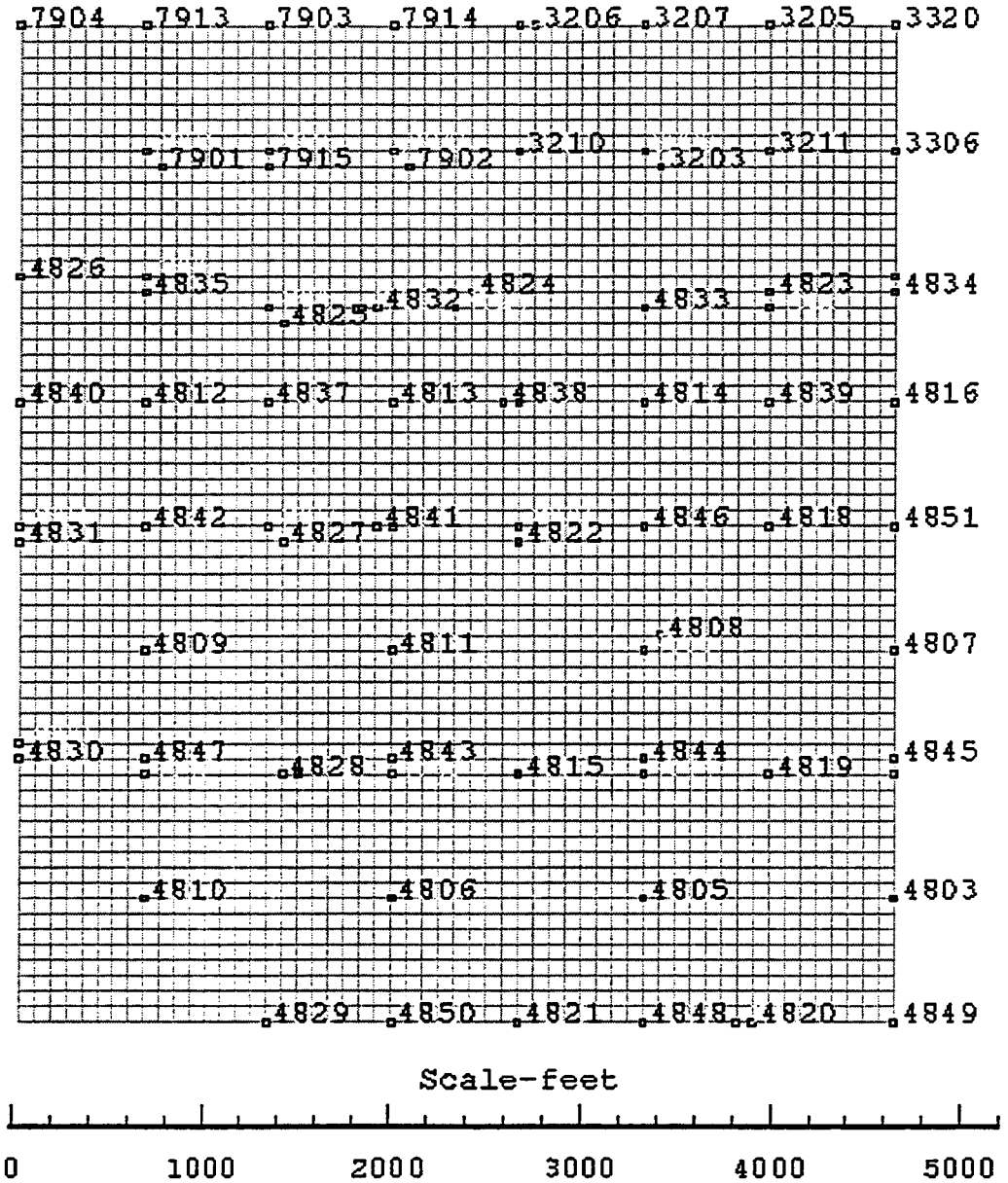

Figure 6-6 56 x 64 areal gridding of the model showing the well locations.

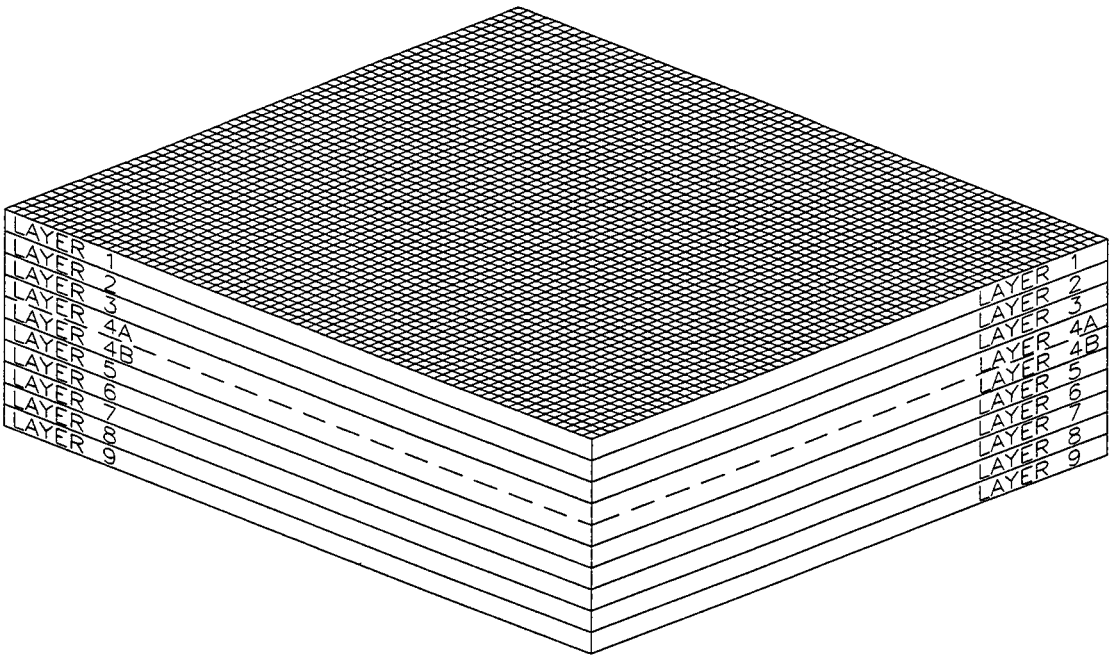

Figure 7-6 Simulation grid showing the layers and 56 x 64 areal gridding.

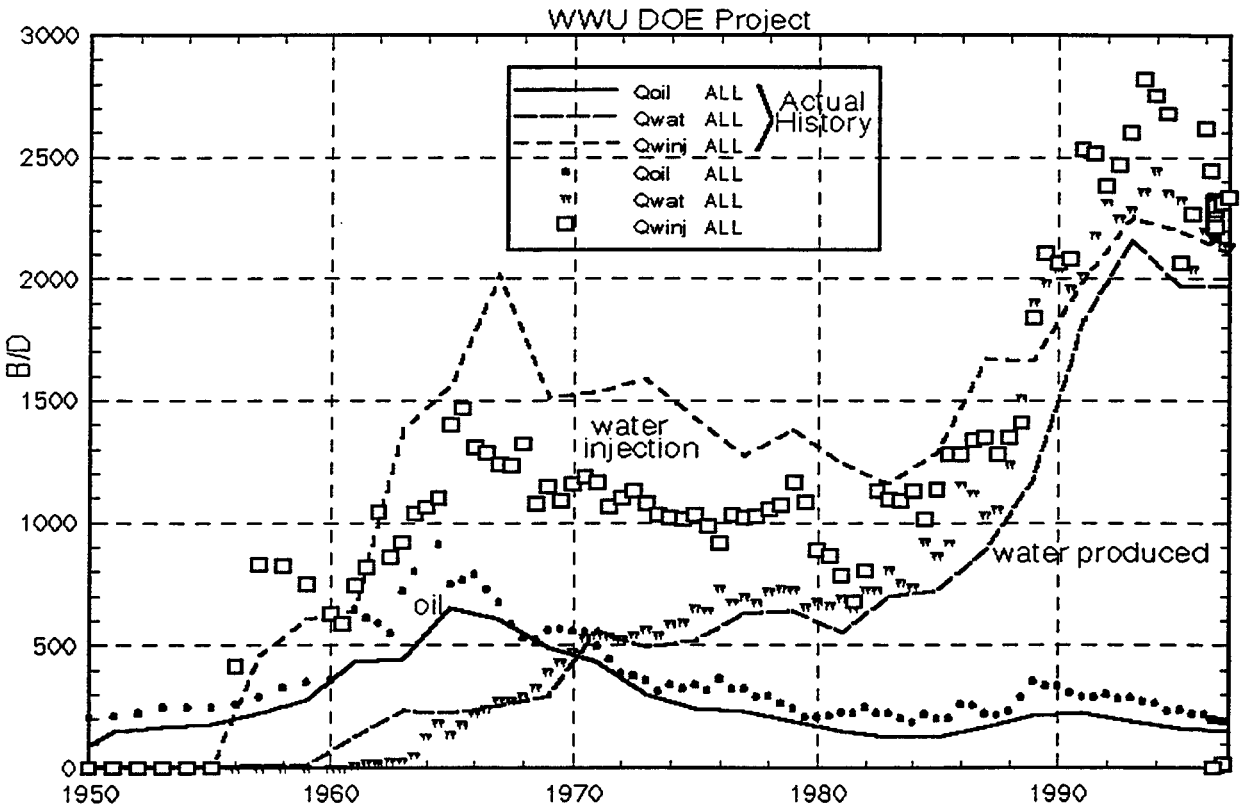

Figure 8-6 Comparison of model historical rates and actual rates

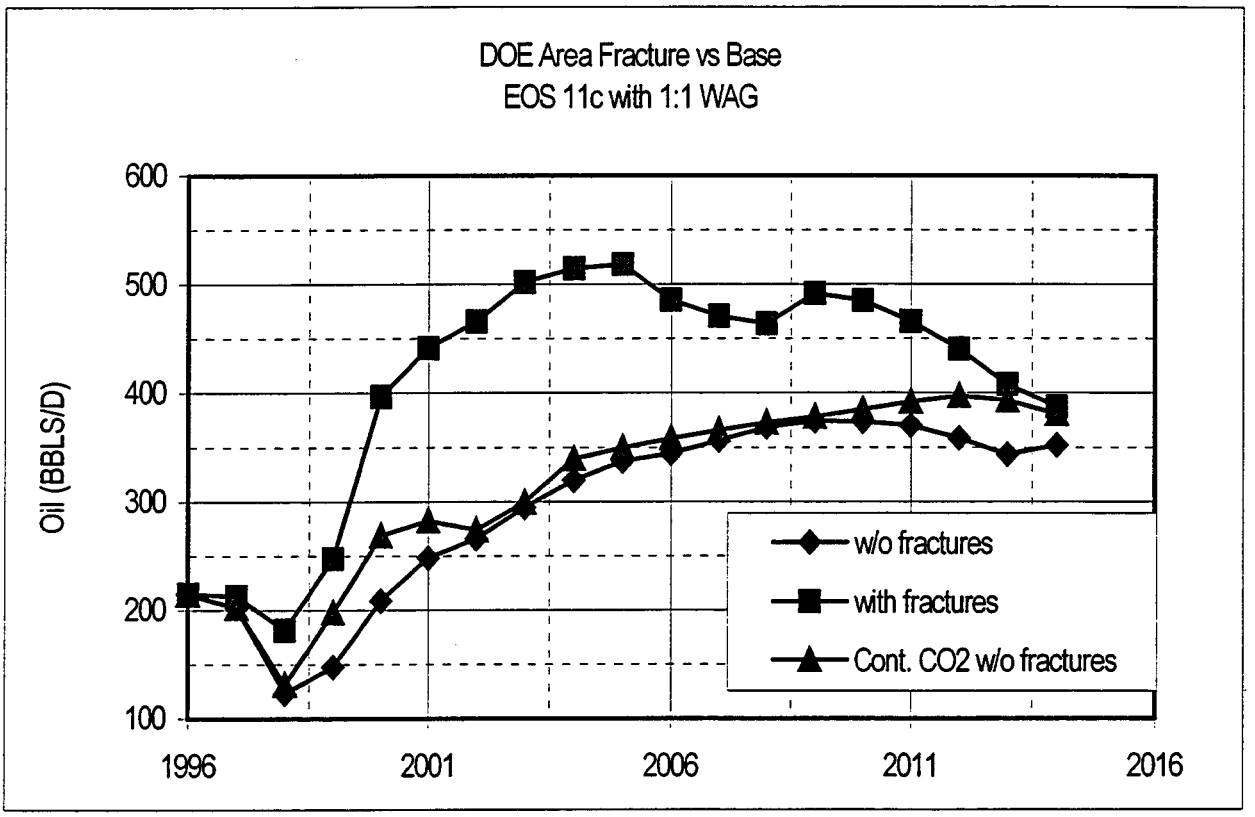

Figure 9-6 Model predicted oil rates for 1:1 WAG after CO2 breakthrough

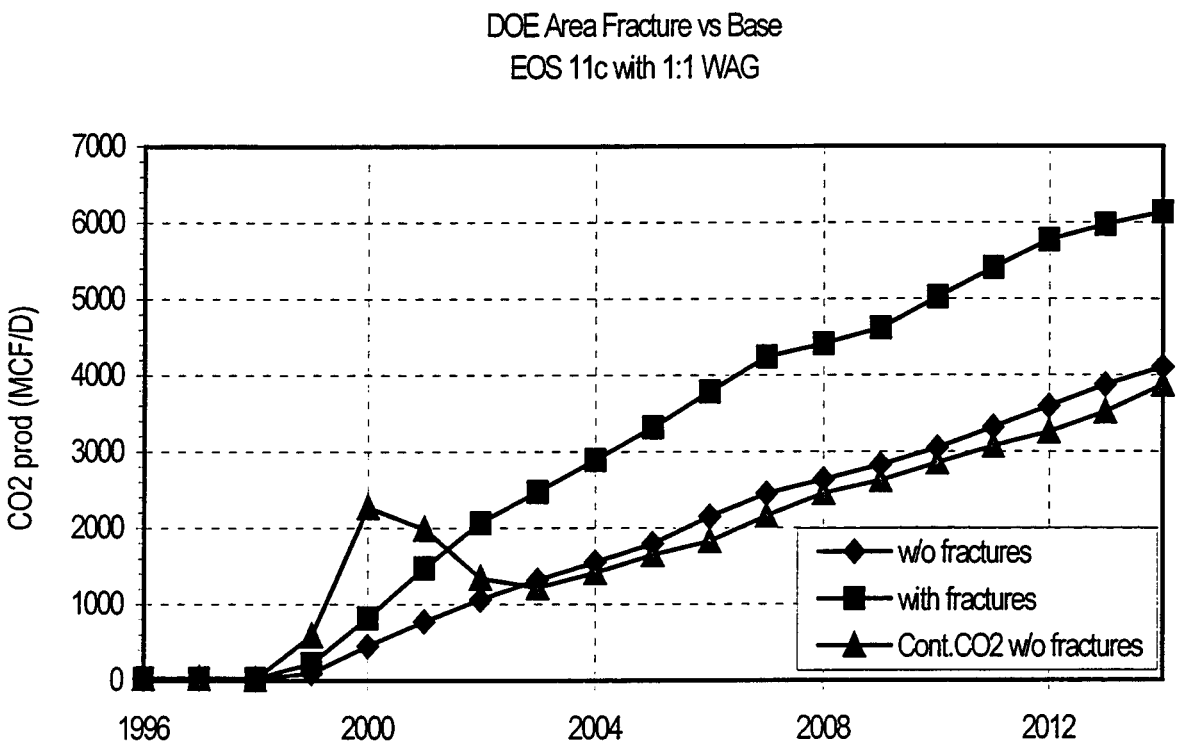

Figure 10-6 Model prediction of CO2 production rates. Continuous CO2 ends in 2000.